**acta physica slovaca vol. 58 No. 2, 155 – 241** **April 2008**

# TOP QUARK PROPERTIES

**Jaroslav Antoš**[1]
*Institute of Experimental Physics, Watsonova 47, Košice, Slovakia*

Received 22 May 2008, accepted 1 July 2008

There is tremendous progress in the study of top quark properties from time when the top quark was discovered by CDF and D0 collaboration in 1995 at TEVATRON collider. In this review we try to summarize results and methods how these results have been achieved. Aim is to emphasize problems and how these problems have been solved. We stay in the Standard model framework and demonstrate how the experimental results give support to this framework.

PACS: 02.50.+s, 05.60.+w, 72.15.-v

KEYWORDS: High Energy Physics, TEVATRON, LHC, CDF, D0, top quark, determination of top quark parameters, Standard Model

## Contents



[1]E-mail address: antos@saske.sk

## 1 Introduction

Top quark was discovered in 1995 by two collaborations CDF and D0 [2] at TEVATRON collider at Fermi National Accelerator Laboratory (FNAL). From time of the discovery of existence of b-quark in 1977 (also discovered at FNAL) one of the most important tasks of HEP community was experimental discovery of partner of b-quark in weak isospin doublet - top quark. Eighteen years of intensive search for this particle was finished and era of experimental study of top quark properties started.

In this article we review current situation in a study of top quark properties, methods and results to determine top quark parameters. There are excellent review articles (e.g [3], [4]) which cover this topic in more details. Ambition of this paper is to update situation in experiments and emphasize some aspects from the author's point of view.
Until now (year 2008) only place to study experimentally top quark properties is FNAL and therefore all quoted experimental results come from two experiments CDF and D0 there.

The paper is organized in the following way:

In the Sec. 2 brief theoretical overview of the top quark properties from a point of view of the Standard Model is given.

In Sec. 3 after brief introduction of detector setup of the experiments CDF and D0 experimental results of the top quark parameter measurements are reviewed. There is always picked up specific published analysis which was from author's point of view interesting (for different reasons - novelty of approach, less model dependence etc.) and is followed in detail. We tried to simplify account and to emphasize important points of a specific analysis.

In concluding remarks improvements which can be expected based on integrated luminosity of the full TEVATRON run II are discussed and tasks which most likely will be left for future measurements at Large Hadron Collider (LHC) and International Linear Collider (ILC) are mentioned.

## 2 Theoretical framework

Standard Model (SM) so far successfully passed all experimental tests and challenges (e.g. [1]). It describes weak, electromagnetic and strong interactions. Only gravitational interaction is left out of SM and we will ignore it in this paper. According to SM structure of basic building blocks of nature can be pictured as in Fig. 1.

In the first row of the picture one can see 3 families of leptons and 3 families of quarks. Quarks and leptons are spin 1/2 (spinor) particles. Quarks can interact with each other by all three kinds of interactions. Each quark can be in one of three color states. Name of these states - color comes from an analogy with everyday life when white light can be decomposed into 3 constituent colors or vice versa. Also three quarks of different color can create white (colorless) object - strongly interacting particle - hadron (more precisely baryon). Also combination of (colored) quark and anti (colored) quark results in colorless hadron (more precisely meson). One can invent colorless combination also from more than three quarks but so far there is no clear evidence that such states exist.

Strong interaction of quarks are described by Quantum chromo-dynamics (QCD) - theory which is integral part of Standard Model. QCD also explains that free quarks cannot be observed

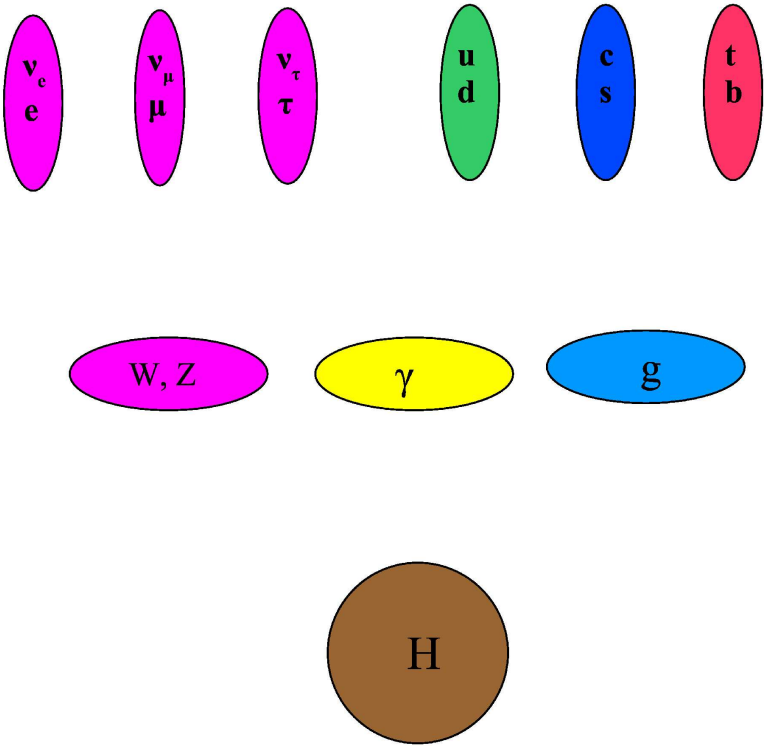


Fig. 1. Structure of fundamental blocks of matter.

in nature - only composite colorless objects with quark constituents or fundamental colorless objects (e.g. leptons). Quarks and leptons are arranged in electroweak isospin doublets. Electric charge of quarks is 1/3 or 2/3 fraction of elementary charge. Upper partner of quark doublet posses +2/3 and lower partner -1/3 electric charge.

Leptons can interact only by electroweak interaction. Symmetry between quark and lepton families (same number of quark and lepton families) is very important from theoretical point of view. Lower partners in lepton doublet posses electric charge -1 (electron, muon and $\tau$ lepton) and upper components electric charge 0 ($\nu_e, \nu_\mu, \nu_\tau$) neutrinos. Neutrinos interact through weak interaction only.

There are three kinds of spin 1 (vector) particles and their role in nature is to mediate interactions between particles. $W^{\pm}$ and $Z^0$-Bosons mediate (are carriers of) weak, photons ($\gamma$) electromagnetic and 8 gluons mediate strong interaction (as a colored objects they cannot be observed as a free particles in nature).

Special role in this schema is reserved for last spin 0 (scalar) particle - Higgs particle. Up to now it is only particle from above structure which was not yet experimentally observed. This particle is responsible for symmetry breaking by which originally massless fundamental particles acquire mass. Main purpose of the new accelerator complex LHC (which will soon be operational) and experiments ATLAS, CMS [5] is discovery and study of the properties of Higgs particle.

### 2.1 The Standard Model predictions about top quark properties

Standard Model (SM) is frequently criticized because there are many independent parameters which need to be supplied to the model. Only after this supply does the Standard Model have a predictive power which can be experimentally verified. Masses of fundamental particles (including top quark) and values of the CKM [6] matrix cannot be determined from the first principles of the model. CKM matrix reflects observation that strong interaction quantum eigenstates of quarks are not the same as eigenstates for the weak interaction. A unitary CKM matrix transforms QCD eigenstates $d, s, b$ quarks into weak interaction eigenstates $d', s', b'$

$$\begin{bmatrix} V_{ud} & V_{us} & V_{ub} \\ V_{cd} & V_{cs} & V_{cb} \\ V_{td} & V_{ts} & V_{tb} \end{bmatrix} \begin{bmatrix} d \\ s \\ b \end{bmatrix} = \begin{bmatrix} d' \\ s' \\ b' \end{bmatrix}. \tag{1}$$

Matrix elements of CKM matrix represent probabilities for charged current transition of one quark to another. e.g. $V_{tb}$ represents probability of charged current transition of top quark to b-quark.

A consequence of unitarity condition for three quark families is

$$|V_{ub}|^2 + |V_{cb}|^2 + |V_{tb}|^2 = 1. \tag{2}$$

From experimentally determined $V_{ub}, V_{cb}$ follows restriction on $V_{tb}$

$$0.9990 < |V_{tb}| < 0.9993. \tag{3}$$

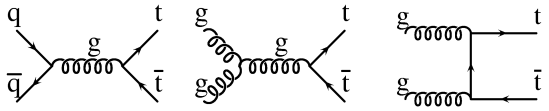


Fig. 2. Lowest order Feynman diagrams for $t\bar{t}$ pair production.

Therefore top quark should dominantly decay into W and b-quark (but one should keep in mind that three quark family condition is crucial for this statement!).

Except for top mass - all other properties of top quark are predicted by Standard Model. According to SM, t-quark as a weak isospin partner of b-quark should have charge +2/3 and spin 1/2. The weak interaction is responsible for both the decay of the muon and the top. The same formula describes both. The top quark width is proportional to the third power of the top quark mass as seen in the formula given below

$$\Gamma_{\rm t} \approx \frac{{\rm G_F m_t}^3}{8\sqrt{2}\pi}, \tag{4}$$

where $\rm G_F$ is the Fermi coupling constant and $m_t$ top quark mass. Top lifetime is inversely proportional to the top width. As one can see from above formula, for top quark mass 170 $\rm GeV/c^2$ lifetime of t-quark is only $\sim 5 \times 10^{-25}$ seconds! Such short lifetime has a consequence. Typical time needed for fragmentation of quarks into hadrons is characterized by time scale $1/\Lambda_{QCD} \sim 3 \times 10^{-24}$ sec. Because top quark lifetime is an order of magnitude smaller than time needed to create hadron from top quark we can draw a conclusion that top quark decays "immediately" into W and b-quark, therefore properties of top quark are directly transfered to decay products (and are not diluted by hadronization process). This property opens a unique opportunity to look at inner quark dynamics!

Dominant top quark production mechanism at hadron colliders is pair production of $t\bar{t}$. Lowest order Feynman diagrams for this process are drawn in Fig. 2.

Basic processes are quark anti quark annihilation and gluon - gluon fusion.

To calculate $t\bar{t}$ cross section for hadron-hadron reaction it is necessary to make convolution of elementary parton-parton cross section over parton distribution functions (PDF)

$$\sigma^{t\bar{t}}_{h_1h_2}(\sqrt{s}, m_t) = \sum_{i,j=q,\bar{q},g} \int dx_i dx_j f_i^{h_1}(x_i,\mu^2) f_j^{h_2}(x_j,\mu^2) \times \hat{\sigma}^{ij\to t\bar{t}}(\rho, m_t^2, x_i, x_j, \alpha_s(\mu^2), \mu^2), \tag{5}$$

where s is center of mass energy squared, $m_t$ - top mass, $x_i$ - fraction of longitudinal momentum of hadron carried by parton i, $f_i^h(x_i,\mu^2)$ is the PDF for parton i probed at energy scale of $\mu^2$ in hadron h, $\alpha_s(\mu^2)$ - QCD strong running coupling constant at energy scale $\mu^2$, $\rho = 4m_t^2/\sqrt{\hat{s}}$, effective center of mass energy squared for partonic process $\hat{s} = x_i x_j s$ and $\hat{\sigma}^{ij\to t\bar{t}}$ cross section for $t\bar{t}$ production by parton - parton interactions.

In [29] the theoretical cross section for $t\bar{t}$ production in $p\bar{p}$ collisions at 1.8 and 1.96 TeV in CMS (TEVATRON run I and II energy) was calculated (for selected top masses assumed) together with careful analysis of uncertainties. e.g. $\sigma^{t\bar{t}}_{p\bar{p}}(1.96, 175) = 6.70^{+0.71}_{-0.88}$ pb, $\sigma^{t\bar{t}}_{p\bar{p}}(1.96, 170)$

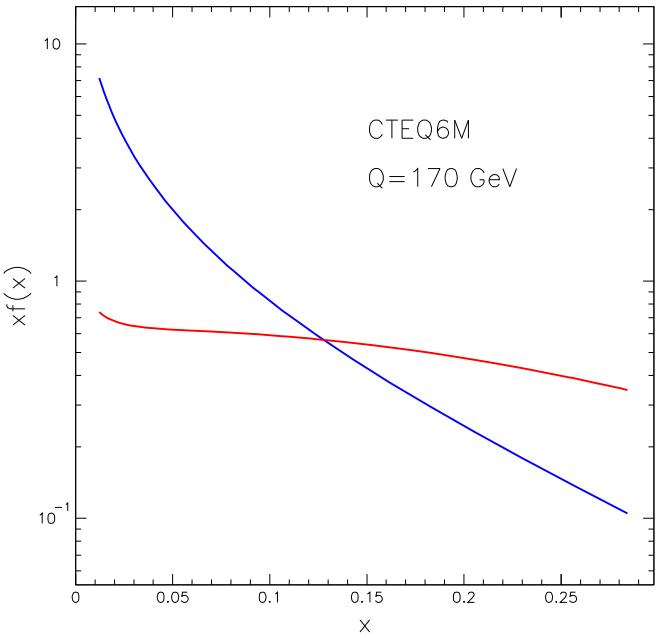


Fig. 3. Probability density to observe gluon (blue), up quark (red) with fraction of longitudinal momentum $x$ in proton probed at energy scale 170 GeV. Curves are based on CTEQ6M parametrization [7], u-quark distribution dominates quark distribution in proton in a given region of the $x$.

$= 7.83^{+0.86}_{-1.04}$ pb. Cross section is dominated by the $q\bar{q}$ production mechanism (80-90%), the gluon-gluon contribution was estimated to be between 10-20%.

At LHC (pp interaction at 14 TeV) fractions are reversed. The reason can be easily understood. Threshold $\sqrt{\hat{s}}$ for $t\bar{t}$ production is $2m_t$ and it corresponds to a typical fraction of longitudinal momentum $x \approx 2m_t/\sqrt{s}$. That means (for $m_t = 175$ GeV/$c^2$) $x = 0.18$ at TEVATRON run II energy and $x = 0.025$ at LHC. As can be seen from Fig. 3 for $x = 0.025$ there is much larger probability for gluon than for u quark to be observed with given fraction of longitudinal momentum of proton. Lower threshold for $x$ is also reason why cross section for $t\bar{t}$ production at LHC is two orders magnitudes higher than in case of TEVATRON while LHC energy is less than order of magnitude higher.

In Tab. I a comparison of selected parameters of TEVATRON and LHC is shown. From this table one can see that cross section for $t\bar{t}$ production at LHC is two order of magnitude higher and luminosity at least order of magnitude higher than luminosity at TEVATRON one can expect at least 3 orders of magnitude larger statistics of produced top quarks at LHC in comparison with TEVATRON. LHC will be top factory and very detailed analysis will be possible there!

Standard Model also predicts possibility for "single top" production by electroweak process. Feynman diagrams for this production mechanism are shown in Fig. 4.

Tab. I. A comparison of the basic parameters for $t\bar{t}$ production at TEVATRON (run I, run II) and LHC.

| Characteristic | Run 1 | Run 2 | LHC |
|---|---|---|---|
| interaction | $p\bar{p}$ | $p\bar{p}$ | $pp$ |
| $E_{CM}$ [TeV] | 1.8 | 1.96 | 14 |
| Luminosity [$cm^{-2}s^{-1}$] | $\approx 10^{31}$ | $\approx 10^{32}$ | $10^{33} - 10^{34}$ |
| $\sigma_{t\bar{t}}(m_t = 175)$ [pb] | 5. | 6.7 | 830 |
| $q\bar{q}$ fraction [%] | 90 | 85 | 5 |
| gg fraction [%] | 10 | 15 | 95 |

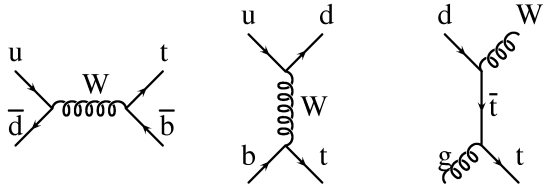


Fig. 4. Feynman diagrams for single top quark production.

The first diagram represents s-channel, second t-channel and last one tW contributions to single top production. According to the Standard Model in the NLO approximation the cross section (for top quark mass 175 GeV/$c^2$) for s-channel is $\sigma(p\bar{p} \rightarrow tb + X) = (0.88 \pm 0.11)|V_{tb}|^2$ pb and for t-channel $\sigma(p\bar{p} \rightarrow tqb + X) = (1.98 \pm 0.25)|V_{tb}|^2$ pb [9]. At TEVATRON tW channel contribution is expected to be negligible.

When considering t channel topology one needs to take into account there are no valence b-quarks in proton (or $\bar{p}$) structure. Therefore b-quark which enters t-channel diagram is always accompanied (compensated) by anti b-quark (and topology in final state is $dt\bar{b}$)!

Observation of single top production will be a very important piece of evidence for Standard Model. This process can be used for a direct measurement of CKM matrix element $|V_{tb}|$, it is a source of $\sim$ 100 % polarized top quarks, t-W-b vertex enters at the production level and therefore by making a measurement of the single top production cross section one can measure the top quark partial width $\Gamma(t \rightarrow Wb)$ and hence the top lifetime! Specifically parton level cross section can be expressed as [10]

$$\hat{\sigma}(ub \rightarrow dt) = \sum_{\lambda=0,+,-} f_\lambda(x = \frac{m_t^2}{\hat{s}}) \Big[ \frac{16\pi^2 m_t^3}{\hat{s}(m_t^2 - M_W^2)^2} \Big] \Gamma(t \rightarrow bW_\lambda^+), \tag{6}$$

where $f_\lambda(x)$ is flux of W - Bosons of a given helicity state $\lambda = 0, +, -$ [11] , $M_W$ is the W-Boson mass, $\Gamma(t \rightarrow bW_\lambda^+)$ - is the partial width for decay of top quark into b and W of helicity $\lambda$.

Standard Model gives definite prediction about spin structure of top quark production and

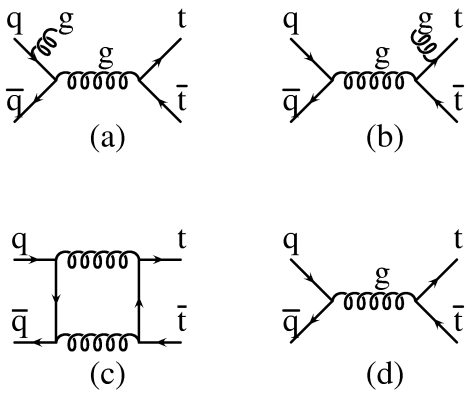


Fig. 5. Interference of diagrams (a) and (b), (c) and (d) has a consequence in forward backward asymmetry for top quark production.

decay. Top quarks produced in pairs by strong interaction are unpolarized (more exactly polarization on level of a few percent is predicted by NLO QCD calculations [12]). Top quark decays through weak interaction $t \rightarrow W^{+}b$ and Standard Model predicts top mass dependent fractions of longitudinal and left-handed W polarization. In the limit of massless b-quark fraction of right handed W polarization should be (according to SM) 0. This topic is treated in more details in section 3.5.

Even if in pair production top and anti-top quarks are unpolarized there is predicted correlation between spins of top and anti top quarks. Origin of correlation can be qualitatively understood in the following way: At threshold $t\bar{t}$ system produced by $q\bar{q}$ annihilation mechanism is dominantly produced in ${}^{3}S_{1}$ angular momentum state [8]. From angular momentum conservation follows that spins of $t$ and $\bar{t}$ should be aligned (point in the same direction). Threshold production of $t\bar{t}$ by gluon-gluon fusion is dominantly produced in ${}^{1}S_{0}$ state and therefore spins of $t$ and $\bar{t}$ should be anti-aligned. Because at TEVATRON $t\bar{t}$ production dominates by $q\bar{q}$ mechanism one can expect to observe spin alignment of $t$ and $\bar{t}$ spins. The topic is treated in more details in section 3.6.

We close this section about Standard Model predictions about top quark properties with prediction of forward backward asymmetry in $t\bar{t}$ production. According to [13] as a consequence of interference of diagrams (a) and (b), (c) and (d) (see Fig. 5) there is forward-background asymmetry in case of $t\bar{t}$ production on level of $\sim 5$ %. At this level top quark is more likely to follow direction of quark (from proton).

## 3 Experimental determination of top quark parameters

Experimental results we will discuss come from the two experiments at TEVATRON – CDF and D0.

TEVATRON is $p\bar{p}$ collider which during run I period (1992-1996) operated using 6 bunches of protons and anti-protons, with 3500 ns between bunch crossings and had center of mass energy 1.8 TeV. Typical peak luminosity was $\approx 10^{31}\mathrm{cm}^{-2}\mathrm{s}^{-1}$. During this period each experiment recorded $\approx 120\ \mathrm{pb}^{-1}$ of data.

In the years 1996-2000 there was a major upgrade of the TEVATRON and also for both of the experiments.
Run II started in March 2001 and is supposed to continue until end of 2009 (2010?). It operates with 36 bunches of protons and anti-protons with bunch spacing of 396 ns and increased center of mass energy 1.96 TeV. Typical peak luminosity is order of magnitude higher than in run I and realistic integrated luminosity which will be achieved by end of run II is 6-8 $\mathrm{fb}^{-1}$!

CDF and D0 are general purpose detector systems composed of the following components:

- vertex detector
- tracking system
- electromagnetic calorimeters
- hadronic calorimeters
- muon system

Both detectors are azimuthally and forward backward symmetric. Both experiments use right-handed orthogonal coordinate systems $(x, y, z)$. Center of coordinate system coincides with center of detector, with *z*-axis along the proton beam direction. The *y*-axis is vertical and *x*-axis points to the center of accelerator ring. There are defined azimuthal angle $\phi$, polar angle $\theta$ and frequently the pseudorapidity $\eta = -\ln(\tan(\theta/2))$ is used. Projection of momentum into transverse $(x, y)$ plane is another frequently used variable $p_T$. This variable is directly related to a curvature of tracks in the magnetic field. In case of calorimetry there is used related variable $E_T = \sum E_i \sin(\theta_i)$. Where $E_i, \theta_i$ are energy of the cell *i* and polar angle of the cell *i* respectively. The summation is over all cells belonging to a given physical object (electromagnetic, hadronic shower).

Vertex detector and central tracker are placed inside solenoid magnet. Vertex detector is supposed to be efficient in identifying vertex of short lived particles. Specifically physical interest is directed to hadrons with b-quark in their structure - B-hadrons (e.g. $\mathrm{B}^{\pm}, \mathrm{B}^{0}$ ) or hadrons with c-quark in their structure - charmed hadrons (e.g. $\mathrm{D}^{\pm}, \mathrm{D}^{0}$). Typical mean lifetime of B-hadrons is $\tau \approx 1.6$ ps or in units $c\tau \approx 500\ \mu$m. Charmed hadrons mean lifetime is shorter $c\tau \approx$ 100-300 $\mu$m. Short lived particle decays into (relatively) long lived, charged (and/or neutral) particles like $\pi, K$ or there is cascade of short lived particles but finally only long lived particles are left. Trajectory of charged particles in magnetic field has helix shape. It can be parametrized by 5 parameters. When charged particle passes through sensor it leaves trace - hit. From hits trajectory can be reconstructed. Long lived particles which come directly from interaction point have impact parameter $d_0$ (closest distance in transverse plane to interaction point) 0 and corresponding

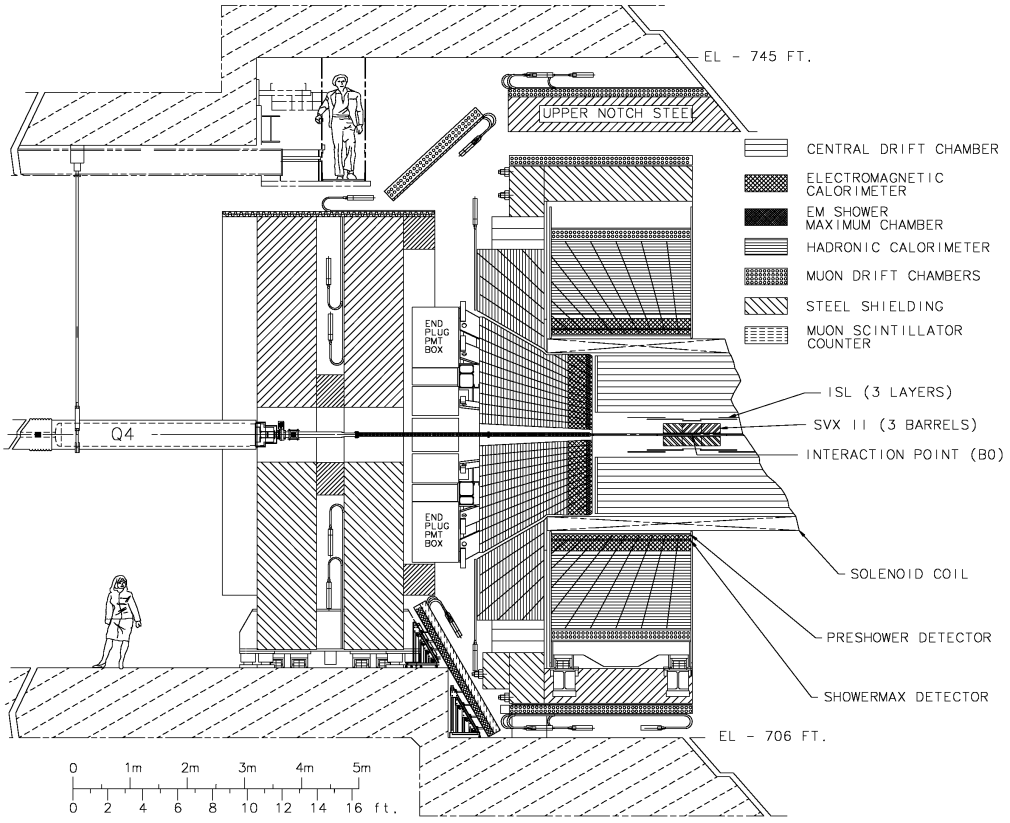


Fig. 6. CDF detector.

coordinate along beam axes ($z_0$) also 0. Naturally within resolution provided by detector. Same quantities for particles which come from decay of e.g. B-hadrons will be non zero.

Vertex detectors have different structure (for CDF and D0) but are based on the same microstrip silicon detector technology.

Detailed description of the CDF detector can be found in [14] and for D0 detector in [15]. Short descriptions can be found on web pages of above collaborations. In our description below we will concentrate just on final performance of subcomponents - resolution and coverage.

### CDF detector

Schematic of CDF detector in elevation view is shown in Fig. 6.
Silicon vertex detector has barrel structure and consists of three parts:

- central SVXII detector consists of 5 layers of double sided silicon sensors
- outer ISL detector consists of two layers of double sided silicon sensors

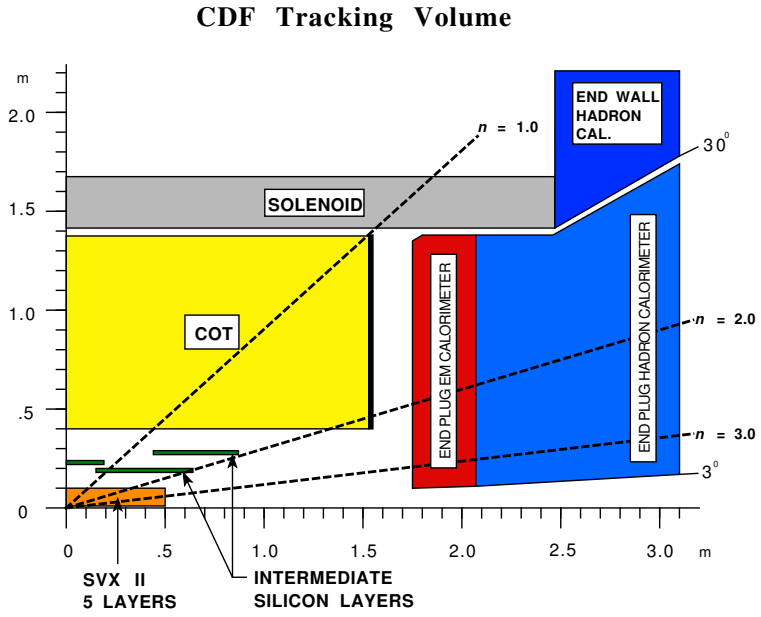


Fig. 7. Longitudinal view of CDF tracking system.

- closest to beam pipe is Layer 00 - single sided silicon sensor

One of the important problems which needed to be solved is radiation hardness specially for Layer 00 which is closest to the beam pipe therefore most prone to radiation damage.

The vertex detector covers region in pseudorapidity $|\eta| < 2$. In the optimal case (combination of ISL and SVXII) the $z_0$ resolution is 70 mum. In the transverse direction the uncertainity in the beamline contributes 30 mum, when combined with the intrinsic resolution of ISL and SVXII, the resulting resolution is 40 mum. Device is capable of reconstructing tracks in 3D. This system is based on tremendous experience of CDF collaboration with silicon vertex detectors. Current system is the third generation of very successful sequence of silicon vertex detectors at CDF!

Cylindrical drift chamber (COT) detector surrounds vertex detector and it is the main tracking device for CDF collaboration. It is 3.1 m long, covers radial range from 40 to 137 cm and provides 96 measurement layers, organized into alternating axial and $\pm 2^\circ$ stereo superlayers. It provides the hit position resolution $\approx 140 \mu$m and the momentum resolution

$$\frac{\sigma(p_T)}{p_T} = 0.0015 \times p_T. \tag{7}$$

The COT also provides information about energy loss of tracks (dE/dx) which can be used in particle identification. COT covers pseudorapidity $|\eta| \leq 1$. Schematic of CDF tracking system is shown in Fig. 7.

Just outside COT with a few centimeters clearance is installed time-of-flight system (TOF) based on plastic scintillators and fine mesh photomultipliers. Resolution of TOF is $\approx 100$ ps.

Superconducting solenoid magnet of length 4.8 m and radius 1.5 m surrounds tracking system and generates 1.4 T magnetic field parallel to the beam axis.

Segmented electromagnetic and hadronic calorimeters cover region $|\eta| < 3.64$. They measure the energy flow of interacting particles. Energy resolution for electromagnetic calorimeter in region $|\eta| < 1.1$ (CEM) is

$$\frac{\sigma(E_T)}{E_T} = \frac{0.135}{\sqrt{E_T}} + 0.02 \tag{8}$$

and in region $1.1 < \eta < 3.6$ (plug) is

$$\frac{\sigma(E)}{E} = \frac{0.16}{\sqrt{E}} + 0.001. \tag{9}$$

Corresponding resolution for hadronic calorimeter in these two separated regions is for central hadron calorimeter

$$\frac{\sigma(E_T)}{E_T} = \frac{0.75}{\sqrt{E_T}} + 0.03 \tag{10}$$

and for plug

$$\frac{\sigma(E)}{E} = \frac{0.74}{\sqrt{E}} + 0.04. \tag{11}$$

The muon system resides beyond the calorimetry. It covers region $|\eta| < 1.5$. There is minimum $p_T$ for muon needed to pass through 5 absorption length of calorimeter (1.5 GeV/c) and region with additional instrumented iron (2 GeV/c). Matching of track in the muon system with track in COT identifies muon.

The beam luminosity is determined by gas Cherenkov counters in forward region $3.7 < |\eta| < 4.7$. They measure the average number of inelastic $p\bar{p}$ collisions per beam crossing.

Very important part of detector system is trigger system which should be able to select interesting events out of a huge number of interactions, and data acquisition system which should be able to cope with huge data flow. One should realize that there is 10 orders of magnitude difference between inelastic $p\bar{p}$ cross section and $t\bar{t}$ production cross section at TEVATRON!

There are three levels of trigger. First level limits rate of events to $\approx$ 18 kHz of selected events based on basic information from tracking system, calorimetry and muon system, level 2 trigger reduces rate to 300 Hz based on more refined information and level 3 trigger has access to the full information and reduces rate to $\approx 75$ Hz which is written to permanent storage.

**D0 detector**

Schematic of D0 detector is shown in Fig. 8.

Most inner part of the detector is silicon vertex detector. Silicon vertex detector has hybrid barrel and disk structure. The central detector covers region $|z| < 32$ cm consists of 6 barrels

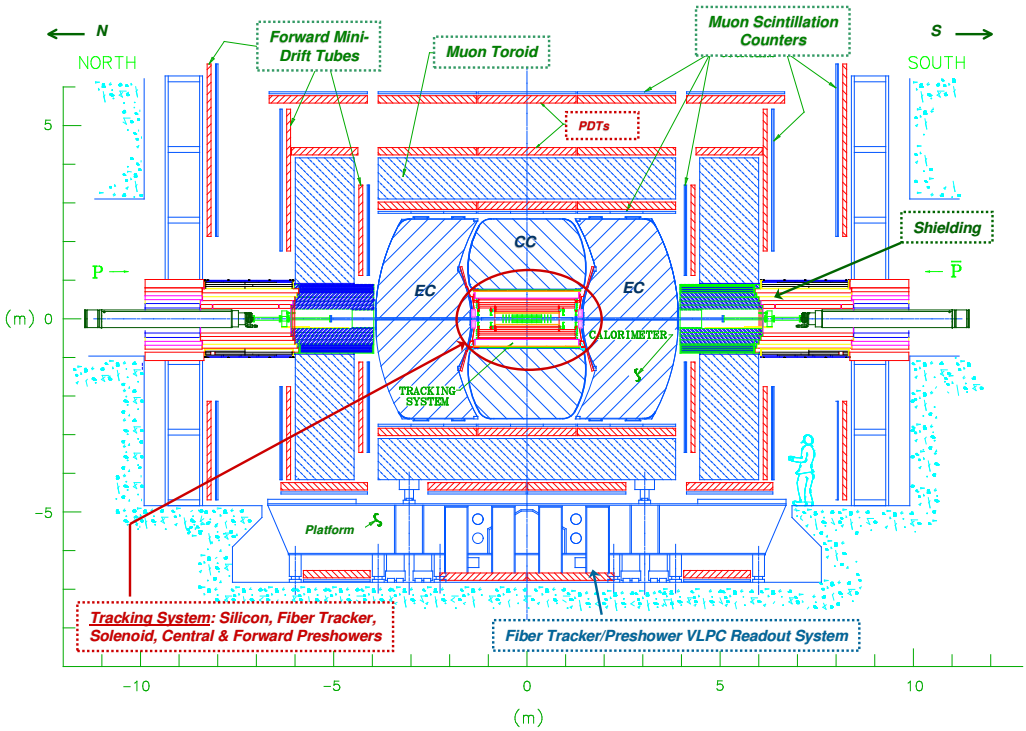


Fig. 8. D0 detector.

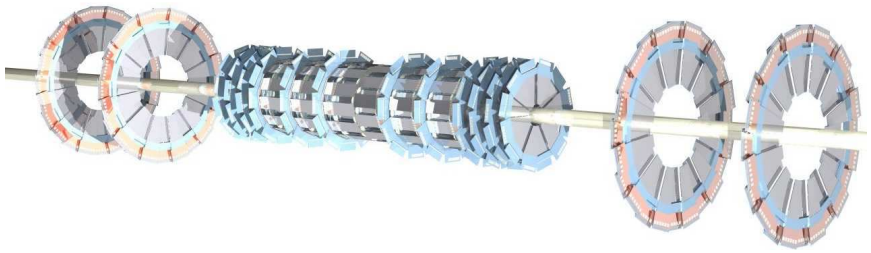

Fig. 9. Disk/barrel structure of silicon vertex detector of D0 collaboration.

with disks interspersed between them. Each barrel consists of 4 radial layers. Each disk module has 12 wedge shaped double sided detectors. The forward detectors consists of six disks of similar design (see Fig. 9). Silicon vertex detector provides tracking information up to $|\eta| = 3$. It gives reconstructed vertex position resolution 15-40 $\mu$m in the transverse plane and 75-100 $\mu$m in $z$, depending on track multiplicity of the vertex.

The central fiber tracker is the main tracking device for D0. It consists of 74000 scintillating fibers mounted on 8 concentric carbon fiber cylinders at radii 19.5 to 51.5 cm. Each cylinder

supports four layers of fibers. The fibers are multi-clad and have diameter 830 $\mu$m. Clear fiber waveguides carry the light for about 10 meters from scintillating fibers to the visible light photon counters!

The combined silicon vertex detector and fiber tracker have excellent tracking performance. Full coverage of combined detector is for $|\eta| < 1.6$ and momentum resolution

$$\frac{\sigma(p_T)}{p_T} = 0.002 \times p_T. \tag{12}$$

These detectors are located inside superconducting solenoid producing magnetic field of 2 T in the beam direction.

Uranium liquid argon sampling calorimeter with fine longitudinal and transverse segmentation provides full coverage $|\eta| < 4$ with energy resolution for electromagnetic showers

$$\frac{\sigma(E)}{E} \approx \frac{0.15}{\sqrt{E}} \tag{13}$$

and for hadronic jets

$$\frac{\sigma(E)}{E} \approx \frac{0.8}{\sqrt{E}}. \tag{14}$$

The muon system is placed around the calorimeters. The central part of muon system covers region $\eta < 1$, forward muon system extends coverage up to $\eta \approx 2$

Trigger system, as in case of the CDF, consists of the three levels. First level (L1) limits rate of events to $\approx 2$ kHz based on basic information from detector components, level 2 (L2) reduces event rate by factor two by using hardware engine and microprocessors associated with specific sub-detectors to provide information for trigger decision tree and at level 3 (L3) candidates passed from L2 are sent to a farm of microprocessors where sophisticated algorithms are implemented and finally event rate is reduced to $\approx 50$ Hz. These events are written to permanent storage.

**Channels, particle and b-jet identification, variables**

As was explained in the section 2.1 according to Standard Model pair $t\bar{t}$ production is dominant mechanism for top quark production at hadronic colliders. Each top (anti-top) quark very quickly decays into W-Boson and b-quark. As a result there are in an event $\mathrm{W}^+, \mathrm{W}^-, \mathrm{b}, \bar{\mathrm{b}}$. Masses of the final decay products are much smaller than top quark mass. Therefore top quark mass is transformed into large kinetic energy of the top decay products!

Decay of W-Bosons determines event topology. W-Boson can decay either into lepton and neutrino or into pair of quarks. If both W-Bosons decay into leptons - final state will consist of 2 leptons of opposite charge $(e, \mu)$ corresponding neutrino and anti-neutrino,$b, \bar{b}$. Such final state is called **"Dilepton channel"**. As a lepton could also be considered $\tau$ lepton but because $\tau$ lepton is from experimental point of view special (e.g. it can decay into hadrons in final state and $\nu_\tau$) it is treated separately.

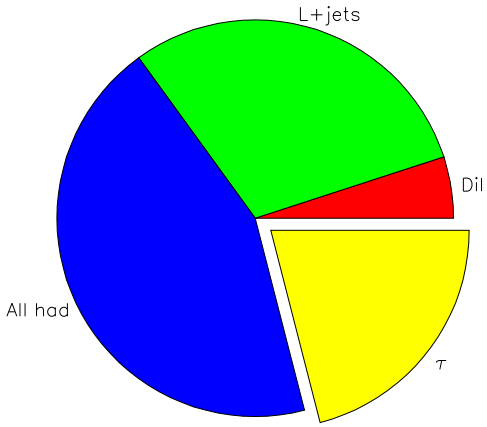


Fig. 10. Pie chart for fractions of different channels.

Quarks cannot be observed as a free particles. They fragment by non perturbative QCD process into collimated jet of hadrons around original quark direction.

Therefore dilepton channel is characterized by 2 opposite charge energetic leptons (e or $\mu$) 2 energetic b-jets and 2 neutrinos.

In case when only one W-Boson decays into e or $\mu$ (and corresponding neutrino) and other decays into quarks, the final state is called **"Lepton + jets channel"**. It is characterized by energetic e or $\mu$ lepton and corresponding neutrino, 2 energetic b-jets and 2 (light) quark jets.

In case when both W-Bosons decay hadronically (into quarks) final state is called **"All hadronic channel"**. It is characterized by energetic 2 b-jets and 4 (light) quark jets.

In consideration of the optimal conditions for jet topology for a given channel one needs to take into account that there can be created additional jets (e.g. by hard gluon radiation). There is also possibility to loose a jet because of jet reconstruction efficiency.

Branching ratios for different channels can be easily estimated. Coupling of W to different weak doublets is the same therefore (if we neglect mass of quarks in comparison with mass of W) also probability for decay is the same. There are 9 possible decays ($3-$lepton doublets$+3$(number of colors)$\times$2quark doublets). Therefore probability for W decay into $e$ or $\mu$ (and corresponding neutrino) is 2/9. Probability to decay into quarks is 2/3. Because decays of two W's are independent it follows that branching ratio for dilepton channel is 4/81, for lepton + jets channel 8/27 and for all hadronic channel 4/9. Rest is accounted by $\tau$ leptons in the final state. Graphically fractions of different channels are shown in Fig. 10.

Identification of electrons is accomplished by a matching of track reconstructed in tracking system with electromagnetic shower in electromagnetic calorimeter. Details should be compatible with electron hypothesis. Ratio (E/p) of measured energy of electron in electromagnetic calorimeter to momentum of corresponding track measured by tracking system should be close to 1.

Identification of muons is accomplished by matching of tracks in tracking and muon system. In corresponding cells in calorimeter deposited energy should be below muon compatibility

threshold.
There are different methods of reconstructing jet kinematic characteristics. CDF collaboration prefers cone algorithm (details can be found in [22]). Raw reconstructed jet $E_T$ is a sum of $E_T$ of calorimetric towers in fixed cone $r = \sqrt{(\triangle\phi)^2 + (\triangle\eta)^2}$ around jet axis. D0 collaboration prefers more sophisticated version of the cone algorithm.
The raw jet energy uses several corrections (see [23]) to get the final energy which should correspond (within resolution) to the energy of the original quark which has materialized as a jet.

For identification of b-jets sophisticated b-tagging algorithms have been developed. In analysis quoted in this paper b-tagging algorithm is based on reconstruction of secondary vertexes of short lived particles inside jet reconstructed from tracks in silicon vertex detector. More details are in section 3.1.2.

Neutrinos, interacting with matter only by weak interaction, do not leave any trace in any part of the detector. But still at least transverse components of (vectorial) sum of transverse momenta of all neutrinos in the event can be estimated by imbalance of the total transverse momentum. Because initial state of $p\bar{p}$ interaction has $\vec{p}_T = 0$ from momentum conservation follows that also sum of $\vec{p}_T$ of all particles created in interaction should be 0. All particles except neutrinos (or neutrino like) leave trace in detector and are accounted for. Therefore, missing transverse energy $\vec{\not{E}}_T$,

$$\vec{\not{E}}_T = -\sum_i \vec{E}_T^{\,i} - \sum_{jets} \vec{E}_T^{\,jets} - \sum_\mu \vec{p}_T^{\,\mu}, \tag{15}$$

represents vectorial sum of transverse momenta of all neutrinos (or neutrino like objects) in the event. The notation $\vec{E}_T^{\,i}$ means transverse energy deposited in cell *i* in calorimeter which was not attributed to any jet, $\vec{E}_T^{\,jets}$ - transverse energy of jet , $\vec{p}_T^{\,\mu}$ - transverse momentum of isolated muon.

### 3.1 Cross section measurement

Cross section is a basic characteristic of a given reaction. This is the first quantity determined when there is a claim of production of a new particle or reaction. This quantity is also usually measured in a less model dependent way than other parameters. A comparison with theoretical prediction gives support or challenge for a theory.

Measurements of cross section in different channels represents statistically independent measurements and consistency of these measurements support idea of measurement of the same process. At small statistics in run I, differences in measurement of cross section in different channels (even if there was no statistically significant difference) gave rise to theoretical speculations about two new particles (not just one top quark) close in mass.

In run II statistics is already more than order of magnitude larger. Speculations from run I can be given support or can be excluded.

Calculation of cross section according to a simple formula looks trivial

$$\sigma_{t\bar{t}} = \frac{N_{obs} - N_{bkg}}{\mathcal{A} \cdot \mathcal{L}}. \tag{16}$$

Formula assumes that in observed number of events ($N_{obs}$) there is only a signal ($t\bar{t}$) and (known) background ($N_{bkg}$) which can be reliably estimated. In denominator there is a product of acceptance ($\mathcal{A}$) and integrated luminosity ($\mathcal{L}$). Acceptance is calculated by using generator for signal (e.g. [16], [17]), GEANT based model for detector simulation, selection and reconstruction procedure as used for the experimental data. One needs to assume specific top mass to calculate acceptance!

#### 3.1.1 dilepton channel

The dilepton channel has an advantage of a simple topology. Signature for this channel are two energetic isolated leptons, (at least) two energetic jets and large missing transverse energy ($\not\!\!E_T$). By a proper kinematic selection it is possible to achieve reasonable signal to background ratio (S/B) without additional requirements (b-tagging or neural net selection)!

Description below follows analysis based on integrated luminosity 1.2 $\mathrm{fb}^{-1}$ collected with CDF detector [18]. Data are collected with inclusive electron or muon trigger which requires electron transverse energy $\mathrm{E_T} > 18$ GeV or muon transverse momentum $\mathrm{P_T} > 18$ GeV/$c$. From this dataset are selected offline events with corresponding isolated leptons $\mathrm{E_T} > 20$ GeV ($\mathrm{P_T}$ >20 GeV/$c$) and another lepton satisfying same $\mathrm{E_T}$ ($\mathrm{P_T}$) condition but looser isolation requirement. Events with more than 2 leptons in a final state are rejected. To suppress Standard Model background couple more conditions are applied:

- $\not\!\!E_T > 25$ GeV. If any lepton or jet is closer than $20^o$ from the $\not\!\!E_T$ direction, condition is strengthened to $\not\!\!E_T > 50$ GeV.
- High $\not\!\!E_T$ significance if ee or $\mu\mu$ invariant mass is in the mass region of Z boson peak.
- At least 2 jets with $\mathrm{E_T} > 15$ GeV (0 and 1 jet category belongs to the control sample).
- The summed transverse energy of leptons, jets and $\not\!\!E_T$ – $H_T > 200$ GeV (the so called $H_T$ cut).

- Two leptons should have opposite charge.

Acceptance for candidate events was calculated by PYTHIA Monte Carlo program [16] simulating $t\bar{t}$ events with top mass $\mathrm{M_{top}} = 175$ GeV/$c^2$ combined with CDF detailed detector simulation and reconstruction package. Acceptance was found $\mathcal{A}$ = 0.808 %.

There are applied corrections for difference between Monte Carlo and data. These corrections are based on experimental data for Z boson to 2 lepton decay. Efficiency of inclusive lepton trigger is taken into account. It is measured in data samples selected by independent set of triggers.

For above event selection there are expected two kinds of background. Background which has physically similar properties as $t\bar{t}$ signal. To this kind of background belongs diboson production (WW, WZ, ZZ) and $Z/\gamma^* \rightarrow \tau\tau$ accompanied by several jets. Another kind of background consist of physical process where some characteristic are mismeasured. To this background belongs $W\gamma$ production where $\gamma$ is mismeasured as a (fake) lepton, $Z/\gamma^* \rightarrow ee, \mu\mu$ where $\not\!\!E_T$ is mismeasured (fake $\not\!\!E_T$) and W accompanied by multiple jets where one jet is mismeasured as a (fake) lepton.

Amount of background from the first category is determined by Monte Carlo, second category is estimated from analysis of data.

Acceptance for signal is based on MC and systematic errors come from several sources - MC generator (it is estimated by comparison of result of two different generators), uncertainty in tuned parameters for initial and final state radiation (ISR/FSR), choice of structure functions (PDF) and most significant item is jet corrections. Purpose of jet corrections is to transform raw reconstructed jet kinematic characteristics to a kinematic characteristics of original quark. To estimate systematic error from this source corrections are changed by $\pm\sigma$ and shift in acceptance is a measure of systematic error. Total estimated systematic error from above sources is 4.2 %. For background there are also systematics related to fake leptons and cross section uncertainties.

Results are summarized in two tables. In Tab. II the comparison of total SM expectation in control region ( 0 and 1 jet topology) demonstrates that amount of the background is well understood. Significant suppression of background is demonstrated in the last two columns by $\mathrm{H_T}$ cut and opposite charge condition for isolated leptons.

In the next table (Tab. III) all selection cuts are applied but data are separated into different

Tab. II. Summary table of background estimates,$t\bar{t}$ predictions and events in 1.2 $\mathrm{fb}^{-1}$ of data for each jet bin. For first three columns all cuts are applied except $\mathrm{H_T}$ cut and opposite charge conditions for leptons. The conditions are subsequently applied for the last two columns. The quoted uncertainties are summed (in quadrature) statistical and systematic uncertainties.

| Events per 1200 $\mathrm{pb}^{-1}$ vs Njet bins. | | | | | |
|---|---|---|---|---|---|
| Source | 0j | 1j | $\geq 2j$ | $\mathrm{H_T}$ | $\mathrm{H_T}$, OS |
| Total background | 139.34±17.96 | 68.55±10.74 | 44.87±9.49 | 30.30±5.89 | 25.56±5.54 |
| $t\bar{t}(\sigma$ = 6.7 pb) | 0.29±0.03 | 7.49±0.58 | 59.53±4.53 | 57.41±4.37 | 55.95±4.26 |
| Total SM expectation | 139.63±17.98 | 76.04±11.10 | 104.40±13.17 | 87.71±8.85 | 81.52±8.92 |
| Data | 143 | 84 | 114 | 88 | 77 |

Tab. III. Summary table by lepton flavor content of background estimates, $t\bar{t}$ predictions and final candidate events in 1.2 $\mathrm{fb}^{-1}$ of data.The quoted uncertainties are summed (in quadrature) statistical and systematic uncertainties.

| Events per 1200 $\mathrm{pb}^{-1}$ after all cuts | | | | |
|---|---|---|---|---|
| Source | $ee$ | $\mu\mu$ | $e\mu$ | ll |
| Total background | 6.86±1.70 | 10.47±2.06 | 8.23±2.30 | 25.56±5.54 |
| $t\bar{t}$ ($\sigma$ = 6.7 pb) | 12.18±0.94 | 13.60±1.04 | 30.17±2.30 | 55.95±4.26 |
| Total SM expectation | 19.04±2.26 | 24.08±2.68 | 38.40±3.90 | 81.52±8.92 |
| Data | 16 | 26 | 35 | 77 |

dilepton flavor categories. Cross section was calculated according to slightly modified eq. (16) to take more carefully into account contribution of different flavor categories.

The result is: $\sigma_{t\bar{t}} = 6.16 \pm 1.05_{stat} \pm 0.72_{syst} \pm 0.37_{lumi}$ pb, where the first uncertainty is statistical, the second is the convolution of the acceptance and background systematics and the third comes from the 6% uncertainty in the luminosity measurement.

### 3.1.2 lepton + jets channel

Lepton + jets channel is a "gold plated" channel for the analysis of many top quark properties. This channel played a crucial role in the top quark discovery.

Advantage of this channel is a large branching ratio (leading to this topology) combined with achievable good signal to background ratio.

Main background consists of the QCD production of W + jets. Trouble with this background is a large uncertainty in the theoretical estimate of cross section by perturbative QCD technique. Different (reasonable) choice of renormalization and factorization scale makes up to factor 2 difference. Fortunately this background (and therefore also uncertainty) can be reduced by requirement of at least one b-jet signature in the event. $t\bar{t}$ signal should have two b-jets therefore signal should pass very well b-jet signature requirement, background is dominated by light quark jets and it will be significantly reduced.

We follow below CDF analysis [19] based on integrated luminosity 1.12 $\mathrm{fb}^{-1}$ of data . The data were collected with an inclusive lepton trigger that requires electron $E_T > 18$ GeV (muon $P_T > 18$ GeV/$c$). Offline selection required isolated electron $E_T > 20$ (muon $P_T > 20$ GeV/$c$), $\not\!\!E_T > 30$ GeV and at least 3 jets with $E_T >$20 GeV. Scalar sum of all transverse energy in event ($\mathrm{H_T}$ cut) should exceed 250 GeV. At least one of the jets should be identified as a b-jet.

For identification of b-jets (b-tagging) is used SecVtx algorithm [20]. This algorithm for identification of b-jets takes advantage of relatively long lifetime of hadrons with b-quark in their structure (B hadrons). Characteristic c$\tau$ for B hadrons is ≈500 $\mu\mathrm{m}$. Therefore (taking into account relativistic $\gamma$ factor for observed mean lifetime in lab. frame) B-hadron travels typically several millimeters from interaction point where it was created until it decays. In critical region around beam pipe there is placed silicon vertex detector with sufficient resolution to find decay vertex close to primary interaction. b-tagging algorithm depends on many details where method-

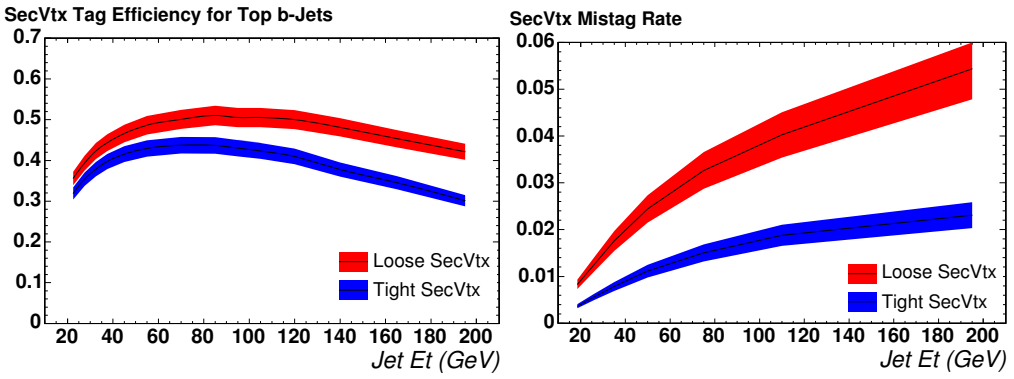


Fig. 11. Left: tagging efficiency for a "tight" and "loose" version of SecVtx algorithm as a function of $E_T$ of b-jets. Right: miss-tag probability for a "tight" and "loose"version of SecVtx algorithm as a function of $E_T$ of b-jets.

ology and detector properties are interconnected but it can be viewed as a black box with two important parameters:

- efficiency to identify b-jet if a given jet really was a b-jet and
- probability to identify as a b-jet jet which was in fact light quark (or gluon) jet. This property is also called miss-tag probability.

As one can imagine these two parameters are correlated. By tuning procedure one can achieve smaller miss-tag probability but price will be smaller tagging efficiency. If efficiency is an issue one can use looser criteria for b-tagging procedure but price will be larger probability to misidentify non b-jet as a b-jet.

There are two versions of SecVtx algorithm at CDF - tight and loose. Properties of these two versions as a function transverse energy of jets ($E_T$) is shown in Fig. 11. By a comparison of efficiency for SecVtx tagger on data and MC, a scale factor $SF = \epsilon_{DATA}/\epsilon_{MC}$ is determined. Scale factor for both cases (loose and tight) was found consistent with SF $\approx 0.95$.

The acceptance was calculated based on PYTHIA MC $t\bar{t}$ production with top mass set to 175 GeV/$c^2$. Naturally, detector simulation, reconstruction and channel selection procedure have been included in the calculation.

Background is dominated by W + jets. This background can be divided into categories of light quark jets (they pass selection criteria due to mis-tag probability) and heavy flavor jets (W + $b\bar{b}$, W+ $c\bar{c}$). There is also expected background from non W category (W signature is faked). Origin of this background is detector mismeasurement and it's amount is determined directly from the data. Last category of the background is di-Boson, single top an Z$\rightarrow \tau\tau$. Amount of this background was estimated by using theoretical cross sections. It was found to be negligible.

Systematic errors have in addition to the same components as in the Dilepton channel (see previous section) uncertainties connected with b-tagging procedure. Systematic error is dominated by jet energy scale uncertainty and b-tagging scale factor uncertainty. Total estimated systematic error was determined to be 11.6 %.

Tab. IV. Summary table of background estimates, $t\bar{t}$ predictions and events in 1.12 $\mathrm{fb}^{-1}$ of data for each jet bin.

| Events per 1120 $\mathrm{pb}^{-1}$ vs Njet bins | | | | | |
|---|---|---|---|---|---|
| Source | 1j | 2j | 3j | 4j | $\geq$ 5j |
| Total background | 854.04±225.17 | 427.52±99.85 | 53.34±13.75 | 16.69±5.95 | 4.72±1.74 |
| $t\bar{t}$ ($\sigma$ = 8.2 pb) | 9.15±0.93 | 72.22±7.35 | 133.68±13.61 | 153.53±15.63 | 53.58±5.46 |
| Data | 1067 | 585 | 185 | 169 | 62 |

Results are summarized in Tab. IV. Category of one and two jet is background dominated and demonstrates consistency of background estimate with data.
Cross section determined by eq. (16) is $\sigma_{t\bar{t}}$ = 8.2 $\pm$ 0.5(stat) $\pm$ 0.9(syst) pb.

### 3.1.3 All hadronic channel

Advantage of All hadronic channel is largest branching ratio in comparison with previous channels. This advantage is more than compensated by huge QCD background one needs to deal with. To get background under control and to achieve reasonable signal to background ratio one needs to implement all analysis artillery (kinematic selection, b-tagging). Below we follow analysis [21].

The All hadronic final state is characterized by the presence of at least 6 jets from the decay of top and anti top quarks. Special multi-jet trigger selects in real time candidates relying on calorimeter information. In the offline analysis jets are identified by grouping clusters of energy in calorimeter cells using fixed cone algorithm with a radius $r = \sqrt{(\triangle\phi)^2 + (\triangle\eta)^2} = 0.4$ [22]. Events satisfying the trigger requirements are reconstructed in terms of final state observables (tracks, vertexes, charged leptons, jets). Retained for further analysis are only events that are well contained in detector acceptance (primary vertex should lie inside luminous region $|z| < 60$ cm). Jet energies are corrected for detector response and multiple interaction. Each jet is required to have $\mathrm{E_T} \geq 15$ GeV and $\eta \leq 2$. Events with identified isolated electrons or muons are removed from the sample and also events with $\not\!\!E_T/\sqrt{\sum E_T} \geq 3\sqrt{\mathrm{GeV}}$ [24]. At this stage called pre-selection simulation shows that fraction of leptonic event is about 14% of the all accepted $t\bar{t}$ events. To avoid overlaps between jets requirement of minimal distance $\triangle r = \sqrt{(\triangle\phi)^2 + (\triangle\eta)^2} = 0.5$ between jets was applied. Background at this stage is expected to be 3 order of magnitude larger than signal! Finally topology is optimized for all hadronic $t\bar{t}$ signal by requirement of the number of selected jets $6 \leq N_{jet} \leq 8$. In the final sample expected signal is about 0.3% and fraction of leptonic $t\bar{t}$ amounts to 5% accepted $t\bar{t}$ events.

To improve signal to background ratio artificial neural network approach is implemented. Artificial Neural Network (ANN) analysis is a technique which resembles biological neural network decision making procedure. This technique has been successfully used in complex pattern recognition problems. Generally there is defined set of sensitive variables which characterizes object to be recognized, there is a procedure to train ANN to recognize certain type of objects and output of ANN gives a degree of recognition. Usually 1 means ANN for a sure recognized

Tab. V. Input variables to the neural network.

| Variable | Description |
|---|---|
| $\sum E_T$ | Scalar sum of the transverse energies of all jets |
| $\sum_3 E_T$ | As above except the two highest $E_T$ jets |
| C | Centrality |
| A | Aplanarity |
| $M_{2j}^{min}$ | Minimum dijet invariant mass |
| $M_{2j}^{max}$ | Maximum dijet invariant mass |
| $M_{3j}^{min}$ | Minimum trijet invariant mass |
| $M_{3j}^{max}$ | Maximum trijet invariant mass |
| $E_T^{*,1}$ | $E_T \sin^2\theta^*$ for the highest-$E_T$ jet |
| $E_T^{*,2}$ | $E_T \sin^2\theta^*$ for the next-to-highest-$E_T$ jet |
| $< E_T^* >$ | Geometric mean over the remaining jets |

object and 0 means that for sure given object is of different kind than signal for which ANN was trained to recognize. Lots of software packages exist for ANN analysis. Most popular in High Energy Physics are JETNET [25] and MLP [26].

For this analysis the MLP package [26] as implemented by ROOT [27] was used. Sensitive variables selected for discrimination between signal and background by ANN are listed in Tab. V. The network was trained on the same-size samples of signal and background events with $6 \leq N_{jets} \leq 8$. Signal was modeled by PYTHIA v6.2 [16] followed by a simulation of the CDF II detector. The top quark mass for training was set to 175 GeV/$c^2$. The background is obtained from multi-jet data events themselves since the signal fraction at initial stage is expected to be very small.

Different structures of ANN have been investigated. Best signal to background ratio was obtained by ANN with 2 hidden layers with 20 and 10 hidden nodes and one output node. On Fig. 12 one can see output node response distribution for $t\bar{t}$ signal and background. To optimize selection by ANN ratio of signal to standard deviation of signal + background was studied as a function of ANN output node cut. Optimal cut was found to be 0.94. Efficiency of this cut for $t\bar{t}$ signal is close to 5 % and S/B $\sim$ 1/12.

Background for $t\bar{t}$ production in all hadronic channel is dominated by QCD heavy flavor pair ($b\bar{b}$,$c\bar{c}$) and (mis-tagged) light quark jet production. Theoretically, there are large uncertainties in estimating this background. Background estimate is based on data in signal depleted region. Events with exactly 4 jets passing pre-selection procedure (without ANN) are expected to have S/B $\approx$ 1/3600 and therefore satisfy criterion for signal depleted sample. Tag rate per jet is evaluated in this control sample and is parametrized in terms of variables sensitive to both the tagging efficiency for true heavy flavored objects and the rate of mistags (false tags). Based on this parametrization one can predict number of b-tagged jets in other samples (with higher jet multiplicity). Difference between prediction and direct result of b-tagging procedure on jets in a given category will be attributed to a $t\bar{t}$ source.

After kinematic and ANN selection there are left 1020 events with 1233 tags in category of $6 \leq N_{jets} \leq 8$. Estimated background amounts to 937$\pm$30 tags. Because this estimate is based

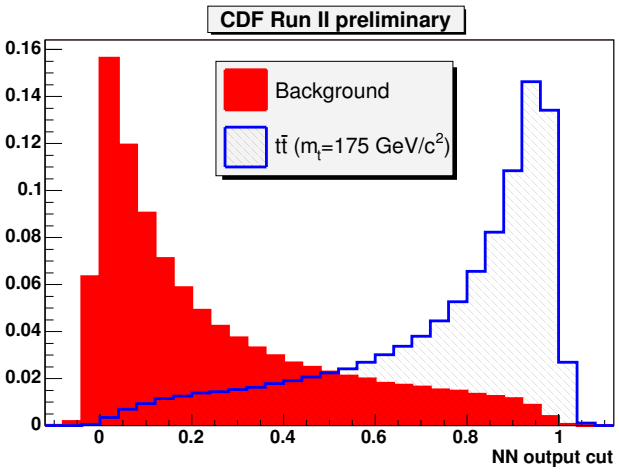


Fig. 12. Response of trained ANN to $t\bar{t}$ signal and background.

on all events passing selection before tagging contribution due to $t\bar{t}$ events should be subtracted. Average number of tags for $t\bar{t}$ events is expected $n_{tag}^{ave} = 0.95 \pm 0.07$. Excess tags are converted to a corresponding number of $t\bar{t}$ events and subtracted from the number of events before tagging and new estimate of background is obtained. After couple iterations the procedure converges. Final number of tags from background sources is reduced to 846±37 tags. Results for different jet topologies are in Tab. VI. Cross section can be extracted by slightly modified eq. (16)

$$\sigma_{t\bar{t}} = \frac{N_{obs} - N_{bkg}}{\epsilon_{kin} \cdot n_{tag}^{ave} \cdot \mathcal{L}_{int}}, \tag{17}$$

where $N_{obs}$ = 1233 and $N_{bkg}$ = 846± 37 are the number of total observed and background tags, respectively, in the signal region $6 \leq N_{jets} \leq 8$, $\epsilon_{kin}$ = 4.8±0.8% is the signal kinematic selection efficiency, $n_{tag}^{ave}$ = 0.95±0.07 is average number of tags in $t\bar{t}$ events and $\mathcal{L}_{int}$ = 1.02±0.06 $\mathrm{fb}^{-1}$ is the integrated luminosity of the data sample. The $t\bar{t}$ cross section was measured to be $\sigma_{t\bar{t}}$ = 8.3 $\pm$ 1.0(stat)$^{+2}_{-1.5}$(syst.)± 0.5(lumi.) pb for a top quark mass 175 GeV/c$^2$.

Relative systematic uncertainties affecting $t\bar{t}$ production cross section dominates jet energy scale uncertainty and uncertainty on average number of tags.

Tab. VI. Observed number of tags, expected background and signal after kinematic and ANN selection.

| Events per 1020 $\mathrm{pb}^{-1}$ vs Njet bins | | | | | |
|---|---|---|---|---|---|
| Source | 4j | 5j | 6j | 7j | 8j |
| Background | 16060±575 | 2750±92 | 536±17 | 255±8 | 146±5 |
| Corrected Background | 15961±677 | 2653±112 | 481±20 | 223±10 | 142±7 |
| $t\bar{t}$ ($\sigma$ = 8.3 pb) | 120±20 | 266±45 | 242±41 | 101±17 | 38±7 |
| Data | 16555 | 3139 | 725 | 349 | 159 |

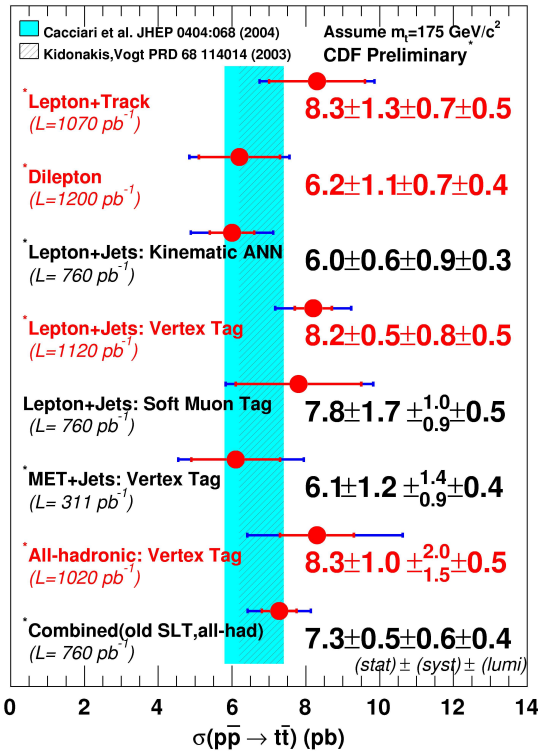


Fig. 13. Measurement of $t\bar{t}$ production cross section by CDF collaboration.

### 3.1.4 Summary

CDF collaboration cross section measurement in dilepton, lepton + jets and all hadronic channel was briefly introduced. There are more details in referenced papers. There are also other analysis produced by CDF collaboration as well as D0 collaboration [28]. CDF collaboration results are summarized in Fig. 13 and D0's results in Fig. 14. As one can see from above plots cross section measurements are consistent between each other for different channels and with theoretical NLO prediction for assumed top mass 175 GeV/$c^2$ [29]. There is also mutual consistency of results between CDF and D0 collaboration.

One may raise a question if these measurements exclude other interpretation of experimental findings than top quark as expected by Standard Model. Standard Model is considered a very successful theoretical concept but there are limitations. As a possible successor of Standard Model is so called Minimal Super-symmetric extension of Standard Model (MSSM). MSSM predicts existence of large number of new particles (to every particle in SM should exist supersymmetric partner). One possibility why so far there does not exist positive observation of any supersymmetric particle is that mass of supersymmetric particles is too large to be observed at TEVATRON. Other possibilities are that they buried in background because of low statistics (integrated luminosity), buried in $t\bar{t}$ candidate events if properties are close to properties of $t\bar{t}$

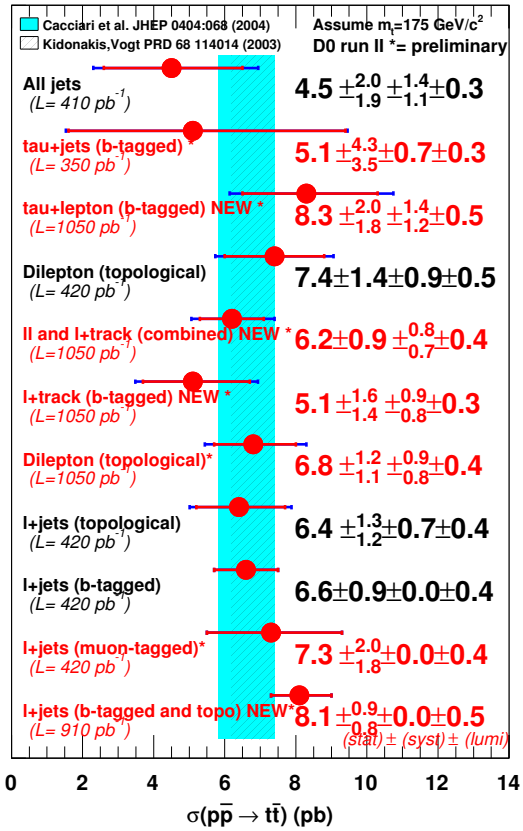


Fig. 14. Measurement of $t\bar{t}$ production cross section by D0 collaboration.

events or even interpretation of $t\bar{t}$ events can be challenged. At right conditions supersymmetric partners to top quark have properties similar to top. As was emphasized in [31] in framework of MSSM mass of scalar top $\tilde{t}_1$ from a theoretical point of view can be made arbitrary low. In this framework one can imagine pair production $\tilde{t}_1\bar{\tilde{t}}_1$ and subsequent decay of $\tilde{t} \to \chi^+ + b$ and $\chi^+ \to W^+\chi^0$. In this case final state will be the same as in case of SM $t\bar{t}$ production. But theoretically cross section for $\mathrm{p\bar{p}} \to \tilde{\mathrm{t}}_1\bar{\tilde{\mathrm{t}}}_1$ at 1.96 TeV is order of magnitude smaller than cross section for $t\bar{t}$ production for the same mass (e.g 175 GeV/$c^2$) of produced particle. Therefore measurement of $t\bar{t}$ cross section (consistent with SM expectation) indirectly rejects $\tilde{t}_1\bar{\tilde{t}}_1$ interpretation of observed events. Naturally question if in addition to $\mathrm{t\bar{t}}$ signal there is also admixture of $\tilde{t}_1\bar{\tilde{t}}_1$ events can be answered only by detailed analysis of large statistic data.

There is also theoretical concept which claims that observed top is in fact particle with same properties as top except charge [32]. This particle decays $X \to W^- + b$. Because other properties are very close (same) just measurement of the $t\bar{t}$ cross section cannot exclude this possibility. Top charge measurement or single top cross section measurement can rule out (or support) this exotic hypothesis!

### 3.2 Top quark mass measurements

A nontrivial question is even from a theoretical point of view definition of top quark mass we want to measure. The quarks have not been observed directly in nature as free particles, quark mass is not observable quantity therefore notion of quark mass relies on a theoretical construction.

There are (at least) two frequently used definitions - pole mass and $\overline{\rm MS}$ mass.

Pole mass is defined as a position of a pole in quark propagator in perturbative QCD. To measure it one needs to be able to measure four momentum of the quark. Because quarks cannot be observed directly there is intrinsic limit on precision to which even in principle quark four momentum can be reconstructed. Light quarks hadronize into jets. Hadronization is nonperturbative procedure by which colored object quark is converted into jet of colorless hadrons. There is an inherent ambiguity of this procedure. Even in principle it is not possible to reconstruct exactly kinematics characteristics of quarks from jets which are composed of hadrons. There is at least uncertainty on level of characteristic QCD scale ($\Lambda_{QCD}$). Point is that to produce colorless final object from colored object there should be picked up at least one quark unrelated to original quark to compensate it's color.

Other frequently quoted definition is $\overline{\rm MS}$ mass.
QCD belongs to re-normalizable theories that means that divergent terms which appear at higher orders of perturbative expansion can be absorbed in such a way that physical (renormalized) quantities remain finite. There are several renormalization schemes which should be equivalent in limit of infinite expansion but in terms of finite perturbation order there can be advantage of using specific scheme because of faster convergence. One of them is $\overline{\rm MS}$ scheme. Relationship between pole (M) and $\overline{\rm MS}$ mass ($\bar{m}$) at a given energy scale $\bar{m}$ is expressed by:

$$M = \bar{m}(\bar{m})[1 + \frac{4}{3\pi}\bar{\alpha}_s(\bar{m}) + ...+] + O(\Lambda_{QCD})$$

where $\bar{\alpha}_s(\bar{m})$ is the strong interaction coupling constant in $\overline{\rm MS}$ scheme at energy scale $\bar{m}$ and $O(\Lambda_{QCD})$ reflects inherent ambiguity of a pole mass on the level of $\Lambda_{QCD}$. In paper [34] is claimed that $\overline{\rm MS}$ mass is free of above ambiguity therefore this quantity can be more precisely determined!

All methods of the top quark mass determination used in TEVATRON experiments determine top quark pole mass. They generally rely on the three assumptions:

- signal is SM $t\bar{t}$ and it's amount was independently determined
- background is known (QCD, WW, Drell - Yan background) and it's amount was independently determined
- there is nothing else in selected $t\bar{t}$ candidate samples except previous two items

Many methods have been developed and used for top quark determination in TEVATRON experiments. They can be divided in two categories:

- methods which rely on use of specific variable sensitive to top mass
- methods which rely on solution to kinematic equations for reconstruction of top mass

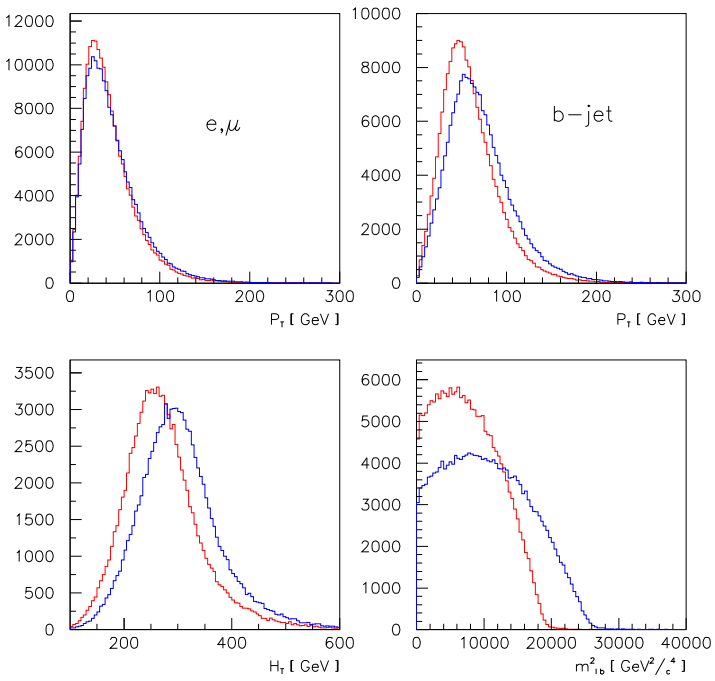


Fig. 15. Distribution of several variables sensitive to top mass. $P_T$ of e,$\mu$ from top decay chain (W), $P_T$ of b-jets, $H_T$ and quadrature of effective mass of lepton and b-jet $m^2_{lb}$. In red color distributions represent top mass 160 GeV/$c^2$, in blue top mass 180 GeV/$c^2$.

### Methods based on single sensitive variables

As a consequence of a large mass of top quark and subsequent cascade decay one can find several variables sensitive to top quark mass. Most popular ones are plotted in Fig. 15. Distributions in this figure have been produced by MC generator PYTHIA [16]. Reaction $p\bar{p} \rightarrow t\bar{t} + X$ at 1.96 TeV was simulated with subsequent decay $t \rightarrow Wb$. In this specific case W was forced to decay to electron or muon and corresponding neutrino. In simulation top quark mass was set to 160 (distributions in red color) or 180 GeV/$c^2$ (distributions in blue color). Range 160 - 180 GeV/$c^2$ represents a very conservative range considering our present understanding of the mass of top quark. One can see from Fig. 15 that $P_t$ of leptons is less sensitive to the top mass than the other variables displayed. But experimentally, isolated leptons from W decay are very well measured. Lower resolution can be compensated by a larger statistic and there can be advantage of lower systematic error by using this variable. But according to the first results this is not the case [35].

$P_T$ distribution of b-jets shows much better sensitivity. But this distribution represents ideal case and great deal of sensitivity is lost when detector resolution is taken into account. Even better sensitivity is seen for $H_T$ (already several times this variable has been mentioned in this

paper) which is defined here as total transverse energy in $t\bar{t}$ production

$$H_T = E_T^{b_1} + E_T^{b_2} + E_T^{l_1} + E_T^{l_2} + E_T^{\nu_1+\nu_2}. \tag{18}$$

The most sensitive variable is effective mass of lepton and b-jet squared ($m_{lb}^2$). Distribution of this variable in limit where we neglect lepton and b-jet masses can be expressed analytically

$$\frac{dN}{dm_{lb}^2} = \frac{6(M_t^2 - M_w^2 - m_{lb}^2)(M_w^2 + m_{lb}^2)}{M_t^6 - 3M_t^2 M_w^4 + 2M_w^6}. \tag{19}$$

This distribution is easily derived based on cascade decay kinematics and SM prediction of $\cos(\theta_l)$ distribution in W rest frame.

From this distribution one can derive relationship between top mass and average effective mass squared of lepton and b-jet ($< m_{lb}^2 >$)

$$M_t = \sqrt{< m_{lb>}^2 + \sqrt{< m_{lb}^2 >^2 + 4 \ < m_{lb}^2 > \ M_w^2 + M_w^4}}. \tag{20}$$

Unfortunately all these relationships work for a "true" effective mass squared of lepton and b-jet where both particles come from decay of the same top quark. In reality in $t\bar{t}$ production in the simplest case there are two leptons and two b-jets in the final state and there is a twofold ambiguity on how to combine them. There are several options on how to pick up correct pairs with reasonable probability. In more detail this problem will be discussed in top charge section of this article. Top mass determination by using $m_{lb}^2$ variable has at least in principle a potential for a method which does not rely on templates.

All above variables have been used for top mass determination in the past. Results and details can be found in [36], [37]. Advantage of methods based on above variables is relative simplicity, disadvantage is poorer resolution in comparison with more sophisticated methods which will be discussed later.

There was recently proposed a very interesting new method [38] to determine top quark mass by a measurement of distribution of transverse distance between vertex from B hadron decay and primary vertex. This method exploits the fact that at TEVATRON t and $\bar{\text{t}}$ are produced almost at rest. In this case boost of b - quark in top decay $\gamma_b \approx 0.4 M_t/m_b$ is proportional to the top mass and therefore also lifetime of B-hadrons and distance traveled by them before they decay. Interesting feature of this method is that for a measurement of top mass is sufficient precise measurement of secondary vertexes by silicon vertex detector and there is no need for a calorimetry measurement (which introduces largest systematic error into measurement by an uncertainty in the jet energy scale). Sensitivity of this method can be judged from Fig. 16. Top mass determined by this method has been published in [39]

All the above methods are based on kinematics of top quark decay. Distributions of sensitive variables are compared with templates produced by MC generator combined with detector simulation and reconstruction package.

There is also a method of top mass determination based on dynamics of $t\bar{t}$ production. If Standard Model is correct one can translate cross section measurement to top mass measurement. There is an exponential dependence of $t\bar{t}$ cross section on top mass (every 20 GeV/$c^2$ increase of mass of top means smaller cross section approximately by factor 2). Just by counting $t\bar{t}$ candidates we can measure top quark mass! More details in combination with kinematic reconstruction will be given later.

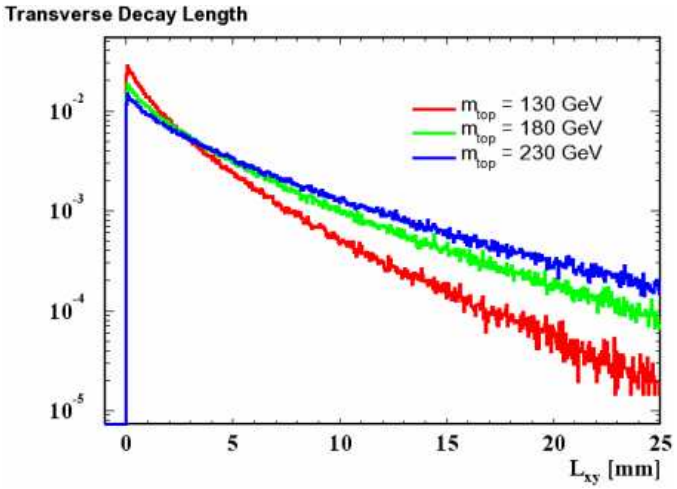


Fig. 16. Distribution of transverse decay length for top mass 130, 180, 230 GeV/$c^2$.

**Methods based on kinematic reconstruction**

Classical way to reconstruct mass of unstable particle is through measurements of kinematic characteristics of all decay products and then to calculate effective mass which will be equal to mass of original unstable particle. In $t \to Wb$ decay there is at least one quark among decay products which cannot be directly measured. There are variety of methods developed for this category of top mass reconstruction. We have chosen 3 methods which will be described in more details. Selected methods have been developed primarily for top mass reconstruction in a specific channel.

### 3.2.1 Dilepton channel

Dilepton channel has one disadvantage in comparison with lept.+ jets or all hadronic channel. There is not enough kinematic constraints to reconstruct even in principle top mass on event by event basis. As one can easily check there are 22 independent variables constraint by 21 kinematic equations! Therefore kinematic reconstruction looks impossible. There is a way around.

Assuming reaction $p\bar{p} \to t\bar{t} + X \to W^+ b W^- \bar{b} + X \to l^+ \nu b l^- \bar{\nu} \bar{b} + X$ following constraints can be used for a kinematics reconstruction

$$\begin{aligned} M_t &= M_{\bar{t}}\,, \\ M_W &= 80.4\,, \\ \vec{P}_b + \vec{P}_{W^+} &= \vec{P}_t\,, \\ \vec{P}_{\bar{b}} + \vec{P}_{W^-} &= \vec{P}_{\bar{t}}\,, \\ \vec{P}_{l^+} + \vec{P}_{\nu} &= \vec{P}_{W^+}\,, \end{aligned}$$

$$\begin{aligned} \vec{P}_{l^-} + \vec{P}_{\bar{\nu}} &= \vec{P}_{W^-}\,, \\ P_{\nu_{1x}} + P_{\nu_{2x}} &= \not{E}_{T\,x}\,, \\ P_{\nu_{1y}} + P_{\nu_{2y}} &= \not{E}_{T\,y}\,, \\ P_{tz} + P_{\bar{t}z} &= P_{t\bar{t}z}\,. \end{aligned}$$

Set of equations represents system with equal number of equations and independent variables. Therefore this set of equations can be solved and as a result top mass will be determined. One can measure kinematic characteristics of leptons, b-jets, x and y components of $\not{E}_T$. But one is not able to measure $z$ component of $\not{E}_T$. Therefore one is not able from experiment to supply right hand side of last equation. This equation is added there to make a system solvable, but question how to get needed information is for a moment overlooked.

Another problem one needs to address is problem of measurement errors. Measured quantities are subjects to experimental errors. To take into account measurement errors it is adopted procedure when all measured quantities are smeared around measured values by amount of expected error. In this approach also last equation in a set can be inserted naturally. It is set $P_{t\bar{t}z} = 0$ with associated error corresponding to width of theoretical $P_{t\bar{t}z}$ distribution (to a very good accuracy Gaussian). Choice of $P_{t\bar{t}z}$ as a "theoretical" input is justified by very weak dependence of this distribution on top mass (in 0 order approximation it depends just on structure functions of quarks and gluons in proton (anti-proton)). Idea of this method was published in [40]. Application to data in [41].

Above set of equations can be reduced to a 4-th order polynomial equation. That means that there can be up to 4 real solutions. In the most probable case there are two solutions. There is also twofold ambiguity of pairing leptons and b-jets corresponding to top decay. Therefore there are up to 8 solutions. One can deal with multiple solutions by assigning appropriate weights. An other approach was taken in [40]. Set conditions were applied and finally just one solution was selected. Still because of a smearing procedure for each event there will be a distribution of reconstructed (raw) top masses. For each event a representative top mass is selected by picking the most probable value from the distribution. There are produced MC templates for range of top mass parameters same way as was described distribution of most probable raw top masses. Distribution of reconstructed (raw) top masses from data is compared with templates and by likelihood fit is determined most probable value of top mass parameter from MC which corresponds to data.

Most recent result by using this method was done for integrated luminosity 1.2 $\mathrm{fb}^{-1}$ [42]. Event selection is the same as in case of cross section analysis in dilepton channel (see section 3.1.1). Selected events have been divided into 2 sub-samples – events with at least one jet b-tagged and events where none of the jets have been b-tagged. b-tagged sample is practically background free. Figure 17 shows distributions of raw top mass templates based on PYTHIA MC [16] for original top mass parameter set to 150, 175 and 200 GeV/$c^2$. There are also superimposed curves from parametrization fit. These distributions represent b-tagged sample but for non b-tagged sample the distributions look very similar.

Figure 18 shows the background distribution of raw top mass when the same procedure has been applied. When amount of signal and background is known (e.g. from cross section analysis) and shape of raw top mass templates is parametrized (as well as background) top mass will

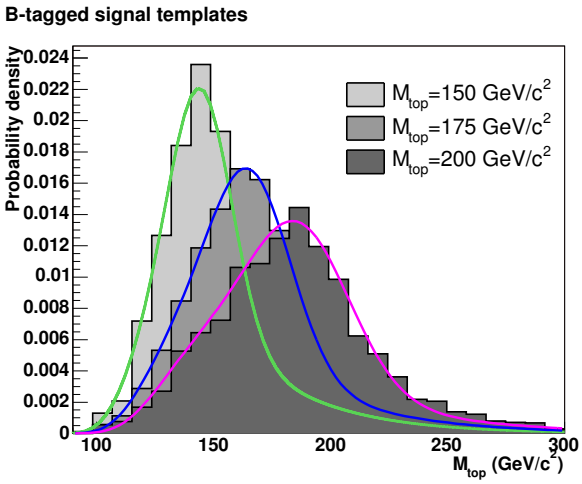


Fig. 17. Distribution of raw top mass for templates for b-tagged templates for top mass 150, 175 and 200 GeV/$c^2$.

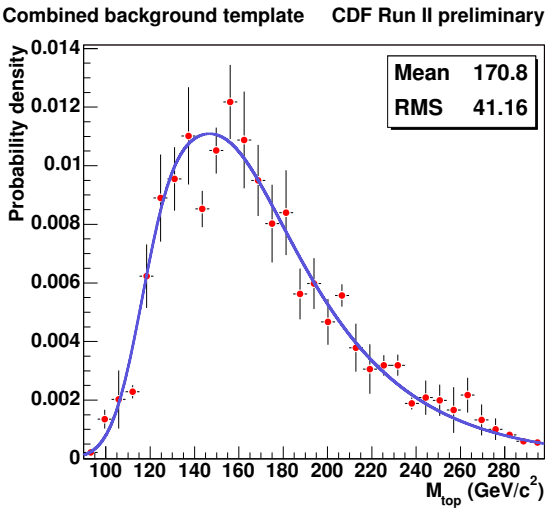


Fig. 18. Distribution of raw top mass for background treated as $t\bar{t}$ signal.

be determined from data by likelihood fit. Definition of likelihood function is given below:

$$\mathcal{L} \equiv \mathcal{L}_{b-tagged} \times \mathcal{L}_{non-tagged}\,, \tag{21}$$

$$\mathcal{L}_{sub-sample} \equiv \mathcal{L}_{shape} \times \mathcal{L}_{nev} \times \mathcal{L}_{bg}\,, \tag{22}$$

$$\mathcal{L}_{shape} \equiv \prod_{i=1}^{n} \frac{n_s \times f_s(m_{t_i}^{rec}, m_t^{orig}) + n_b \times f_b({m_{t_i}}^{rec})}{n_s + n_b}\,, \tag{23}$$

$$\mathcal{L}_{nev} \equiv \frac{e^{-(n_s+n_b)}(n_s+n_b)^N}{N!}\,, \tag{24}$$

$$-ln(\mathcal{L}_{bg}) \equiv \frac{(n_b - n_b^{exp})^2}{2\sigma_{n_b}^2}\,, \tag{25}$$

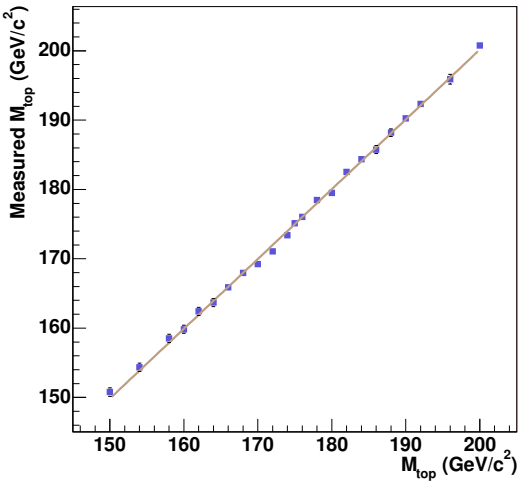


Fig. 19. Test of the top mass reconstruction procedure by pseudo-experiments.

where top mass $m_t^{orig}$, number of background events $n_b$ and number of signal events $n_s$ are fit parameters. The number of background events is constrained by Gaussian term $\mathcal{L}_{bg}$ and total number of events by Poisson term $\mathcal{L}_{new}$, $f_s(m_{t_i}^{rec}, m_t^{orig})$ is a parametrization of signal as function of $m_t^{orig}$ and $f_b({m_{t_i}}^{rec})$ parametrization of background. Fit parameters are determined by maximum likelihood method.

Procedure was tested by pseudo-experiments where randomly picked up events from a pool of MC signal events for a given mass are combined with randomly picked up events from a pool of background events and form a set for which the top mass is determined by a given procedure. As one can see from Fig. 19 at least in the range of top masses between 160 - 200 GeV/$c^2$ original top mass and reconstructed one from pseudo-experiments (average) correspond well to each other.

Finally method is applied to data. In Fig. 20 distribution of raw top mass and fit is displayed. Top mass was determined to be $\mathrm{M_{top}} = 169.7^{+5.2}_{-4.7}$(stat) GeV/$c^2$.

The total systematic error is 3.1 GeV/$c^2$. The largest single source of systematic error is the jet energy scale which has a value of 2.9 GeV/$c^2$.

Final result is $\mathrm{M_{top}} = 169.7^{+5.2}_{-4.7}(\mathrm{stat}) \pm 3.1(\mathrm{syst})$.

**Combination with cross section mass dependence**

By a small modification of the likelihood function eq. (22) the top mass dependence of cross section can also be included in a fit and the top mass resolution improved. The expected number of signal events can be expressed as:

$$n_s(M_{top}) \quad = \quad \sigma_{t\bar{t}}(M_{top}) \cdot a(M_{top}) \cdot \mathcal{L}^{int} \cdot p_{mass}^{rec}\,, \tag{26}$$

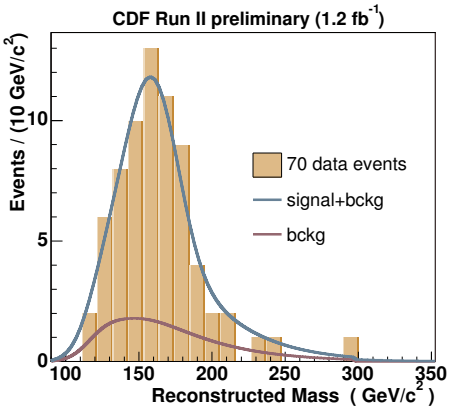


Fig. 20. Top mass fit to data.

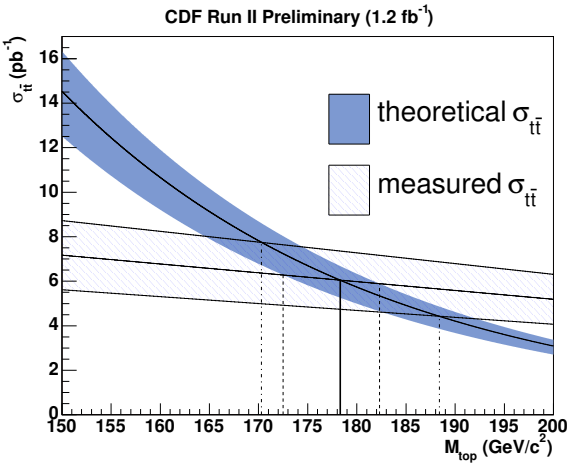


Fig. 21. Extraction of top mass from top mass dependence of theoretical cross section and top mass dependence of measured cross section.

where $\sigma_{t\bar{t}}(M_{top})$ is theoretical dependence of $t\bar{t}$ cross section as a function of top quark mass, $a(M_{top})$ is the acceptance, $\mathcal{L}^{int}$ is an integrated luminosity and $p^{rec}_{mass}$ is the probability to reconstruct raw top mass. Fitted parameters after this modification of likelihood function will be $M_{top}$ and $n_b$. This way about 20 % top mass resolution improvement can be achieved.

Reconstruction of top quark mass by kinematic reconstruction (and templates) was done in previous section. One can also estimate top mass just by combination of theoretical prediction of top mass cross section dependence and cross section measurement [43] and compare these two measurements if they are compatible. In Fig. 21 extraction of top mass from top mass dependent

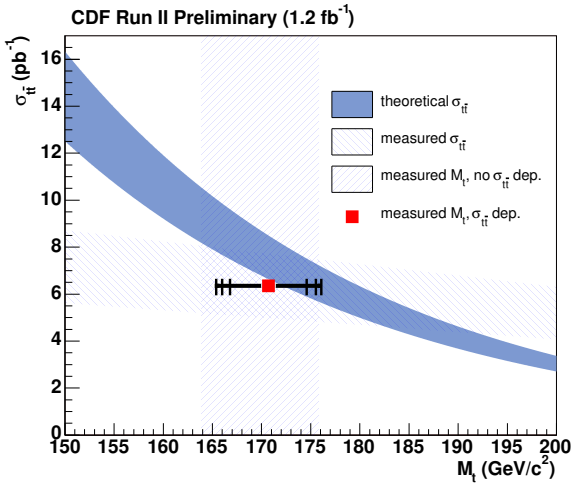


Fig. 22. Top mass measurements by combination of kinematics and cross section measurement. The blue solid bands shows theoretical $t\bar{t}$ cross section within its uncertainties. Hatched areas mark the cross section measurement as a function of top mass and independent top mass measurement based on kinematics and templates (see Fig. 20). Red square with error bars mark the measured top mass by combined cross section and kinematics method (see text).

theoretical cross section and from top mass dependent (acceptance) measured cross section is demonstrated. Result is $\mathrm{M_{top}} = 178.3^{+10.1}_{-8.0}(\mathrm{stat.})^{+4.0}_{-6.0}(\mathrm{syst.})\mathrm{GeV/c^2}$. It is important to note that two very different methods of determining the top mass give compatible result!

Results by using combination of top mass cross section dependence and kinematics based on modification of likelihood function eq. (22) by eq. (26) have been published in [44]. Reconstructed top mass was found (see Fig. 22) $\mathrm{M_{top}} = 170.7^{+4.2}_{-3.9}(\mathrm{stat}) \pm 2.6(\mathrm{syst}) \pm 2.4(\mathrm{theor})$. Improvement in statistical error was expected. Improvement in systematic error is because cross section constrained kinematic reconstruction of top mass is less sensitive to uncertainty in jet energy scale. It is still dominant source of systematic error but its estimated value is 1.8 GeV/$c^2$ (to be compared with 2.9 GeV/$c^2$ in case of traditional kinematics approach). Second most significant contribution to systematic error is uncertainty on estimate of integrated luminosity. Systematic uncertainty on top mass from this source was found to be 1.1 GeV/$c^2$.

Delicate question is treatment of uncertainty on calculated theoretical cross section. A conservative approach was adopted (after discussion with authors [29] ) and systematic error from this source is written down separately.

### 3.2.2 Lepton + jets channel

As was already mentioned lepton + jets channel is a gold plated channel for most top properties analysis. In comparison with dilepton channel advantage for top mass analysis is not only higher statistics but also number of kinematic constrains is larger than number of independent variables.

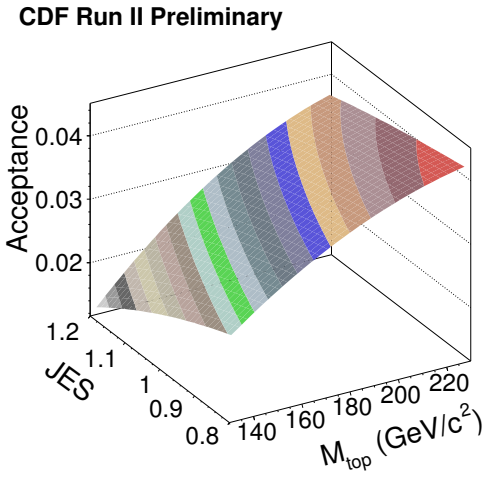


Fig. 23. Acceptance dependence as a function of JES and top mass.

Therefore system is over-constrained. Specifically for 21 kinematic equations (constraints) there are 19 independent variables (if we use same conditions as in case of dilepton channel). Disadvantage is increased level of ambiguity for association of jets with correct decay chain item. In lepton + jets channel for top mass reconstruction there are selected events with isolated lepton and 4 jets (for cross section measurements at least 3 jets are required). From these 4 jets there are 12 different combinations for assignment of these jets to specific items of top decay chain ( b-jet combined with W leptonically or hadronically decaying, jets associated with hadronic decay of W). In case when one of the b-jets is b-tagged and its assignment will be strictly assigned to either hadronic or leptonic W (not to W decay) number of ambiguities is reduced to 6. In case when two b-jets are b-tagged, not tagged jets are assigned to W hadronic decay and there is still twofold ambiguity of assignment of b-tagged jets to leptonic or hadronic decaying W.

We follow CDF analysis published in [45] where more details can be found. In this analysis two major improvements are implemented to improve resolution. For top mass reconstruction are used not only kinematic constraints but also top mass dependent dynamical information based on LO matrix element for $t\bar{t}$ production and for W + jets background. Second improvement concentrates on improving most significant systematic uncertainty - jet energy scale. W bosons which decays hadronically into two jets is used for "in situ" calibration of jet energy scale. Fitted parameters in this case will be $\mathrm{M_{top}}$ and jet energy scale.

Selection requires one isolated lepton with $E_T > 20$ GeV (e), $P_T > 20$ GeV/c ($\mu$), exactly 4 jets with $E_T > 15$ GeV and pseudo-rapidity $|\eta| < 2.0$, at least one of the jets should be b-tagged, $\not\!\!E_T > 20$ GeV and for $\not\!\!E_T < 30$ GeV azimuthal angle between leading jet and $\not\!\!E_T$ should be inside $0.5 < \triangle\phi < 2.5$. The last condition reduces non W background while retaining most of the signal. Figure 23 shows dependence of acceptance as a function of top mass and jet energy scale (JES).

In Tab. VII expected contribution to the signal and background for 955 $\mathrm{pb}^{-1}$ sample is com-

Tab. VII. Signal, background and data passing selection criteria (integrated luminosity 955 $\mathrm{pb}^{-1}$).

| Source | Expected number of events |
|---|---|
| W + jets | $14.5 \pm 5.1$ |
| non-W | $5.2 \pm 2.6$ |
| EWK | $2.2 \pm 0.5$ |
| Total | $22 \pm 8.2$ |
| $t\bar{t}$( $\sigma = 8.0\mathrm{pb}, \mathrm{M_{top}} = 170\mathrm{GeV/c^2}$) | $145.1 \pm 16.5$ |

pared with data. Core of the method is definition of likelihood function. Likelihood function was defined:

$$\mathcal{L}(M_{top}, JES, C_s; \vec{x}) \propto \prod_{i=1}^{N} [C_s P_{t\bar{t}}(\vec{x}; M_{top}, JES) + (1 - C_s) P_{W+jets}(\vec{x}; JES)]. \quad (27)$$

Probability density for $t\bar{t}$ signal and dominant background (W+jets) is based on calculation of elementary processes cross section on parton level $\frac{d\sigma(y)}{dy}$ convoluted over parton distribution functions PDF's and detector resolution for observed variables x. It is claimed that dominant background adequately represents also non W+jets backgrounds

$$P(\vec{x}) = \frac{1}{\sigma} \sum_{permjets} \int \frac{d\sigma(\vec{y})}{dy} f(\tilde{q_1}) f(\tilde{q_2}) W(\vec{x}, \vec{y}) d\tilde{q_1} d\tilde{q_2} dy. \quad (28)$$

$W(\vec{x}, \vec{y})$ describes detector resolution effects. It represents normalized probability of observing jet with $E^{jet}$ when a parton with $E^{parton}$ was produced. It is assumed that there is no correlation between different partons/jets. $W(\vec{x}, \vec{y})$ was determined by parameterizing the jet response in fully simulated $t\bar{t}$ created by MC [16] including detector simulation and resolution. PDFs $f(\tilde{q_i})$ take into account the flavors of colliding quark and anti-quark and are given by CTEQ5L [48]. The final state described by $\frac{d\sigma(y)}{dy}$ contains 6 particles which introduces 20 integration variables. This number is reduced to 5 by imposing energy momentum conservation and also Dirac delta functions inside $W(\vec{x}, \vec{y})$.

Sum over all jet permutations means in case of one b-tagged jet 6 permutations of different jet assignments to proper items in top decay chain and in case of two b-tags (for two different jets) 2 permutations.

Jet energy scale is defined as ratio of observed jet energy to true jet energy $JES = E^{obs}_{jet}/E_{jet}$ and probability density $P(\vec{x})$ is evaluated as a function of assumed jet energy scale. It is also assumed that same jet energy scale factor is also valid not only for light quark jets but also for b-jets. Deviation from this assumption is treated as a systematic error.

$C_s$ represents fraction of signal. One can use eq. (27) to fit $C_s$ as a function of input signal fraction (S/(S+B)). From result in Fig. 24 for top mass 172.5 and JES=1 one can see that even for case of 100% signal fraction from fit is close to 0.8. This apparent discrepancy is explained by fraction of jets in signal which cannot be matched to partons. In this case given procedure treats

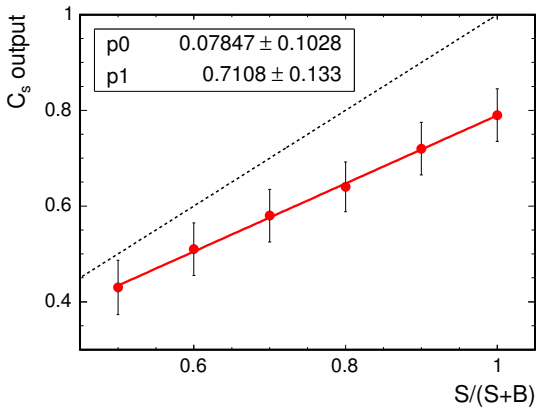


Fig. 24. Dependence of fitted output signal fraction $C_s$ as a function of input signal fraction S/(S+B) and a comparison with an ideal case.

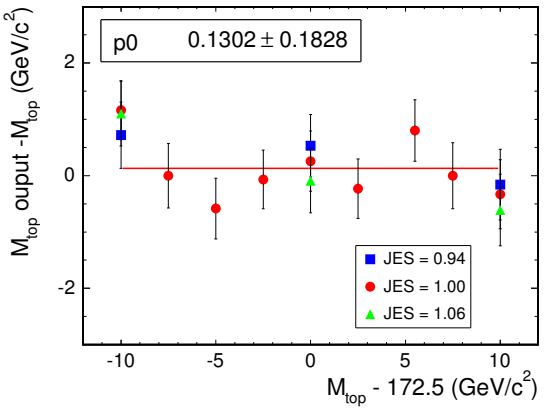


Fig. 25. Linearity check of reconstructed top mass as a function of input top mass for 83% of signal and 17% of background. Input JES was fixed at 0.94, 1.0 and 1.06 values.

them as background. On subsample of signal when all jets are matched to partons fitted signal fraction is 1. Linearity check of reconstructed (output) top mass as a function of input top mass for fixed input jet energy scale from 0.94 to 1.06 is presented in Fig. 25 for 83% signal and 17% background. Within statistical errors reconstructed top mass in a given range is unbiased. When this procedure is applied to data the result is $\mathrm{M_{top}} = 170.8 \pm 2.2(\mathrm{stat.}) \pm 1.4(\mathrm{syst.})$ GeV/$c^2$. Here statistical uncertainty includes uncertainty 1.5 GeV/$c^2$ due to jet energy scale. Systematic errors are dominated by uncertainty from initial and final state radiation which was estimated to be 1.1 GeV/$c^2$.

### 3.2.3 All hadronic channel

From the point of view of ratio of number of kinematic constraints (19) to number of independent variables (16) all hadronic channel looks suited best for top mass reconstruction. But large background and also large level of ambiguity of association of the jets with correct decay chain items give rise to the question: Can the top quark mass be reconstructed in this channel? For 6 jets in this channel there is 90-fold ambiguity for assignment of these jets to proper items in top decay chain, in case when one jet is b-tagged 30-fold ambiguity remains and with 2 b-tagged jets still 6-fold ambiguity persists.

We follow a method [49] first used by CDF for a data set correspoding to an integrated luminosity of 310 pb$^{-1}$. The method is based on event by event likelihood and uses all 90 possible jet permutations. Using likelihood fit two parameters are determined: top mass $\mathrm{M_{top}}$ and signal fraction (called also sample purity) $\mathcal{P}$.

Event selection is based on multi-jet trigger which relies solely on calorimetry. It requires at least 4 clusters with transverse energy $E_T > 15$ GeV and scalar sum of transverse jet energies exceeds 125 GeV. Offline there are imposed kinematic requirements based on scalar sum of transverse jet energies and event shape observables. Full description is given in [56]. For the final top quark mass measurement are considered only events with exactly six jets, each with $E_T > 15GeV$ and pseudo-rapidity $|\eta| \leq 2$. Jets are identified as clusters of energy deposits in the calorimeter segments (towers) which fall within a cone radius $r = \sqrt{\triangle\phi^2 + \triangle\eta^2} = 0.4$. The jet energies are calibrated based on instrumental calibration analysis of the data control sample [57]. There are applied additional jet-pattern corrections, specific to $t\bar{t}$ which are parametrized independently for b-quark jets and light quark jets. In order to reduce background it is imposed requirement that at least one jet should be b-tagged. But this information is not used to reduce ambiguity of the jet assignments. Instead weight factor for each jet is defined using CDF jet probability algorithm [63] which takes into account probability that jet originates from the b-quark.

By applying energy momentum conservation, momenta of t and $\bar{\mathrm{t}}$ are derived, the two top quark masses $m_i^{1,2}$ and their estimated uncertainties $\sigma_i^{1,2}$ are determined. In kinematic fit constraint on W mass 80.4 GeV/$c^2$ and natural width are implemented. All 90 possible permutations of jets assignments are applied, equality of $m_i^{1,2}$ is not imposed. Weight factor is defined:

$$w_i = exp(-\frac{1}{2}\chi^2) \prod_{j=1}^{2} p_j^b \prod_{j=3}^{6} p_j^q, \tag{29}$$

where exponential term is a measure of compatibility of a given jet combination with $t\bar{t}$ kinematics, second factor determines probability that b-jet assignment is correct and the last term probability that 4 jets assigned to W decay into light quarks are consistent with this assignment.

Likelihood consists of two terms. Signal likelihood is a convolution of two Breit-Wigner distributions $F_{BW}(m'_j|M_{top})$ with two Gaussians $G(m'_j|m_i^j, \sigma_i^j)$ which describes the experimental resolution. $\sigma_i^{1,2}$ is uncertainty in reconstructed top quark masses $m_i^{1,2}$

$$\mathcal{L}_i^{sig}(M_{top}) = \prod_{j=1}^{2} \int G(m'_j|m_i^j, \sigma_i^j) F_{BW}(m'_j|M_{top}) dm'_j. \tag{30}$$

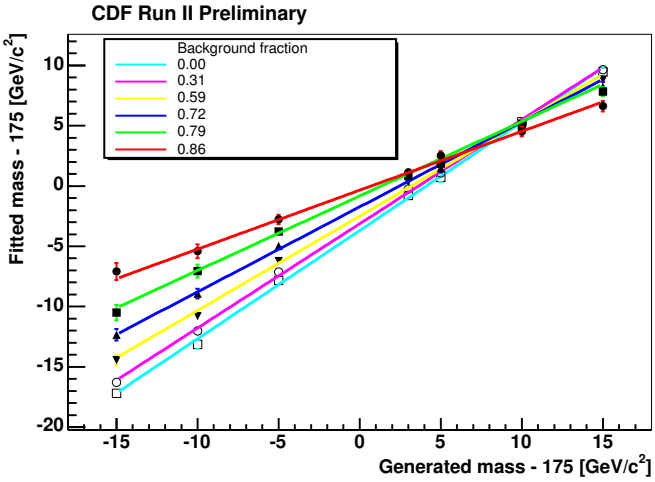


Fig. 26. Calibration curves for dependence of fitted top mass as a function of input top mass for different background fractions.

The $M_{top}$ independent likelihood term $\mathcal{L}_i^{bg}$ corresponds to the two-dimensional posteriori probability density function of $m_i^{1,2}$ obtained from ALPGEN [47] MC multi-jet QCD background. All MC events pass through detector simulation, reconstruction and event selection procedure same as data.

Likelihood for a given event j and total likelihood are defined:

$$\mathcal{L}^j(M_{top},\mathcal{P}) = \sum_{i=1}^{90} w_i[\mathcal{P}\mathcal{L}_i^{sig}(M_{top}) + (1-\mathcal{P})\mathcal{L}_i^{bg}]\,, \tag{31}$$

$$\mathcal{L}_{tot}(M_{top},\mathcal{P}) = \prod_{j=1}^{N_{ev}} \mathcal{L}^j(M_{top},\mathcal{P})\,. \tag{32}$$

Top mass extracted from likelihood fit will be biased due to presence of wrong jet combinations, background events, jets assigned from initial and final state radiation. In Fig. 26 a comparison of fitted mass for pseudo-experiment samples as a function of input mass and background fraction is presented. Calibration curves are used for a final determination of top mass. $Pull = \frac{M_{top}-m_{gen}}{\sigma_{res}}$ is very sensitive variable to correct top mass reconstruction. If procedure is correct, mean of pull distribution should be equal to 0 (if reconstructed top mass $M_{top}$ is unbiased) and have width 1 (if $\sigma_{res}$ correctly represents uncertainty on reconstructed top mass). These properties should be constant as a function of input top mass ($m_{gen}$). As can be seen from Fig. 27 constancy condition is honored. But width is wider by about 17% and therefore for final determination of uncertainty on top mass estimated uncertainty is appropriately inflated. When 290 events of data have been analyzed by above procedure purity was found to be $\mathcal{P} = 0.21 \pm 0.07$ and top mass $M_{top} = 177.1 \pm 4.9(stat)$ for this sample. From systematic errors the most significant is jet

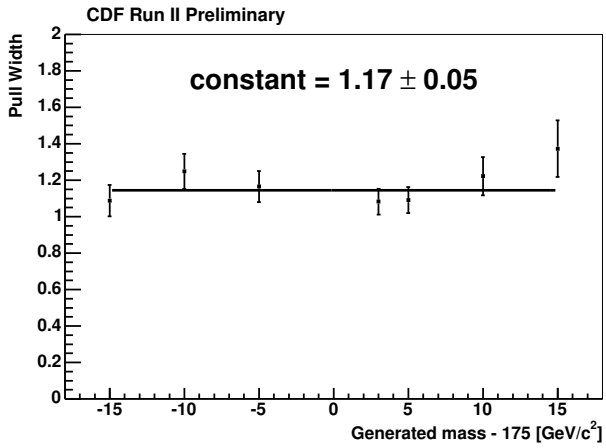


Fig. 27. Pull width dependence as a function of input top mass.

energy scale uncertainty. It amounts to 4.4 GeV/$c^2$. The total systematic error was estimated to be 4.7 GeV/$c^2$.

### 3.2.4 Summary

All methods for top mass reconstruction rely on an assumption of known background and $t\bar{t}$ signal. These assumptions are tested in details and there was not found any discrepancy which could undermine this assumption.
Statistical error $\sigma_{M_{top}}$ can be roughly estimated as

$$\sigma_{M_{top}} \approx \frac{\sigma_{res}}{\sqrt{N_{sig}}}\,, \tag{33}$$

where $\sigma_{res}$ is intrinsic top mass resolution of the method and $N_{sig}$ is number of signal events. Rough estimate $\sigma_{res} \approx 30$ GeV/$c^2$ gives a quick guess what top mass resolution can be achieved for a given number of signal events.

Presented examples of methods for top mass reconstruction have features which are specific for a given channel but other can be (with a slight modification) applied to other channels too. A combination of cross section and kinematics can be used in lept. + jets channel and all hadronic channel too. In situ calibration of jet energy scale can be used also in All hadronic channel. This is a very important way how to reduce systematic error of uncertainty on jet energy scale. And this uncertainty is reduced with increasing statistics!

Already at present statistical and systematic errors are very close. Statistical errors are reduced with increasing statistics however same does not work for systematic errors. One of the most significant systematic errors after jet energy scale uncertainty is uncertainty from initial and final state radiation. Systematic errors will present main challenge in future precise measurements of top mass.

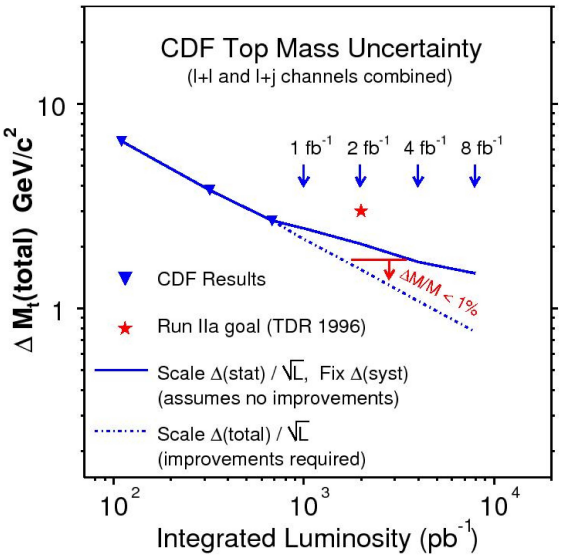


Fig. 28. Expected total top mass error (systematic and statistical added in quadrature) dependence as a function of accumulated statistics (for more detail see text).

In Fig. 28 one can see prediction for dependence of the total error (systematic and statistical errors added in quadrature) as a function of the statistics. Statistical error is expected to be inversely proportional to the square root of statistics. If systematic error will be fixed, expected behavior will follow upper curve. If systematic error will go down same way as statistical one dependence will follow lower curve. In situ energy calibration is an example how systematic error can be improved with increased statistics. But then there will dominate other components of systematic errors. Most likely outcome is dependence between two curves. It should be also mentioned that goal in the CDF TDR proposal for top mass measurement was total precision of 3 GeV/$c^2$ which was already achieved.

Both experiments CDF and D0 used variety of methods to reconstruct top quark mass in the three discussed channels. Summary of CDF results is in Fig. 29. For D0 summary results are in Fig. 30. From these results one can draw a conclusion that within experimental uncertainties measurement of top quark mass in different channels executed by different methods are consistent with the statement that mass of the same physical object was measured - Standard Model top quark!

In case when we have a confidence that in different decay channels same physical object was measured one can combine different measurements (even from both experiments CDF and D0) to improve precision of top quark mass measurement. Proper procedure which takes into account correlations between different measurements and contributing items to measurements was developed [50]. The most recent (spring 2008) combined result from CDF and D0 experiment is $\mathrm{M_t} = 172.6 \pm 0.8(\mathrm{stat}) \pm 1.1(\mathrm{syst})$.

Most attention to a top mass measurement is attracted due to a possibility to estimate mass of

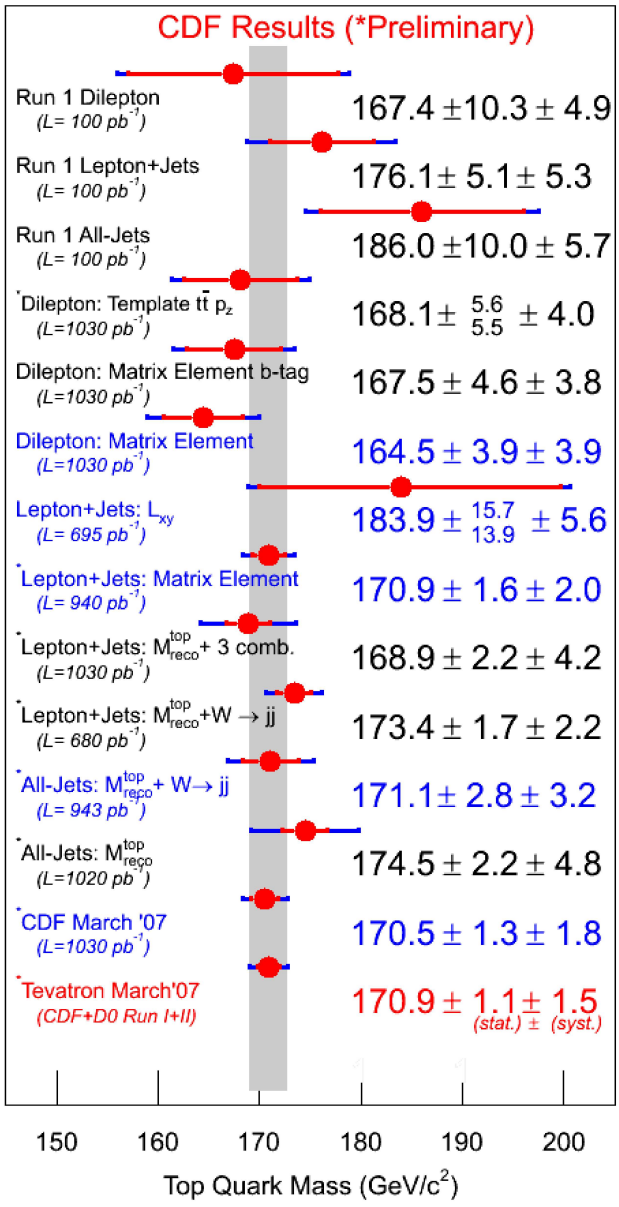


Fig. 29. Summary of top mass measurements by the collaboration CDF.

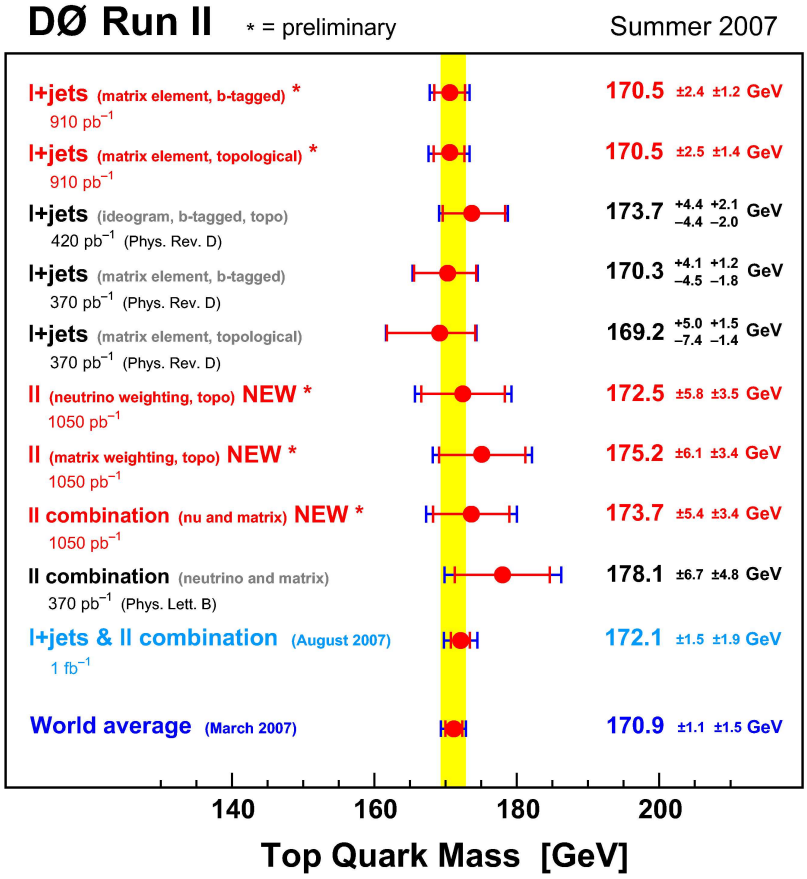


Fig. 30. Summary of top mass measurements by the collaboration D0.

Higgs particle by precise measurement of mass of W boson and top quark mass. Constraints on SM Higgs or MSSM Higgs given by LEP2 and TEVATRON measurements of top mass $\mathrm{M_t} = 172.6 \pm 1.4$ and $\mathrm{M_W} = 80.398 \pm 0.025$ GeV/$c^2$ are in Fig. 31 produced by authors of [51]. Precision top quark and W boson mass measurements (blue circle) limits region of Higgs mass (if Standard Model is correct) or possible masses of SUSY particles if MSSM theoretical description is correct.

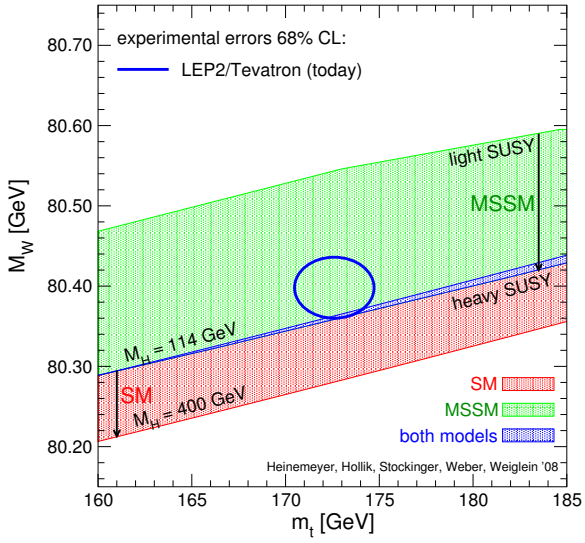


Fig. 31. Allowed region for range of $\mathrm{M_t}$ and $\mathrm{M_W}$ in case when Higgs mass is varied from 114 GeV/$c^2$ and SM assumed (red band) and allowed region determined by a scan over possible SUSY particle masses in case of MSSM (green band).

### 3.3 Single top production

Pair production of t and $\bar{\mathrm{t}}$ quarks by strong interaction can be considered theoretically and experimentally (as can be seen from previous sections) as well established. Theory predicts existence also another mechanism of single t ($\bar{\mathrm{t}}$) quark production by electroweak interaction. Theoretical cross section for single top production is expected to be about 40% of pair production cross section however signal is so deeply burried in background that it presented challenge to find evidence for single top production. Experimental evidence for this channel was found twelve years after top quark discovery was announnced! Evidence was established by D0 collaboration [52] and latter supported by CDF [55]. This analysis is a milestone in analysis in high energy physics. It completely relies on advanced methods of statistical treatment. As was demonstrated in previous sections advanced treatments like Artificial Neural Network based methods can be very useful and improve precision of a given measurement. But it was never only way how to get result up to now.

Conditions to find a signal in single top channel are following: signal to background ratio 1:15-20, number of events after final selection is even lower than what is expected from background only (uncertainty on background level is much larger than expected signal) and signal and background in terms of a single sensitive variables look indistinguishable. Can the existence of a signal under these conditions be established? It is clear that classic counting approach fails. Below we follow procedure proposed by D0 collaboration [52] by which the first evidence for this channel was claimed.

Data have been analyzed at the integrated luminosity 0.9 $\mathrm{fb}^{-1}$, triggers required a jet and electron or muon. Search focuses on top quark in lepton channel mode - isolated lepton, high $\not\!\!E_T$ and b-jet which is accompanied by b-jet in s-channel production and light quark and b-quark in t-channel production (it is rarely reconstructed because it is produced mainly in forward direction and low $\mathrm{E_T}$). Main background consists of W boson in association with jets, pair production of $t\bar{t}$ and cases when jet was mismeasured as lepton (fake leptons) - multi-jet, non W background.

Specifically, jets are reconstructed by cone algorithm with radius $r = \sqrt{(\triangle\eta)^2 + (\triangle\phi)^2}$=0.5 to cluster energy deposits in the calorimeter. The leading jet was required to have $E_T > 25$ GeV and pseudo-rapidity $|\eta| < 2.5$, the second leading jet $E_T > 20$ GeV and $|\eta| < 3.4$ and subsequent jets $E_T > 15$ GeV and $|\eta| < 3.4$. Requirement for events was exactly one isolated electron with $P_T > 15$ GeV/$c$ and $|\eta| < 1.1$ or one isolated muon with $P_T > 18$ GeV/c and $|\eta| < 2.0$. Only events satisfying condition $15 < \not\!\!E_T < 200$ GeV and $\not\!\!E_T$ should not be aligned or anti aligned in azimuth with lepton or selected jets. One or two of the jets have been required to be identified as originating from long lived b hadrons by neural network b-jet tagging algorithm.
For simulation of signal SINGLETOP NLO MC event generator was used, it was checked that it reproduces s-channel and t-channel kinematics according to direct NLO theoretical calculations [9]. Interface to Pythia [16] is used for hadronization of generated partons.
To simulate $t\bar{t}$ and W + jets backgrounds ALPGEN leading order MC package [47] was used and interfaced with PYTHIA for hadronization. Normalization of $t\bar{t}$ was based on integrated luminosity and predicted cross section [30]. The multi-jet background was modeled using data that contain non-isolated lepton but otherwise resemble the lepton + jets data set. W + jets background combined with multi-jet background is normalized to lepton + jets data set separately for each channel (defined by lepton flavor and jet multiplicity) before b-jet tagging. In W + jets simulation $\mathrm{Wb\bar{b}}$ and $\mathrm{Wc\bar{c}}$ components are scaled by $1.5 \pm 0.45$ factor. MC events are input to

GEANT [53] simulation of D0 detector. Differences between data and simulations are corrected by proper weights.

Selection procedure passed 1398 b-tagged lepton + jets data events. Expected amount from single top signal there is $62 \pm 13$. Results for expected signal, background and data are summarized in Tab. VIII. There is no signal over expected background visible. Next step is to calculate multivariate discriminants that separate signal from background and thus enhance probability to observe single top quarks. Decision tree technique (see specific references in [52]) is used to create these discriminants. A decision tree is a machine-learning technique that applies cuts iteratively to classify events. Discrimination power is claimed to be further improved by averaging over many decision trees constructed using the adaptive boosting algorithm AdaBoost. Based on analysis of signal and background 49 sensitive variables have been identified. The variables may be classified into three categories: individual object kinematics, global event kinematics and variables based on angular correlations. Those with most discrimination power include the invariant mass of all the jets in the event, the invariant mass of the reconstructed W boson and the highest $\mathrm{E_T}$ b-tagged jet, the angle between the highest $\mathrm{E_T}$ b-tagged jet and lepton in the rest frame of the reconstructed top quark, and lepton charge times the pseudorapidity of the untagged jet. It is claimed that reducing number of variables always reduces sensitivity of analysis.

Events are divided into 12 channels based on lepton flavor ($e$ or $\mu$), jet multiplicity (2,3 or 4) and number of identified b jets (1 or 2). Boosted decision tree (DT) is applied to each of the 12 channels for three searches: tb+tqb, tqb, and tb. A boosted decision tree produces a quasi-continuous output distribution $O_{DT}$ ranging from 0 to 1. Closer to 0 means more background like event, closer to 1 more signal like. Distribution of $O_{DT}$ in signal enhanced region is displayed in Fig. 32. There is seen excess of single top signal over background!

To convert excess of signal into measured cross section Bayesian approach was applied. Binned likelihood was formed as a product over all binned channels (lepton flavor, jet multiplicity, tag multiplicity) of the decision tree discriminant, separately for tb+tqb, tqb, and tb analysis. Poisson distribution for observed counts was assumed and flat nonnegative probabilities for the signal cross section. Systematic uncertainties have been taken into account by assuming their Gaussian prior. The final posterior probability density is computed as a function of the production cross section. As a measured cross section is considered peak position in posterior probability density and symmetric 68% region determines uncertainty of measurement. A posterior probability density distribution as a function of tb + tqb cross section is shown in Fig. 33. There

Tab. VIII. Number of expected and observed events in 0.9 $\mathrm{fb}^{-1}$ for e and mu, 1 b-tag and 2 b-tag channels combined as a function of 2-4 jets.

| Events per 900 $\mathrm{pb}^{-1}$ after all cuts | | | |
|---|---|---|---|
| Source | 2j | 3j | 4j |
| tb | $16 \pm 3$ | $8 \pm 2$ | $2 \pm 1$ |
| tqb | $20 \pm 4$ | $12 \pm 3$ | $4 \pm 1$ |
| Total background | $686 \pm 41$ | $460 \pm 39$ | $253 \pm 38$ |
| Data | 697 | 455 | 246 |

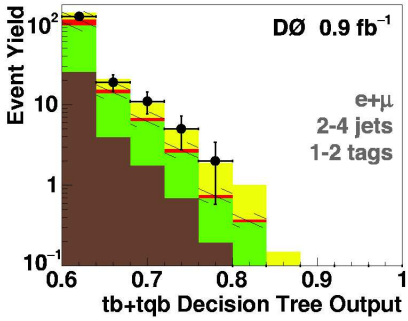


Fig. 32. Distribution of output from boosted decision tree for sum of all 12 channels for tb+tqb search. Points represent data. Different contributions drawn there (in ascending order) are multi-jets, W+jets, $t\bar{t}$ and single top scaled according to measured cross section.

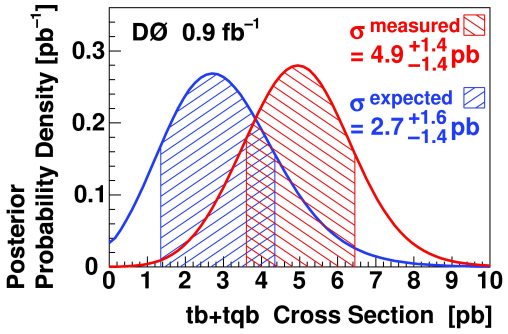


Fig. 33. Expected SM and measured Bayesian posterior probability densities for the tb + tqb cross section. Shaded lines indicate 1 standard deviation above and below peak positions.

is also included expected distribution based on Standard Model. By above procedure was measured single top cross section $\sigma(p\bar{p} \to tb + X, tqb + X) = 4.9 \pm 1.4$ pb which is consistent with expectation from Standard Model. Same procedure was applied separately for tb, tqb channels. Result $\sigma(p\bar{p} \to tb + X) = 4.2^{+1.8}_{-1.4}$ pb and $\sigma(p\bar{p} \to tqb + X) = 1.0 \pm 0.9$ pb. The uncertainties include statistical and systematic components combined.

In Fig. 34 is addressed a question what is a probability that observed result can be obtained from background only hypothesis. From ensemble of 68150 background-only pseudo-datasets, with all systematic uncertainties included, background fluctuates to give SM cross section 2.9 pb or higher 2.9% cases which correspond to 2.1 standard deviations for a Gaussian distribution. The probability that background fluctuates up to produce the mesured cross section 4.9 pb or greater is 0.035% corresponding to 3.4 standard deviations in Gaussian model. The same exercise was repeated with pseudo-datasets where single top signal was included on level expected from SM. Probability to measure cross section 4.9 pb or larger was found to be 11%.

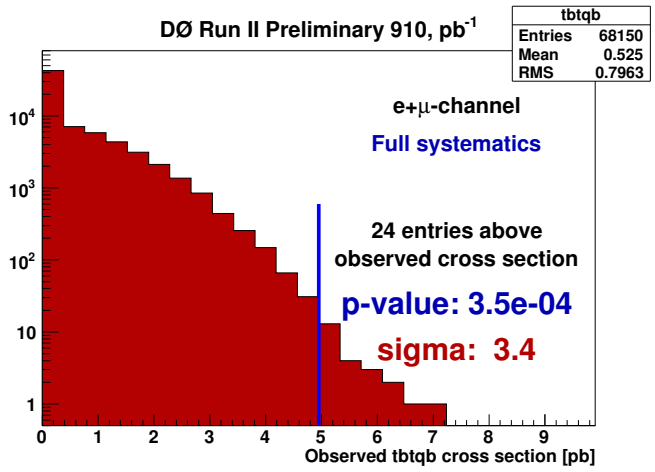


Fig. 34. Test of procedure of measurement cross section on background-only pseudo-datasets.

From above discussion follows that significance of the result (3.4 $\sigma$) was a result of upward fluctuation of signal in D0 experiment. This can also explain why CDF had problems to find evidence for single top production (lack of upward fluctuation) but finally both experiments CDF and D0 claim to see evidence for single top production in their experiments. By using different multivariate statistical approaches both experiments find consistent results. Summary of D0 and CDF results are in Fig. 35. As one can see from a comparison that both results (D0 and CDF) are consistent with Standard Model expectations however cross section measured by D0 is factor 2 larger than cross section measured by CDF. As was already several times mentioned upward fluctuation can be a reason. In high energy physics to state that new process was observed there needs to be reached significance better than 5 standard deviations from a contrary hypothesis that given process was not observed. There is a good chance that with integrated luminosity about 4 $\mathrm{fb}^{-1}$ both experiments CDF and D0 will be able to claim observation of this process!

Task of detailed studies of single top production will be probably left for next generation of HEP experiments at LHC which should start at the end of this year (2008).

Importance of experimental evidence for single top production by experiments D0 and CDF is not only in finding another evidence supporting standard model picture of nature. For experimental high energy physics is of at least the same importance successful exploration of new methods of analysis which are able to isolate tiny signal inside huge background. These methods will find even more challenging application in search for Higgs boson. Not to mention that single top production will be for Higgs search a background which needs to be well understood and under control.

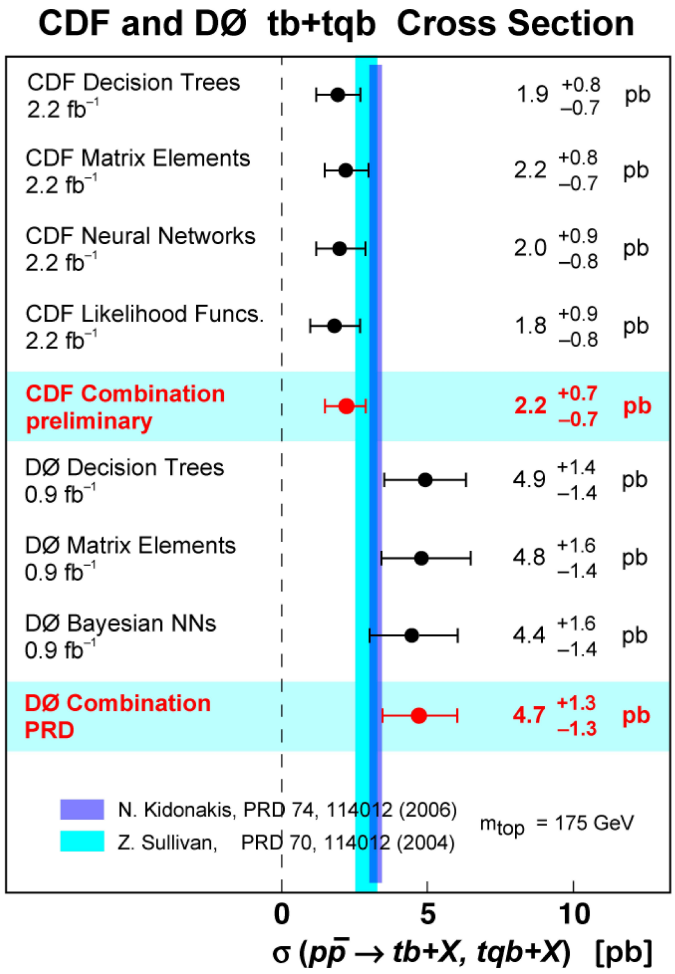


Fig. 35. Summary of measurements of single top cross section by D0 and CDF collaboration.

### 3.4 Top Charge

There does exist alternative model [32] which claims even better agreement with electroweak data than Standard Model. There is large number models which claim that in low energy limit they give the same or better description as Standard Model. Some of them are considered (e.g MSSM) to be a possible successors of the SM.

What makes this model [32] special is that in this model is postulated existence of exotic particle with all properties same as top quark except charge. Charge of exotic particle is 4/3 (in comparison with 2/3 for top). According to this theory what was discovered as top quark is in fact exotic quark. True top quark mass (according to [32]) is much larger ($\approx$ 270 GeV/c$^2$). Therefore only by measurement of top charge one can distinguish between SM and exotic model. More exactly there are also other verifiable differences - let's call exotic particle XM top.

XM top lifetime is longer by factor $\approx$ 18. Therefore does not hold usual argument of SM that hadronization cannot occur. In case of XM top it can. But consequences could escape experimentalists attention.
Cross section for single XM top production is about factor 18 smaller [33]. Therefore if single top production gains discovery level XM top will be in trouble.

In any case, independent of existence or nonexistence of alternative models, task for experimentalist is to measure top charge and make clear underlying assumptions which led to a given measurement.

Basically there are two approaches to measure top charge:

- Based on electromagnetic coupling (measurement of cross section $t\bar{t}\gamma$ ). This measurement will wait for LHC.
- Based on reconstruction of charges of decay products - b and W.

At TEVATRON one needs to consider limited statistics. That can be at some level compensated by an appriory information.

Reconstruction of top charge in $t\bar{t}$ production from decay to b and W can be simplified to a reconstruction of sign of b-jet charge, W charge and decision to what is correct pairing of Ws to b-jets (there are two W and two b-jets in final state). We consider only 2 channels – dilepton channel or lept. + jets channel.

b-jet charge can be determined by identification of decay products (e.g. $B^{\pm}$,$D^{\pm}$, lepton) associated with b-jet.

There is also well known procedure to determine jet charge by weighted sum of charges of the tracks associated with jet. Specifically, following formula is known to work:

$$Q_{jet} = \frac{\sum |\vec{p}_i.\vec{P}_{jet}|^{0.5} Q_i}{\sum |\vec{p}_i.\vec{P}_{jet}|^{0.5}}\,, \tag{34}$$

where $\vec{p}_i, Q_i$ is momentum and charge of a track associated with a jet and $\vec{P}_{jet}, Q_{jet}$ momentum and charge of the jet. Methods based on identification of specific particles associated with b-jet suffer from relatively low identification efficiency. Therefore approach based on eq. (34) was preferred.

Reconstructed b-jet charge distribution by eq. (34) $P_b(x)$ is generally a function of $x$ in the

range <-1.,1.>. Because of CP symmetry of $p\bar{p}$ reaction it should hold relation between b and $\bar{b}$ reconstructed charge distribution $P_b(x) = P_{\bar{b}}(-x)$. This relation can serve also as a consistency check.

One more step can be taken to simplify problem. If reconstructed b-jet charge is smaller than 0 it is considered -1/3, if it is greater than 0 it is considered +1/3. Probability to obtain this way correct charge ($P_b^c$) or wrong charge ($P_b^w$) is the following:

$$P_b^c = \int_{-1}^{0} P_b(x)\,dx, \tag{35}$$

$$P_b^w = \int_{0}^{1} P_b(x)\,dx. \tag{36}$$

There hold the following trivial relations: $P_b^w = 1 - P_b^c$, $P_b^c = P_{\bar{b}}^c$, $P_b^w = P_{\bar{b}}^w$. Let's denote $P^{++}$ probability to measure +2/3 top charge, charge given top hypothesis true and $P^{--}$ is probability to measure -4/3 given exotic hypothesis is true. $P^{++}$ can be determined based on probability of correct pairing and probability of correct b-jet charge reconstruction:

$$P^{++} = P_b^c P_{lb} + (1 - P_b^c)(1 - P_{lb}). \tag{37}$$

Here, $P_{lb}$ is a probability for a correct pair combination of lepton and b-jet from the same top decay. It is also called Purity.

In case when only difference in top and exotic particle hypothesis is charge formulas for $P^{++}$ and $P^{--}$ will be the same. Also assumption that these two hypothesizes are mutually exclusive seems plausible. Therefore we have binomial problem (there are only two possible and exclusive outcomes) to solve. What is probability to observe $N^{++}$ or less pairs out of N pairs of lepton and b-jet if top hypothesis is true?

$$P(N^{++}) = \sum_{i=0}^{N^{++}} \binom{N}{i} (P^{++})^i (1 - P^{++})^{N-i}. \tag{38}$$

In case of exotic hypothesis considered true one needs to replace ++ to $--$ in above formula. Relation eq. (38) in fact represents formula for P-value calculation (standard statistics) given true corresponding hypothesis (top).

Task of reconstructing top (exotic) charge can be reformulated in the following way: Let's have binomial distribution of known individual probability p. There is an ambiguity if p holds for (++) or $(--)$ combination. $H_0$ hypothesis can be formulated for either option. Rejecting one hypothesis means support for the other.

**Background treatment**

Background is supposed to contribute with equal probability (0.5) to both charge combinations (top and exotic). This statement should be cross-checked in both MC and Data! Probability to measure +2/3 charge when top hypothesis is true taking into account correct $t\bar{t}$ and background fractions is:

$$P_{comb}^{++} = P^{++} P_F^{t\bar{t}} + 0.5 P_F^{Bkg}, \tag{39}$$

where $P_F^{t\bar{t}}$ and $P_F^{Bkg}$ are $t\bar{t}$ and background fractions respectively. For P-value calculation $P^{++}$ in formulas eq. (38) should be replaced by $P^{++}_{comb}$. Treatment of exotic hypothesis is straightforward.

### 3.4.1 P-value distribution

Standard statistical treatment is to set $\alpha$ level (usually 0.05 or 0.01) and calculate P-value. P-value was defined by e.g eq. (38). It is a random number and probability to observe value smaller than $\alpha$ when hypothesis under consideration is true is $\alpha$. This is true for continuous probability distribution functions but not exactly true for discontinuous ones. Let's calculate probability distribution of P-value defined by eq. (38),

$$n(P_l, N) = \binom{N}{P_l^{-1}(N^{++})} (P^{++})^{P_l^{-1}(N^{++})} (1 - P^{++})^{N - P_l^{-1}(N^{++})}, \tag{40}$$

where $P_l^{-1}(N^{++})$ is an inverse function to $P_l$ (value of $N^{++}$ corresponding to value of $P_l$). $P_l$ can acquire only discreet values depending on N. Probability to observe $P_l \leq \alpha$ is

$$P_{\alpha,N} = \sum_{P_l \leq \alpha} n(P_l, N). \tag{41}$$

The probability to reject a true hypothesis at a given alpha level is given by eq. (41).
What is probability to reject the exotic hypothesis (based on same $\alpha$ level) when top hypothesis is true? In this case P-value probability distribution has a form:

$$n^{ex}(P_l, N) = \binom{N}{P_l^{-1}(N - N^{++})} (P^{++})^{P_l^{-1}(N - N^{++})} (1 - P^{++})^{N - P_l^{-1}(N - N^{++})}. \tag{42}$$

Probability to observe $P_l \leq \alpha$ is

$$P^{ex}_{\alpha,N} = \sum_{P_l \leq \alpha} n^{ex}(P_l, N). \tag{43}$$

In Fig. 36 a two dimensional distribution of probability (based on eq. (43)) to reject "wrong" hypothesis at 95% CL as a function of purity and number of measurements is shown. It is quantatively expressed by the rather trivial message that for high purity a sufficently modest number of measurements is needed to reject the wrong hypothesis, but for low purity a very large number of measurements is needed.

### 3.4.2 Treatment of uncertainty of individual probability

In case of individual probability ($P^{++}$) is known with some uncertainty what is probability to reject true hypothesis based on $\alpha$ level cut and what is probability to reject wrong hypothesis based on the same cut? Probability to reject true hypothesis based on $\alpha$ level cut is in this case a

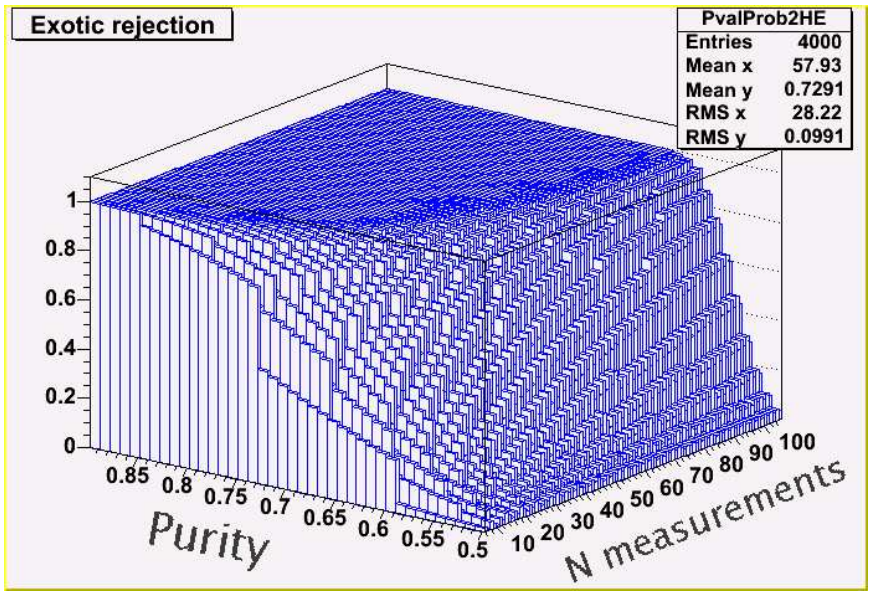


Fig. 36. Two dimensional distribution of probability to reject "wrong" hypothesis at 95% CL as a function of purity and number of measurements.

convolution of formula 41 over distribution of individual probability function. Formula eq. (38) is modified:

$$P(N^{++}) = \sum_{i=0}^{N^{++}} \binom{N}{i} \int f(P^{++})(P^{++})^i (1-P^{++})^{N-i} dP^{++}\,, \tag{44}$$

where f($P^{++}$) is distribution function of $P^{++}$. All previous formulas have the same form only relation (38) is replaced by (44).

### 3.4.3 Bayes Factor

Statistical treatment based on rejection of hypothesis with observed P-value lower than preset $\alpha$-cut can lead to a situation e.g. when both hypotheses are accepted or rejected. This kind of drawback is eliminated by Bayes Factor approach.

In statistics Bayes Factor (BF) is a standard tool for a comparison of two hypothesizes. Odds of one hypothesis over other. Convention is:

| 2 ln(BF) | evidence |
|---|---|
| 0-2 | Not worth mentioning |
| 2-6 | positive |
| 6-10 | strong |
| $> 10$ | very strong |

In our case definition of Bayes factor is following:

$$BF = \frac{\int prob^{SM}(N^{++}, N, p).f(p)dp}{\int prob^{Ex}(N^{++}, N, p).f(p)dp}\,, \tag{45}$$

where $prob^{SM}(N^{++}, N, p)$ - probability to observe $N^{++}$ pairs out of N for a given purity p, f(p) - we assume Gaussian distribution of purity where mean is estimated purity and $\sigma$ estimated uncertainty on purity.

**Statistical analysis**

Now we have all tools ready for statistical analysis. Following strategy in statistical analysis was decided [58]:

- Standard Model hypothesis is considered true. Standard Model hypothesis will be rejected only if P-value under assumption this hypothesis is true is found smaller than 0.01.
- Bayes Factor will be calculated.
- Probability to reject SM hypothesis (by 1% cut) if exotic hypothesis is true will be calculated.

### 3.4.4 Monte Carlo Study

Below analysis follows CDF results [58]. For top charge study two channels have been used: lepton + jets channel and dilepton channel. There are similarities in treatment in both channels but there are also differences. There is needed to establish procedure for determination of b-jet charge and procedure for assignment of b-jet and lepton from the same top decay. In Fig. 37 distribution of b-jet charge calculated according to eq. (34) is shown. Tracks used in calculation have been selected around cone $r = \sqrt{(\triangle\phi)^2 + (\triangle\eta)^2} = 0.4$ around jet axis. To get rid of charge asymmetry (excess of positive charge because of interaction with detector material) $P_T \geq 1.5$ GeV and impact parameter $|d_0| < 0.03$ cm cuts have been implemented. If the charge calculated by using eq. (34) is smaller than 0, then jet is considered b-jet (charge -1/3). If the charge is greater than 0, then jet is $\bar{\text{b}}$-jet(charge +1/3). The result of the above algorithm is the probability for obtaining the correct b-jet charge is about 60%.

Next problem one needs to solve is a right combination of lepton and b-jet from the same top decay. This problem is approached differently in dilepton channel and lept. + jets channel.

In dilepton channel two leptons and two b-jets represent two fold ambiguity how leptons and b-jets can be combined. There are four possible combinations of effective mass squared between lepton and b-jet ($M^2_{lb}$). In Monte Carlo simulation one "knows" which combination is "correct", which combination is "wrong". In Fig. 38 there are two superimposed distributions - maximal value of $M^2_{lb}$ for "correct" combination and for "wrong" one. One can see that for top mass 170 $\mathrm{GeV/c^2}$ contribution of "correct" combination in region of $\mathrm{M^2_{lb}} > 21000$ $\mathrm{GeV^2}/c^4$ is negligible. Therefore if in an event a combination with $M^2_{lb} > 21000$ $\mathrm{GeV^2}/c^4$ occurs, the

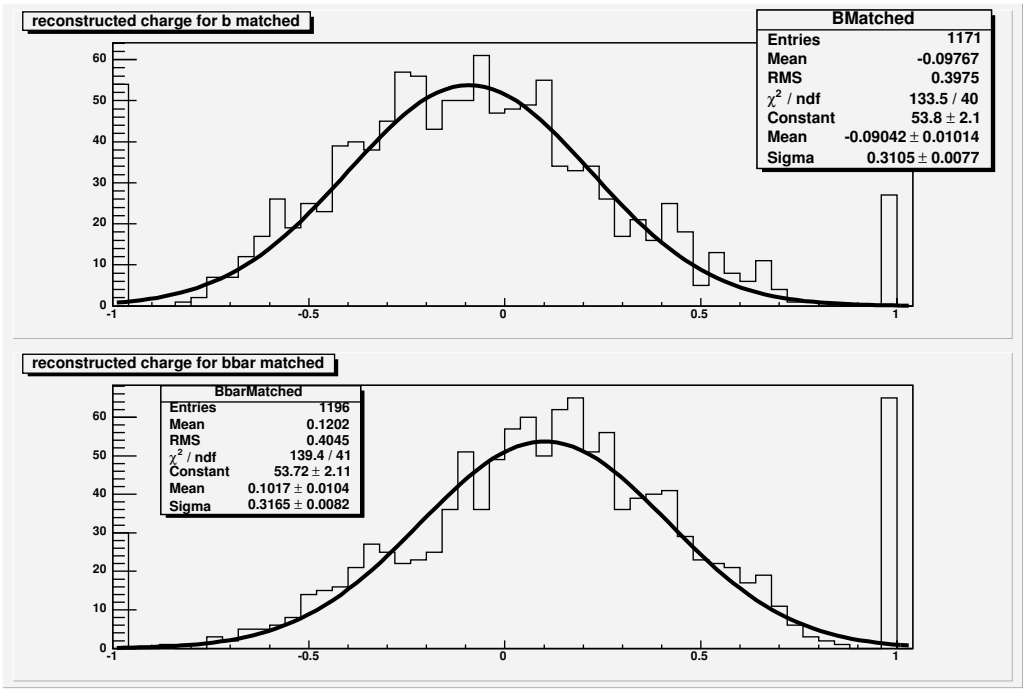


Fig. 37. Charge distribution for matched b-jets (upper plot) and $\bar{\text{b}}$-jets.

choice of complementary combination is with very high probability the right choice. Probability for correct assignment this way is close to 95% and efficiency (probability to observe in an event $M_{lb}^2 > 21000$ GeV$^2/c^4$) close to 40%.

In lept.+ jets channel correct pairing is estimated by kinematic reconstruction of the event. Probability of correct pairing this way is close to 83%.

As a result one obtains certain number of pairs of lepton and b-jet which support the top hypothesis (charge 2/3) and certain number of pairs which support exotic hypothesis (charge 4/3). Under conditions of CDF experiment and a given analysis based on MC simulation it was expected in 1.5 fb$^{-1}$ integrated luminosity to observe $171.07 \pm 25.66$ pairs from "signal" and $8.23 \pm 3.55$ pairs from background (the combined result from lept.+jets and dilepton channels).

### Scale factor between Data and simulation

Detector simulation combined with physical event generator is tuned after many tests and comparisons with real experiment to reproduce most of features of experiment very well. Still question how reliable is e.g. probability of b-jet charge determination based on MC needs to be answered. It can be answered by determination of "scale factor" which converts probability of correct b-jet charge determination in MC to corresponding measurement in real experimental data. Roughly idea is simply to select b-jets from trigger lepton enhanced dijet sample. Lep-

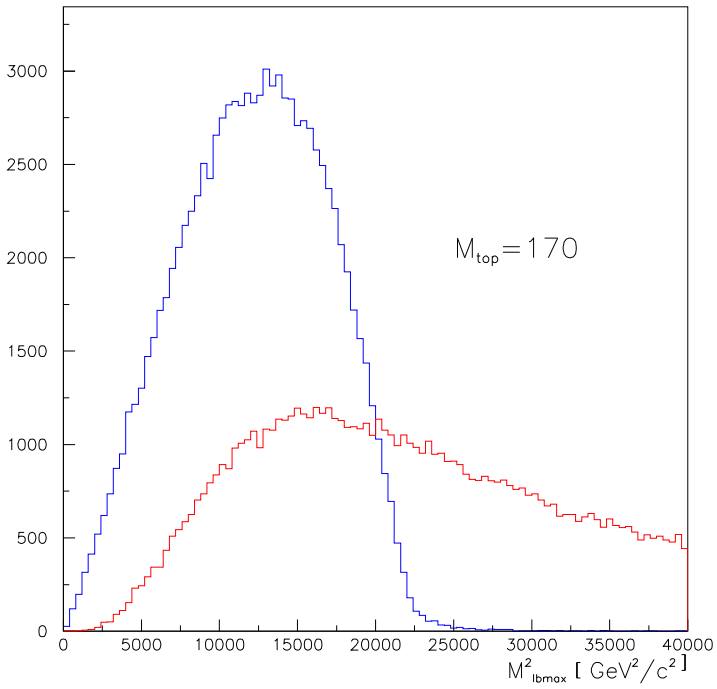


Fig. 38. Distribution of max $M^2_{lb}$ for correct pairing (blue) and wrong pairing (red).

ton associated with jet enhances probability that a given jet is a b-jet. Leptons from b-hadrons semileptonic decay have a characteristic transverse momentum distribution (details can be found in e.g. [64]) and one can statistically determine fraction of true b-jet in a sample. Charge of lepton determines charge of b-jet. Second jet in a dijet sample (so called "away jet") is considered to have opposite sign to semileptonic jet (see Fig. 39). This jet is used for determination of b-jet charge by eq. (34). Scale factor determined by above procedure was found within statistical and systematic errors equal to 1.

**Final result**

Above procedure has been applied to 1.5 $\mathrm{fb}^{-1}$ CDF data. Probability to determine correctly top charge (taking into account also scale factor) for signal was estimated to be $P_s = 0.572 \pm 0.003(stat) \pm 0.008(syst)$ for background $P_b = 0.505 \pm 0.005$ (background is expected to contribute equally to top and to exotic hypothesis. The result is consistent with this statement). There have been found 124 pairs supporting SM hypothesis and 101 pairs supporting exotic one (combined lept. + jets and dilepton channel result).

P-value (under assumption of SM hypothesis true) was found 0.31 - consistent with the assumption and calculated Bayes Factor 12.01 means very strongly support for SM (top charge 2/3) in comparison with exotic hypothesis (charge 4/3). Probability to reject SM hypothesis (P-value

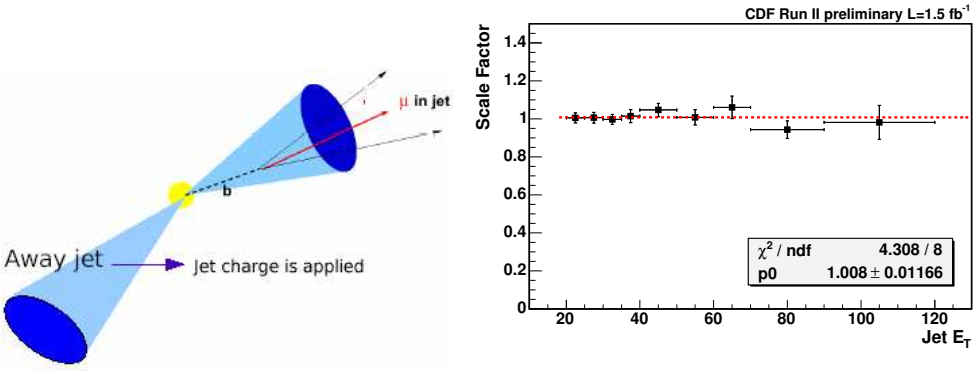


Fig. 39. Idea for determination b-jet charge purity from enhanced b-dijet data (left) and dependence of scale factor as a function of b-jet $E_T$ (right).

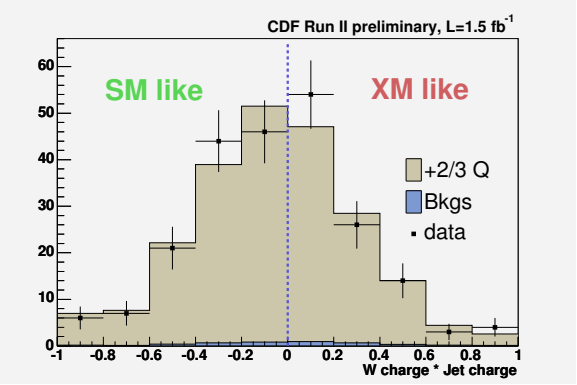


Fig. 40. Distribution of product of W Boson charge and associated jet charge (determined according to eq. (34)). Points representing data are compared to the result expected at the same conditions in case of SM top (+2/3 Q). Background is very small, barely visible in this figure.

$< 0.01$ under assumption of SM true) in case when exotic hypothesis is in fact true was found 87%. Therefore exotic hypothesis is claimed to be rejected with 87 % probability.

In Fig. 40 one can see distribution quantity which is product of W charge and b-jet charge calculated according to eq. (34) paired by pairing procedure to W. This product would be in case of absolute precision and SM true equal exactly to -1/3.

Another easy way how to view result is through Fig. 41. In Fig. 41 there are superimposed two curves and marked two regions. Blue line, border of blue region represents P-value under assumption of SM top hypothesis for $N^{++}$ number of pairs supporting this hypothesis out of 225 pairs. Red border has same meaning for exotic hypothesis. Probability for correct determination of top charge (purity) was set to value 0.572. One can immediately judge from figure P-value in case SM hypothesis assumed true or XM hypothesis assumed true. Green line repre-

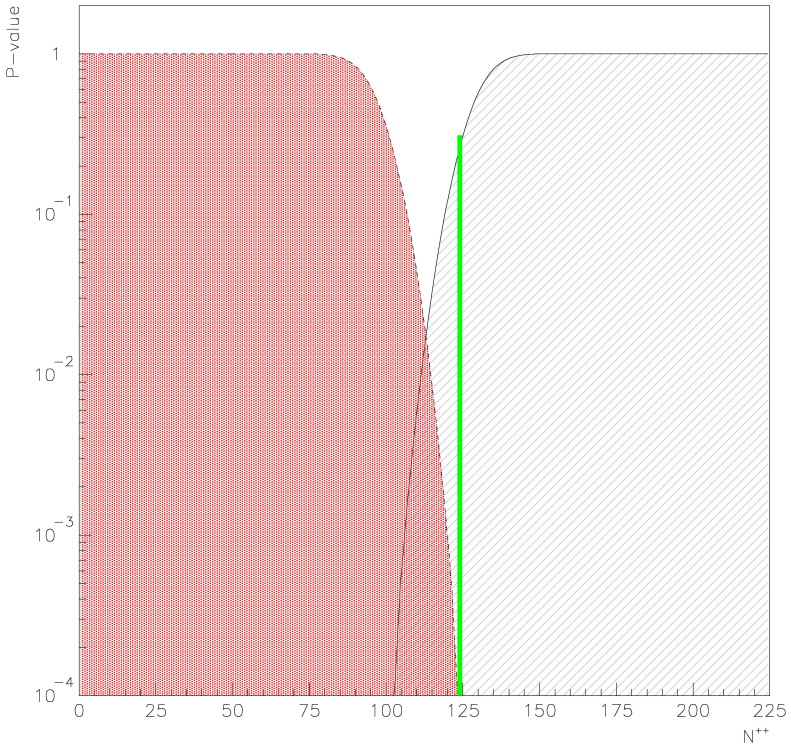


Fig. 41. Probability to observe $N^{++}$ pairs or less supporting SM top if SM hypothesis is true - blue curve (region) and complementary case when exotic hypothesis (XM) is correct. Probability to correctly determine top charge was set to $P_s = 0.572$

sents experimental result $N^{++} = 124$ and one can see that it corresponds to P-value $\approx 0.3$ under assumption SM hypothesis true or $\approx 10^{-4}$ under assumption of XM true. This is just good order of magnitude estimate because e.g. uncertainty on purity was not taken into account.

### 3.5 Measurement of W-Boson helicicity in top decays

According to the Standard Model the top quark decays into W and b-quark with almost 100% probability and very fast (see 2.1). Short lifetime prevents hadronization of top quark therefore its properties are transfered directly to decay products without modification caused by hadronization! This is a unique property of the top quark! Standard Model makes specific prediction about W polarization in case of $\mathrm{t} \rightarrow \mathrm{Wb}$ decay. Precise measurement of W polarization can reveal new physics beyond the Standard Model (if it takes place).

A short description of W helicity expectations in top rest frame predicted by Standard Model is given below.

W-Boson as a vector (spin 1) particle can have projections of spin on the direction of motion (helicity) +1,0,-1. We talk about right-handed, 0 (longitudinal) and left-handed helicity states. In the b-quark massless limit in top decay (because V-A charge current weak interaction responsible for decay) b-quark can be only left handed and $\bar{\mathrm{b}}$-quark (in $\bar{\mathrm{t}}$ decay) only right-handed. Top quark spin is $\frac{1}{2}$ and only options for $W^+$ helicity states therefor are left-handed ($W_-$) and longitudinal ($W_0$). In case of $\bar{\mathrm{t}}$ decay – $W^-$ helicity states can be right-handed ($W_+$) and longitudinal ($W_0$). These are the only options on how to combine the W with a left-handed b-quark to produce spin projection consistent with top $\pm 1/2$. In Fig. 42 there is the graphical explanation.

If what we call top quark is in fact an exotic quark as predicted in [32] which decays to $W^+$ and $\bar{\mathrm{b}}$ then naively one would expect that W helicity can be only 0 and right-handed! But as it turns out [33] in this exotic model prediction about W helicity is the same as in case of SM! However, for the exotic model we are considering the SM assumption about fast decay preventing hadronization or spin flip are not valid. The reason being this particular model [32] predicts the lifetime of the exotic top quark will be 18 times larger than the SM top quark! Therefore really conclusive possibility to rule out exotic option is to measure top charge!

Standard Model gives specific prediction about fraction of cases when top quark decays into definite helicity states of W-Boson. e.g. for longitudinal fraction $F_0$ SM in the tree approximation

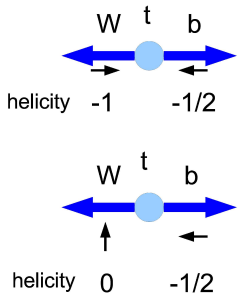


Fig. 42. Decay of top quark into W and b in top rest frame. Upper part represents top spin projection +1/2, W helicity -1 and b-quark helicity -1/2 (both left-handed), Lower part represents top spin projection -1/2, W helicity 0 (longitudinal) and b-quark helicity -1/2 (left-handed).

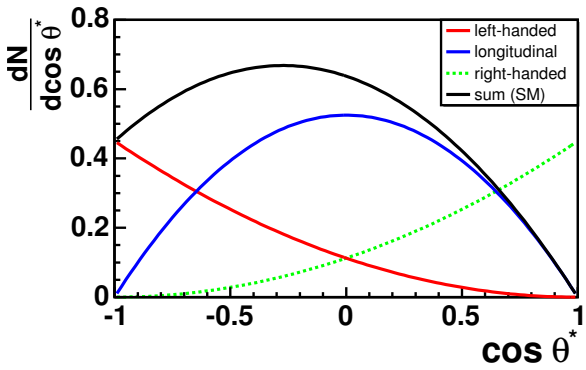


Fig. 43. Expected angular distribution of leptons in W rest frame in case $W_-, W_0, W_+$ helicity states compared to SM expectation.

predicts:

$$F_0 = \frac{\Gamma(t \to W_0 b)}{\Gamma(t \to W_0 b) + \Gamma(t \to W_+ b) + \Gamma(t \to W_- b)} = \frac{M_t^2}{2M_W^2 + M_t^2}. \quad (46)$$

In Standard Model $\Gamma(t \to W_+ b)$ is (close to) 0. Naturally there holds equality $F_+ + F_- + F_0 = 1$.

Therefore for top mass 175 GeV/$c^2$ SM predicts $F_0 = 0.7$, $F_- = 0.3$ and $F_+ = 0$.
The W-Boson polarization is reflected in angular distribution of leptons from $W \to l\nu$ decay. Generally $\cos(\theta^*)$ distribution is expressed by:

$$\frac{dN}{d\cos(\theta^*)} \propto F_- \cdot \frac{3}{8}(1 - \cos(\theta^*))^2 + F_0 \cdot \frac{3}{4}(1 - \cos^2(\theta^*)) + F_+ \cdot \frac{3}{8}(1 + \cos(\theta^*))^2 , \quad (47)$$

where $\theta^*$ is the angle between momentum of the charged lepton in the W rest frame and the momentum of the W-Boson in the top quark rest frame. In Fig. 43 are shown $\cos(\theta^*)$ distributions for different helicity states of W and for SM expectation.

Below we follow procedure and results published by the CDF collaboration [59]. The analysis is done using the lept. + jets channel. Selection requirements are close to one used for cross section measurement (see section 3.1.2). There is an extra requirement that event is removed if lepton and another object form effective mass in Z-Boson mass window. In the data sample corresponding to integrated luminosity 1.9 fb$^{-1}$ there are 484 $t\bar{t}$ candidate events. Background was estimated to be 86.53 events. It's composition was discussed in detail in section 3.1.2.

It is necessary to fully reconstruct four momenta of t and $\bar{t}$. One can think that it would be sufficient to reconstruct top quark associated with W which undergoes semileptonic $W \to l\nu$. But to find out which jet in the event is most probably associated with W from top quark decay one needs to try different jet associations and to reconstruct t and $\bar{t}$ four momenta.

Measured momenta of jets and $\not\!\!E_T$ are corrected to parton level. $\not\!\!E_T$ corresponds to transverse momentum of neutrino from leptonic decay of W-Boson. Longitudinal component of neutrino can be reconstructed when constrain on W mass in W-Boson semileptonic decay is applied. This

way longitudinal component of neutrino will be obtained as a solution of a quadratic equation. In 70% cases there are two real solutions and both have to be taken into account. In 30% cases solutions become complex. In this case *x* and *y* componets of $\not\!\!E_T$ are varied (starting from the measured values) until imaginary part of the solution vanishes. In this case there is single solution.

All jets in the event (not only 4 leading jets) are considered for assignment to the two b-quarks and the two light quarks (from hadronic W decay). Therefore number of hypotheses considered for complete kinematic reconstruction is quite large - $N_\nu \cdot N_j \cdot (N_j-1) \cdot (N_j-2) \cdot (N_j-3)/2$. Where $N_\nu$ is number of neutrino solutions and $N_j$ number of jets. For each hypothesis is calculated quantity $\psi$ which gives quantitative estimate how well given hypothesis matches the $t\bar{t}$ configuration,

$$\psi = P_\nu \cdot P_{b-light} \cdot \chi^2,$$

where $P_\nu$ is the weighting factor for the calculated longitudinal component of neutrino, $P_{b-light}$ is a measure of likeness that for a given jet assignment true light quarks are assigned as the b-quarks, $\chi^2$ is a measure how well within expected uncertainties reconstructed W mass from assigned jets corresponds to $M_W$, $M_{top}$ leptonic to $M_{top}$ hadronic and fraction of transverse energy from two top quarks in event to total transverse energy.

$\psi$ is calculated for each hypothesis in the event and hypothesis with smallest $\psi$ is chosen to be used for a calculation of $\cos(\theta^*)$ distribution.

Extraction of helicity fraction $F_+$ and $F_0$ from measured $\cos(\theta^*)$ distribution was performed by binned likelihood fit. The likelihood function $L(a)$ (where "a"stands for the free parameters - helicity fractions)

$$L(a,\beta) = e^{-\frac{(1-\beta)^2}{\sigma_\beta^2}} \cdot \prod_{k=1}^{N_{bins}} \frac{\mu_k^{exp}(a,\beta)^{n_k} e^{-\mu_k^{exp}(a,\beta)}}{n_k!}. \tag{48}$$

$\mu_k^{exp}(a,\beta)$ denotes the number of events expected to be observed in bin k of the reconstructed $\cos(\theta^*_{rec})$ and $n_k$ actually measured number of events in the same bin. $\mu_k^{exp}(a,\beta)$ is a sum of the expected number of events from signal $\mu_k^{sig,exp}$ and background $\mu_k^{BG,exp}$:

$$\mu_k^{exp}(a,\beta) = N_{sig} \cdot \mu_k^{sig,exp}(a) + N_{BG} \cdot \mu_k^{BG,exp} \cdot \beta\,,$$

and $\mu_k^{sig,exp}$ is calculated via

$$\mu_k^{sig,exp} \propto \sum_i \mu_i^{sig}(F_0,F_+) \cdot \epsilon_i \cdot S(i,k).$$

The starting point is the theoretically predicted number of signal events in each bin $\mu_i^{sig}(F_0, F_+)$ (dependence on $F_-$ is eliminated by constrain $F_0 + F_+ + F_- = 1$). Event selection acceptance depends on $\cos(\theta^*)$ therefore for each bin is applied different event selection efficiency $\epsilon_i$. The migration matrix S takes migration effects due to the finite resolution of detector and the reconstruction method into account. The matrix element $S(i,k)$ represents probability for an event with true $\cos(\theta^*)$ in bin i to contribute to bin k. Both migration matrix and selection efficiency $\epsilon_i$ have been checked to be independent of W helicity fractions.

$\mu_k^{BG,exp}$ is the normalized background estimate derived from the background templates.

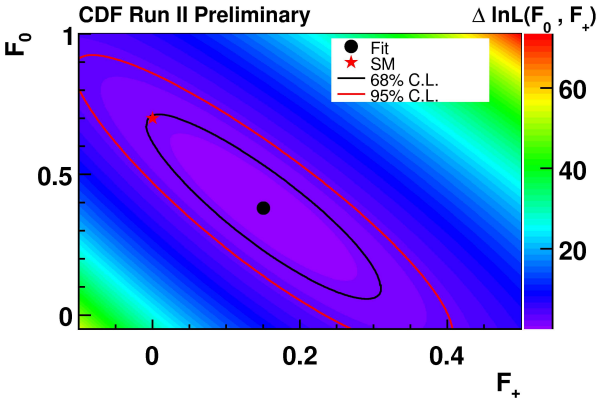


Fig. 44. $\triangle \ln L$ dependence as a function of $F_+, F_0$ around fitted value (black point). Position of SM predicted value for $F_+, F_0$ is marked by red star. The black line indicate 68% CL contour, red one 95% CL.

$N_{BG} \cdot \beta$ is the total number of background events. Gaussian term in likelihood (48) constrains number of background events to estimated expected value within estimated error.

Number of the signal events $N_{sig}$ is determined from number of observed events $N_{obs}$ and number of background evens as $N_{sig} = N_{obs} - N_{BG} \cdot \beta$.

Data are separated into exactly one b-tag and more than one b-tag categories. Likelihood function is separately calculated for each category and product of these two likelihoods is the combined likelihood used to perform a fit of W-Boson helicity fractions. Fit was executed under three separate conditions:

- Fit to determine $F_0$ when $F_+$ is fixed to 0 (as expected from SM).
- Fit to determine $F_+$ when $F_0 = 0.7$ (as expected from SM).
- A two dimensional fit to determine simultaneously $F_0, F_+$.

Systematic uncertainty was studied by means of pseudo-experiments (PE). The systematic uncertainty is given by the difference between mean fit result for PE with systematic affected sample and the mean fit result for default sample. Three most relevant sources of systematic errors have been identified - jet energy scale uncertainty, final state radiation uncertainty and background shape. Nominal value of top quark mass in systematic studies was 175 GeV/$c^2$. Uncertainty on top mass was not included in systematic uncertainties but there was performed a check in $\pm 5$ GeV/$c^2$ region around top mass 175 GeV/$c^2$ and it was demonstrated that fit reproduces well W helicity fractions (which are top mass dependent).

Results: Performing the fit with fixed $F_+ = 0$, the fraction of helicity 0 W-Bosons was determined to be $F_0 = 0.66 \pm 0.10(stat) \pm 0.06(syst)$. When $F_0$ was fixed to $F_0 = 0.7$ right-handed fraction of W-Bosons $F_+$ was found $F_+ = 0.01 \pm 0.05(stat) \pm 0.03(syst)$. Background parameter $\beta$ was determined $\beta = 1.02 \pm 0.20$. Assuming $F_0 = 0.7$ the 95% CL for $F_+$ was determined to be $F_+ < 0.12$. The simultaneous fit of $F_0$ and $F_+$ yielded the results $F_0 = 0.38 \pm 0.21(stat) \pm 0.07(syst)$, $F_+ = 0.15 \pm 0.10(stat) \pm 0.05(syst)$ and $\beta = 1.0 \pm 0.2$. The corresponding distribution of $-\triangle \ln L$ is shown in Fig. 44. Both results are consistent with SM prediction for W helicity fractions.

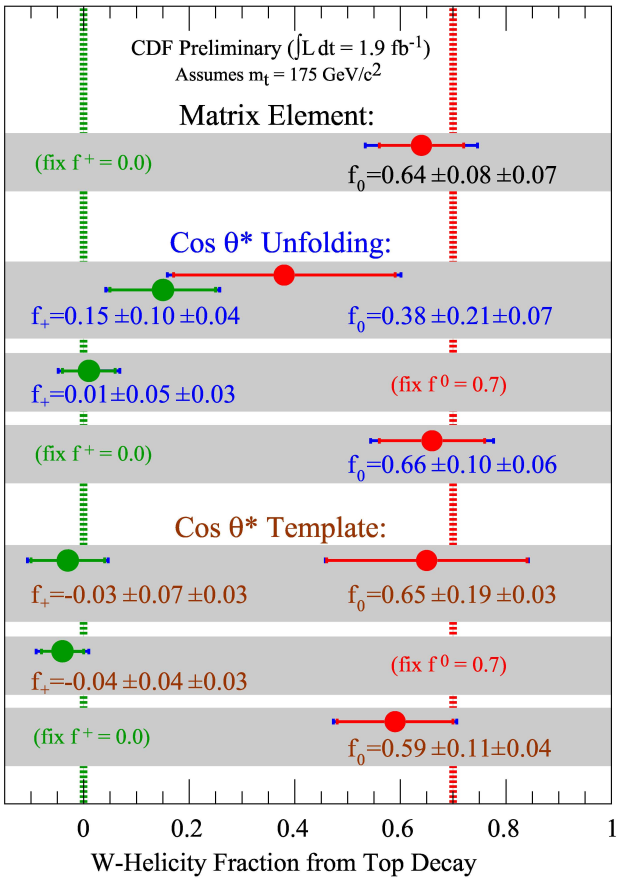


Fig. 45. Summary of the results of CDF collaboration on W helicity fraction measurements.

Consistent results have been obtained by several other independent analysis at CDF [60], [61] and D0 [62].

As can be seen from Fig. 45 different methods point to the same conclusion - support for SM prediction. Consistency with Standard Model prediction for W helicity fractions means also indirect support for other prediction of SM implicitly assumed - very short lifetime of SM top quark which prevents hadronization or spin flip for top quark to happen.

### 3.6 Spin - Spin correlations

Correlations between spins of $t$ and $\bar{t}$ in $t\bar{t}$ production have been extensively theoretically studied in the past [65]. Interest in these studies was provoked by unique feature of the top quark - very fast decay, mean lifetime order of magnitude smaller than time needed for hadronization or spin flip. Therefore spin properties of top quark are directly transferred to the decay products. These correlations are very sensitive to a new physics, deviations from the Standard Model. The large correlations in an appropriate reference frame have been predicted in Standard Model framework.

So far there are no (statistically significant) experimental results about t and $\bar{\text{t}}$ spin correlations. Therefore in this section we will try to analyze situation from an experimentalist point of view how these correlations can be approached and what kind of problems can be faced.

It is well known [71] that best analyzer of top spin is charged lepton from the decay chain $t \to Wb \to l\nu b$. Therefore we concentrate on dilepton channel.

A two-dimensional distribution (in an appropriate reference frame) of $\cos(\theta_+), \cos(\theta_-)$ (for lepton with charge + and - respectively) has a simple form (see e.g. [71]):

$$\frac{1}{\sigma}\frac{d\sigma^2(p\bar{p} \to t\bar{t} \to l^+l^-X)}{d\cos\theta_+ d\cos\theta_-} = \frac{1}{4}(1 - C \cdot \cos(\theta_+)\cos(\theta_-))\,, \tag{49}$$

where *C* is spin-spin correlation coefficient in a given reference frame. One can define variable

$$z = \cos(\theta_+)\cos(\theta_-) \tag{50}$$

and derive from the 2 dimensional distribution eq. (49) a one dimensional distribution

$$\frac{1}{\sigma}\frac{d\sigma(p\bar{p} \to t\bar{t} \to l^+l^-X)}{dz} = -1/2 \cdot (1 - C \cdot z) \cdot \ln(|z|). \tag{51}$$

Very attractive feature has distribution:

$$\frac{-1}{\ln(|z|)}\frac{1}{\sigma}\frac{d\sigma(p\bar{p} \to t\bar{t} \to l^+l^-X)}{dz} = 1/2 \cdot (1 - C \cdot z). \tag{52}$$

The correlation coefficient is proportional to the slope. No information is lost in going from the two-dimensional eq. (49) to the one dimensional eq. (52). Dealing with one dimensional distribution, specially in case of low statistics should be an advantage.

Standard Model prediction in NLO approximation [67] for TEVATRON and LHC is summarized in Tab. IX.

Tab. IX. A comparison of the NLO Standard Model prediction for spin-spin correlation coefficient in beam and helicity frames in case of TEVATRON an LHC.

| Reference frame | TEVATRON | LHC |
|---|---|---|
| $C_{beam}$ | 0.806 | -0.072 |
| $C_{hel}$ | -0.389 | 0.311 |

As one can see from above comparison Standard Model predicts larger correlations in the case of TEVATRON. But this drawback in case of LHC will be more than compensated by three orders of magnitude larger expected statistics.

There are several options how to determine correlation coefficient *C*;

- by a fit to a two-dimensional distribution described by eq. (49);
- from eq. (49) follows:

$$C = -9 < \cos t\theta_+ \cos t\theta_- >; \tag{53}$$

- from endpoints of distribution eq. (49)
  for points (1,-1) and (-1,-1) follows:

  $(-1,-1) \rightarrow$ 1/4(1-C) = $N_-$
  $(1,-1) \quad \rightarrow$ 1/4(1+C)= $N_+$

  then

$$C = \frac{N_+ - N_-}{N_+ + N_-}; \tag{54}$$

- from asymmetry of "same side" and "opposite side" pairs.
  Let's define same side

$$N_s = \int_{-1}^{0}\int_{-1}^{0} \frac{d\sigma^2}{d\cos\theta_+ d\cos\theta_-} d\cos\theta_+ d\cos\theta_- + \int_{0}^{1}\int_{0}^{1} \frac{d\sigma^2}{d\cos\theta_+ d\cos\theta_-} d\cos\theta_+ d\cos\theta_-$$

  and opposite side

$$N_{op} = \int_{-1}^{0}\int_{0}^{1} \frac{d\sigma^2}{d\cos\theta_+ d\cos\theta_-} d\cos\theta_+ d\cos\theta_- + \int_{0}^{1}\int_{-1}^{0} \frac{d\sigma^2}{d\cos\theta_+ d\cos\theta_-} d\cos\theta_+ d\cos\theta_-$$

  one can easily see that

$$C = 4 \cdot \frac{N_{op} - N_s}{N_{op} + N_s}; \tag{55}$$

- from a fit to $z$ distribution eq. (51);
- according to eq. (52) $z$ distribution has linear dependence. Fit to this dependence determines correlation coefficient.

In a limit of the infinite statistics all these determinations should be equivalent. In case of modest statistics, one of the above maybe the best choice because of selection and reconstruction biases.

**Reference frames**

Because results crucially depend on a choice of reference frame we decided to devote special paragraph to this topic. We also realized that there are at least two definitions of the beam frame defined by theorists who calculated correlation coefficient in these frames. Ambiguity in definition of above frames in the literature was resolved with help of original authors [68, 69]

We consider three reference frames:

- Beam reference frame I.
- Beam reference frame II.
- Helicity reference frame.

**Beam frame I [68]**

There are defined four vector QL $\equiv (0, 0, 1, 1)$ and QR $\equiv (0, 0, -1, 1)$ in lab frame (in case of TEVATRON means in fact CMS frame). QR is transformed by Lorentz transformation into top rest frame. Cosine of angle between transformed QR and lepton from top decay in top rest-frame is $\cos(\theta_+)$. $\cos(\theta_-)$ is defined by using QL and $\bar{t}$ rest frame same way.

**Beam frame II [69]**

QL $\equiv (0, 0, 1, 1)$ in lab frame is transformed to "Zero Momentum Frame" (frame where $t\bar{t}$ system has 0 momentum). Lepton four momenta are transformed to ZMF first and then to corresponding top (for + charged lepton) and $\bar{t}$ (for negative charge lepton). $\cos(\theta_+)$ is defined by direction of QL in ZMF and charge + lepton in top rest frame. $\cos(\theta_-)$ is defined by direction of QL in ZMF and negative charge lepton in $\bar{t}$ rest frame.

**Helicity frame**

There is a general agreement on definition of helicity frame. What may be unusual for novice is importance of ZMF stage.
Top, anti top and leptons four momenta are transformed to ZMF first and then from this frame to top (anti top) rest frame. Direction from top (anti top) rest frame to ZMF frame is the helicity axis. Angle between this direction and direction of lepton in a given rest frame is the wanted angle in the helicity frame.

### 3.6.1 Spin-spin correlation coefficient determination from different MC generators

For a test of discussed procedures for determination of spin correlation coefficient we employed two event generators – Pythia [16] and TopRex [70]. In fact TopRex does use interface to Pythia. By means of these generators $p\bar{p} \rightarrow t\bar{t} + X$ reaction at 1.96 TeV is generated and t ($\bar{\text{t}}$) is forced to decay in leptonic mode (dilepton channel). Top mass was set to 170 GeV/$c^2$ for purpose of these tests.

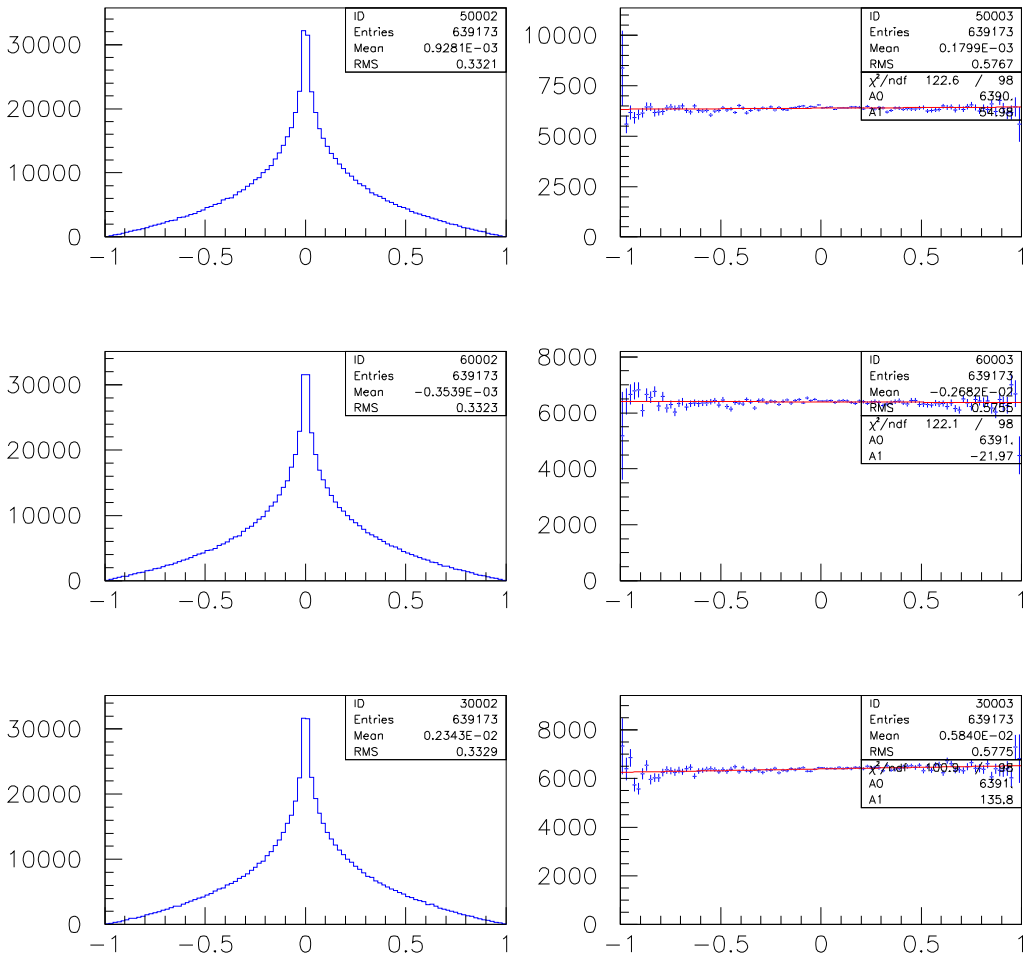


Fig. 46. Using standard Pythia the distributions for the variable $z$ are generated in the left column, while the right column shows z distribution weighted by $-1/\ln(|z|)$. The top row is for Beam frame I, the middle for Beam Frame II, and the bottom for the Helicity frame.

### Standard Pythia - ideal case

In the standard Pythia (at least up to version 6.x) spin correlations in $t\bar{t}$ production are not included. However spin content of individual t ($\bar{\text{t}}$) is correctly propagated along t ($\bar{\text{t}}$) decay chain. Just spin of t and $\bar{\text{t}}$ are not correlated. In the ideal case, "true" - generator level top four vectors are used in the transformations between appropriate frames. In Fig. 46 distribution of variable $z$ (see eq. (50)) in beam frames I,II and helicity frame is shown (left column). Right column displays $z$ distribution weighted by $-1/\ln(|z|)$. Absence of spin-spin correlation is easily identified by flat shape of this distribution.

Tab. X. The $t\bar{t}$ spin-spin correlation parameter determined in different ways.

| Method | $C_{\mathrm{beamI}}$ | $C_{\mathrm{beamII}}$ | $C_{\mathrm{helicity}}$ |
|---|---|---|---|
| LO (CTEQ5) [71] | – | 0.910 | -0.456 |
| LO (CTEQ6L) [72] | – | 0.928 | -0.471 |
| -9$<$ z $>$ | -0.711 $\pm$ 0.004 | 0.9 $\pm$ 0.004 | -0.468 $\pm$ 0.004 |
| Fit (eq. 52) | -0.711 $\pm$ 0.004 | 0.904 $\pm$ 0.004 | -0.467 $\pm$ 0.004 |
| Asymmetry (SS,OS) | -0.711 $\pm$ 0.005 | 0.905 $\pm$ 0.005 | -0.466 $\pm$ 0.005 |
| End Points 2D | -0.6 $\pm$ 0.03 | 0.858 $\pm$ 0.02 | -0.5 $\pm$ 0.03 |

**Modified Pythia - TopRex - ideal case**

In TopRex $t\bar{t}$ spin-spin correlations are correctly included. We use version 4.11 where LO matrix element is implemented. One can compare spin correlations in two dimensions for beam frame I and II in Fig. 47 and helicity frame in Fig. 48. The same $z$ distribution as in Fig. 46 (standard Pythia) is presented in Fig. 49 (TopRex). One can clearly see difference between previous case. More precisely, relevant conditions for spin correlations generated by TopRex are $M_t = 170\ \mathrm{GeV/c^2}$ and PDF structure function CTEQ5L.

In Tab. X is result of determination of spin-spin correlation coefficient by different approaches.

The first two items in the table are published results of theoretical calculations using leading order matrix element but different PDF structure functions. Other items are different estimates of correlation coefficient based on analysis of TopRex generated events.

There is a good agreement between different ways of determination of correlation coefficient and also between LO theoretical prediction and above determinations. As one would expect at high statistics different approaches give at high statistic very close results.

One can make a very rough estimate of the needed statistics to distinguish between correlation coefficient as expected from Standard Model and no correlations at 3 $\sigma$ accuracy. To achieve this correlation coefficient should be estimated with precision better than 0.3 (prediction for corr. coef. from SM in LO approximation in beam frame is $\approx 0.9$). As one can see from Fig. 49 rms of (unweighted ) distribution in variable $z$ is for all frames $\approx 0.3$. If we use estimate of correlation coefficient based on eq. (53) estimate of error is:

$$\sigma(C) = \frac{9rms(z)}{\sqrt{N}}\,, \tag{56}$$

where $N$ is number of events. Result is $\approx$ 80 events. This estimate should be considered as a lower limit because all input data are taken from ideal condition set up. Any real measurement needs to look very carefully into issues relating to selection and reconstruction biases.

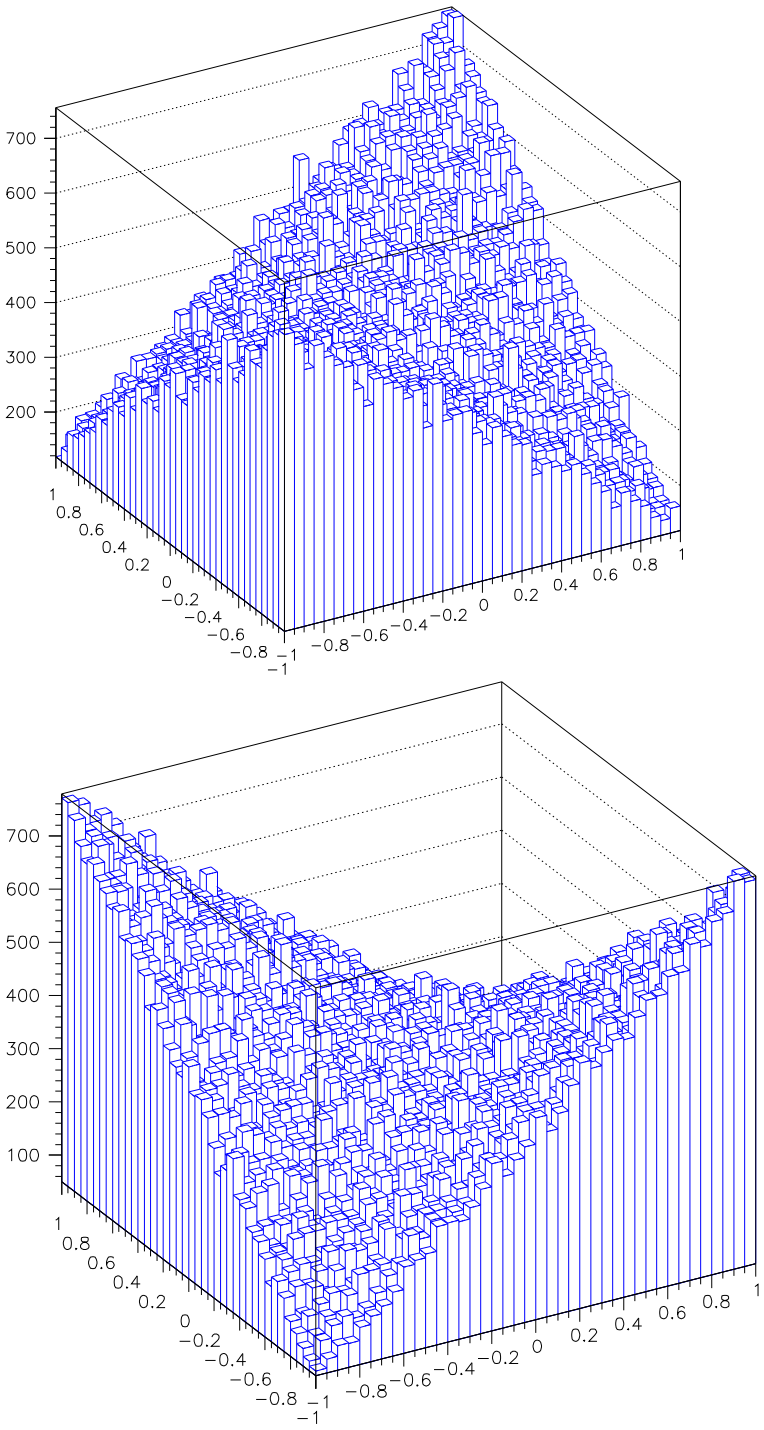


Fig. 47. A two dimensional distribution of $\cos(\theta_1) \times \cos(\theta_2)$ in beam frame I (upper plot) and beam frame II (lower plot) - TopRex.

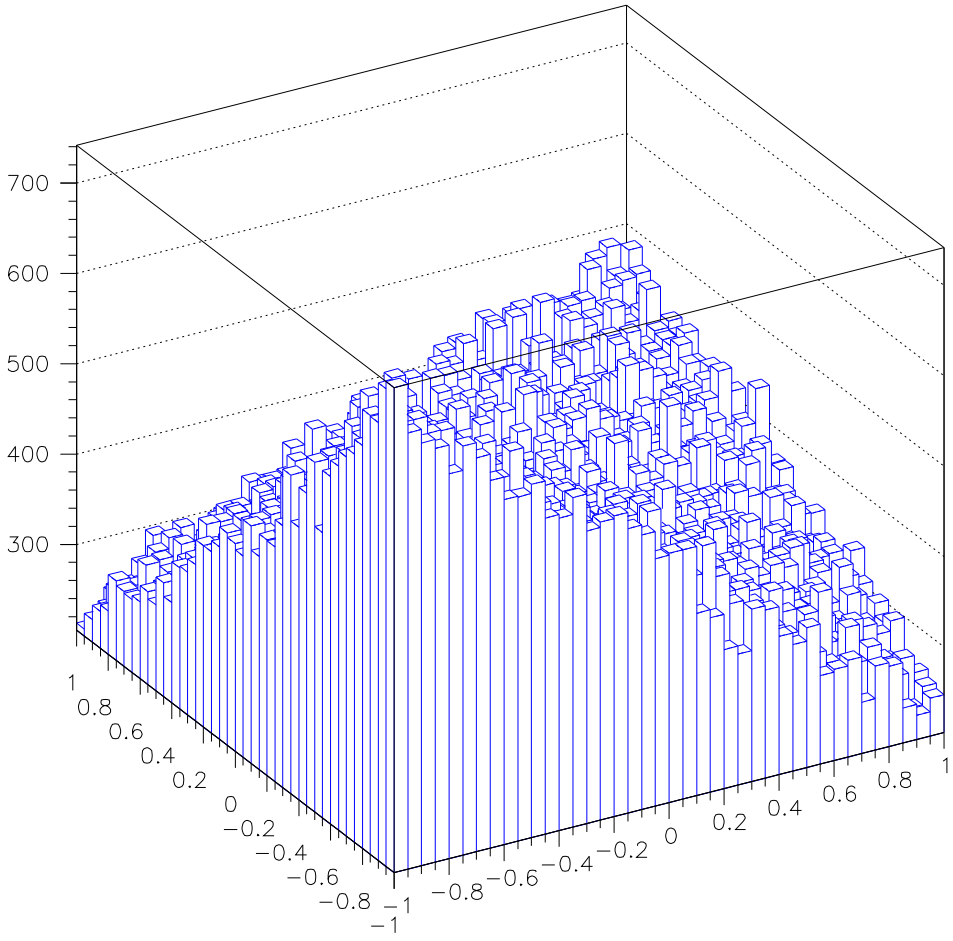


Fig. 48. A two dimensional distribution of $\cos(\theta_1) \times \cos(\theta_2)$ in helicity frame - TopRex.

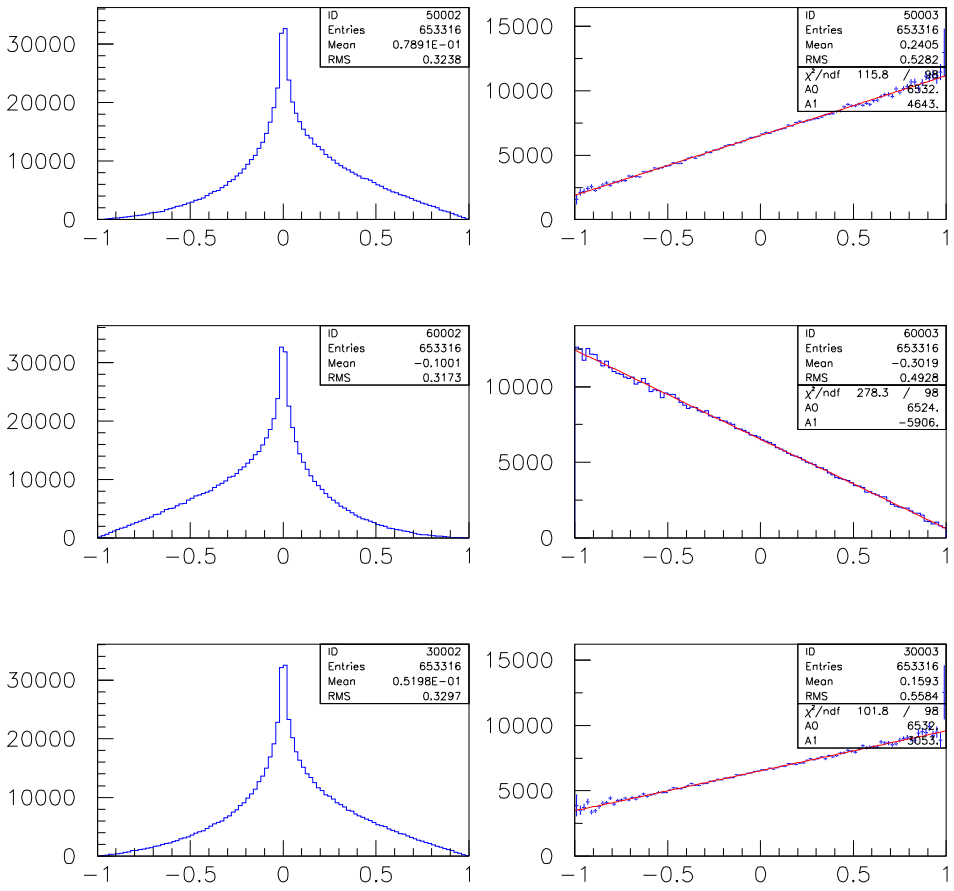


Fig. 49. Distribution of variable $z$ in beam I,II frames and helicity frame (see text).

### 3.7 Measurement of top quark width and lifetime

Top quark lifetime and width are related through Heisenberg's uncertainty relation. Therefore, if one is able experimentally to measure one quantity it implicity also measures the other one.

Lifetime can be measured directly if it is long enough that resolution of detector can distinguish it from 0. Otherwise measurement will result in the upper limit. It can be measured indirectly if there is relationship between observed specific feature and top lifetime and if some calibration is possible. e.g. one can imagine that amount of radiated gluons directly from top quark is proportional to the top quark lifetime.
Top quark width can be measured directly by top mass measurement. It can be measured indirectly e.g. by single top cross section measurement (see 2.1).

Two of the above mentioned options have been already realized and details are discussed below.

#### Direct measurement of top quark lifetime

A direct measurement of top quark lifetime was addressed by a CDF study [73]. This study had no chance to measure the top quark lifetime if the Standard Model is correct. But it is important to make measurement even in such case (otherwise if we strictly believe in the Standard Model any measurement is not necessary).

Idea behind this measurement is to measure with best precision detector allows distance between interaction point of $\mathrm{p\bar{p}}$ scattering and decay vertex of $W^{\pm}$ from $t \to Wb$ decay.

Study [73] is based on statistics 318 $\mathrm{pb}^{-1}$ collected by CDF collaboration between March 2002 and September 2004. Selection of enhanced $t\bar{t}$ candidate sample is close to one explained in section 3.1.2 - cross section measurement based on lept. + jets channel. Basically, isolated lepton, at least 3 high $E_T$ jets (at least one of them b-tagged), $\not\!\!E_T > 20$ GeV are required. Requirements are strengthened on quality of reconstructed track corresponding to lepton ($e$ or $\mu$) in silicon vertex detector - at least three measurements in $r - \phi$ layers (transverse plane) for each track are required. Rejected are also events when effective mass of isolated lepton based on "tight" criteria and track passing loose lepton criteria requirements have effective mass between 76 and 106 GeV/$c^2$.

Finally, 97 electron tracks and 60 muon tracks for measurement of top quark lifetime have been selected.

As sensitive variable for a measurement of top lifetime is selected impact parameter $d_0$ of lepton from W-Boson decay. Impact parameter is defined as smallest distance between transverse projection of track and collision point. More precisely, implemented definition is: $d_0 = Q(\sqrt{x_0^2 + y_0^2} - \rho)$, where $x_0, y_0$ are x,y coordinates of center of circle (track of charged particle in magnetic field forms helix in space or circle in transverse plane), $\rho$ is radius of the circle and Q sign of charge of the track.

Impact parameter resolution is measured by using leptons from $Z^0$-Boson dilepton decay (Drell-Yan sample). Pair of leptons of the same flavor, opposite charge, satisfying tight lepton criteria with effective mass in range between 83 and 106 GeV/$c^2$ have been used for impact parameter resolution study. In Fig. 50 impact parameter distribution for electron and muon tracks is shown.

These distributions represent intrinsic detector resolution which includes uncertainty of the

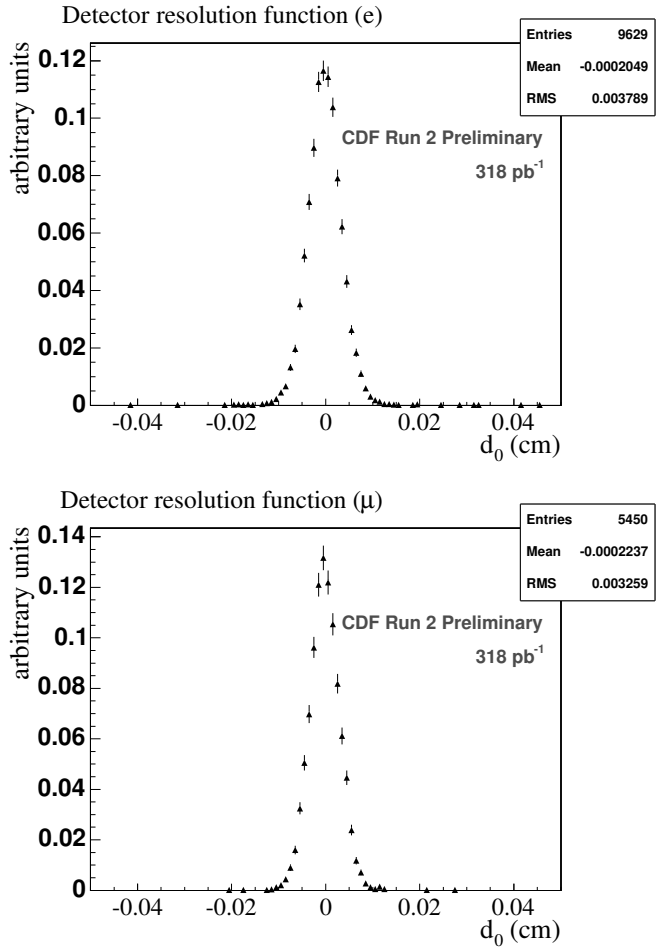


Fig. 50. Impact parameter resolution for isolated electrons and muons from $Z^0$ decay.

beam position ($\approx 25\ \mu m$) as well as intrinsic resolution of the single track helix parametrization.

Background to $t\bar{t}$ production is dominated by "prompt" leptons from W-Boson decay. In W-Boson decay there is the $\tau$ decay fraction present and $\tau$'s mean lifetime is relatively large ($c\tau \approx 90\ \mu m$). Another component which broadens impact parameter distribution is QCD component of background (non W background) where leptons come from heavy flavor (b,c jets). Electrons from electron positron conversion which somehow pass through selection procedure are also source of fake "long lifetime" component. And also muons from cosmic which passed cosmic ray filter. Sum of these "long lifetime" contributions and "prompt component" for electron and muon tracks are shown in Fig. 51.

Based on experimentally determined impact parameter resolution by convolution of resolution with exponential decay of preset lifetime of top templates for $c\tau$ in range of 0-500 $\mu m$ have been produced. See Fig. 52. Binned likelihood method is used to fit combination of background and signal templates to data. Result of a comparison of data and the best fit is shown in Fig. 53. Fit converges to 0 lifetime. Statistical Feldman-Cousins (FC) [75] approach is used to estimate correspondence between measured and true lifetime at 95 % confidence level (CL). Result (which takes also into account systematic errors) is presented in Fig. 54.

From FC analysis follows that at 95 % CL mean lifetime $c\tau$ of top quark is smaller than 52.5 $\mu m$ or $1.75 \cdot 10^{-13}$ s!

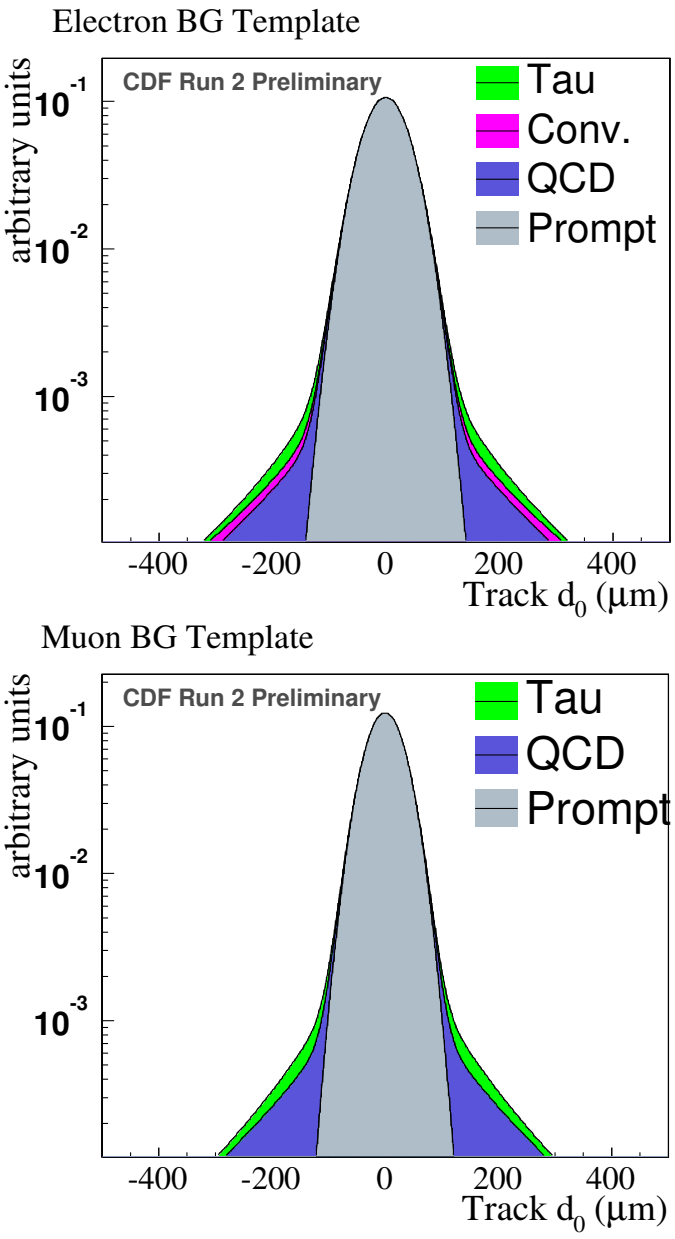


Fig. 51. Influence of different kind of background on impact parameter distribution for electron and muon tracks.

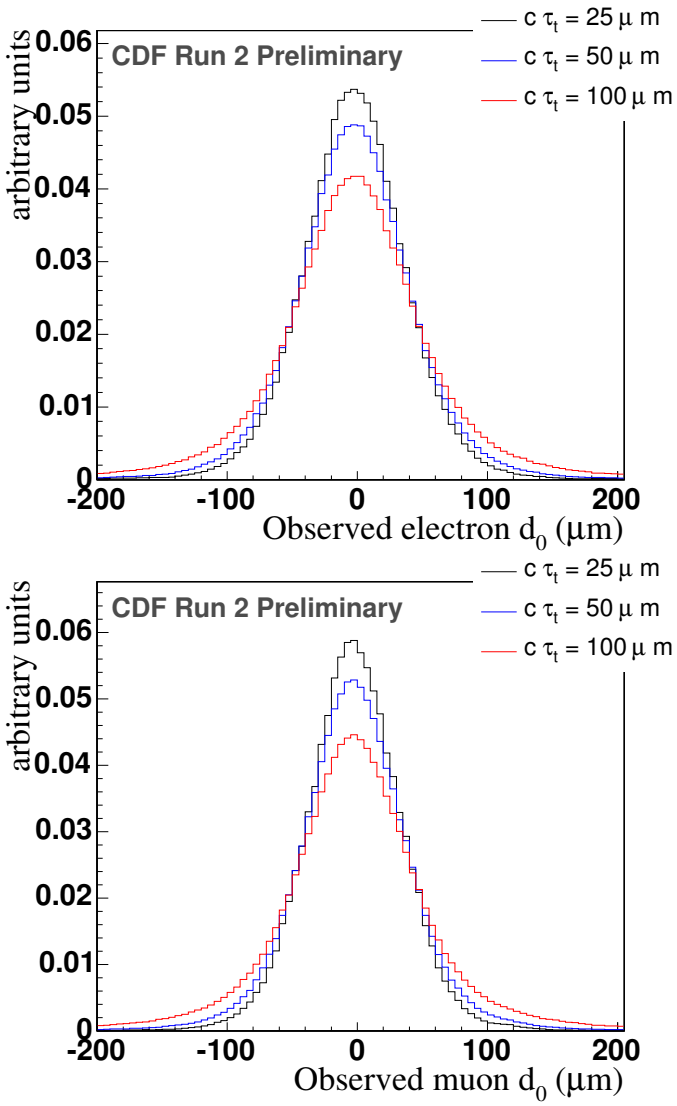


Fig. 52. Templates for $t\bar{t}$ signal simulated for different top lifetimes for electron and muon tracks impact parameter distribution.

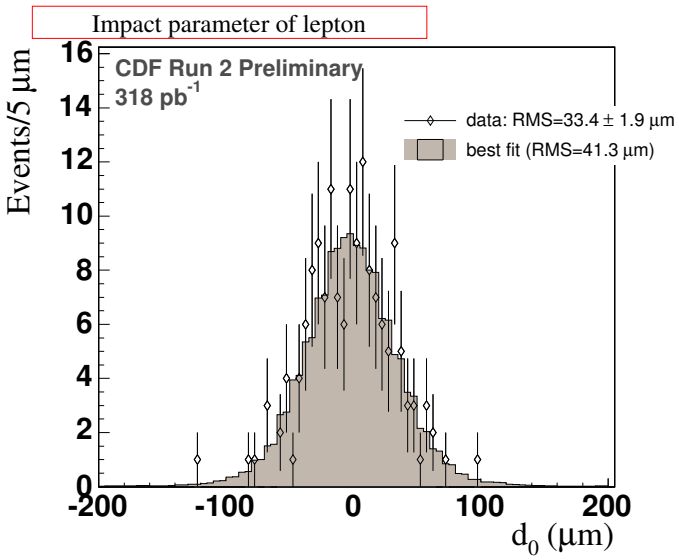


Fig. 53. A comparison of impact parameter distribution of leptons for $t\bar{t}$ candidates and best fit by templates.

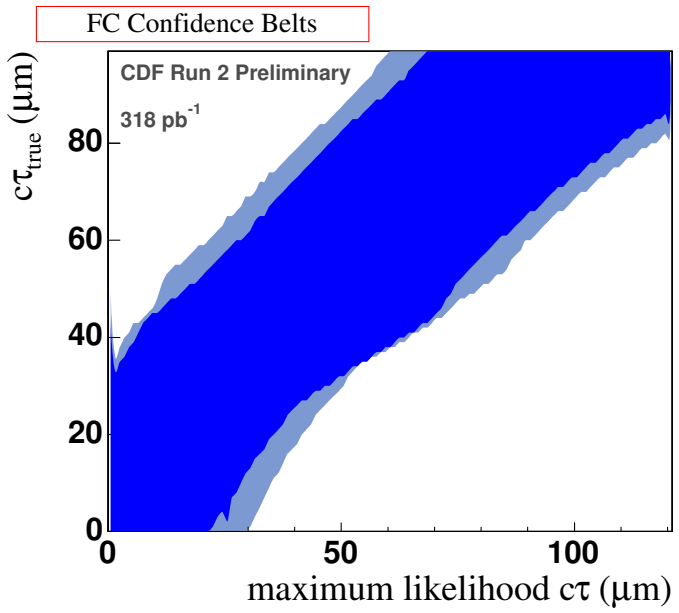


Fig. 54. Feldman-Cousins confidence level bands between measured and true top $c\tau$ measurement.

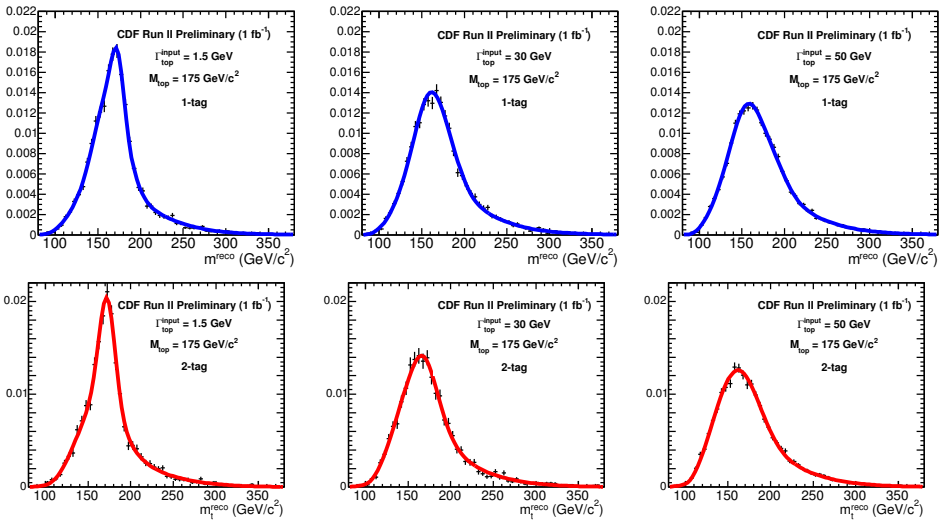


Fig. 55. Parametrization fits to the reconstructed top mass distributions for$\Gamma_t^{input}$ 1.5, 30, and 50 GeV. Top: 1- b-tag sample, Bottom: 2-b-tag sample.

### Top quark width measurement

Question of top quark width is addressed by another CDF analysis [74] based on statistics of integrated luminosity $\approx 1$ fb$^{-1}$.
Idea behind this analysis is to use top mass reconstruction and templates for different top width and to fit it to data. Analysis was done on statistics 1 fb$^{-1}$ sample, lept. + jets channel. Main difference in event selection in a comparison with section 3.1.2 is that 4 jets are required but in case when 2 jets are b-tagged there is applied relaxed criterion on 4-th jet selection. In this case fourth jet is required to have $E_T > 8$ GeV only (each of other jets must have at least $E_T > 15$ GeV). Selection passed 171 events with one jet b-tagged (expected signal / background ratio 3.7) and 82 events with at least 2 b-tagged jets (S/B = 10.6).

Top mass reconstruction follows well tested procedure [46] used in the past many times for reconstruction of top quark mass by a comparison of reconstructed observable top mass with templates created for preset values of top mass parameter. In top quark width study top quark mass is considered known, fixed to $M_{top} = 175$ GeV/$c^2$ and templates are produced for range of different top width $\Gamma_t^{input}$. Top quark width parameter is appropriately set in generator PYTHIA [16] and generated events pass through detector simulation and event reconstruction chain. Finally, above selection procedure is applied and by using observable top mass reconstruction procedure [46] top mass observable is reconstructed. Distribution of top mass observables ($m_t^{reco}$) for a given $\Gamma_t^{input}$ forms a template. Templates are normalized and parametrized and probability density function $P_s(m_t^{reco}; \Gamma_t^{input})$ is created.

Examples of parametrization for $\Gamma_t^{input}$ 1.5, 30, and 50 GeV is shown in Fig. 55. An a priori estimate for background composition is used to obtain $m_t^{reco}$ shapes for background.

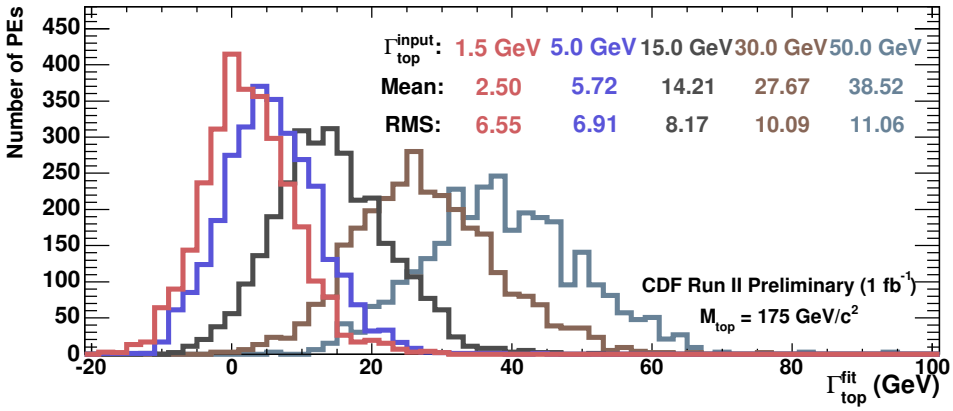


Fig. 56. Fitted width distribution for 3000 pseudo-experiments using MC samples with various $\Gamma_t^{input}$.

The reconstructed top mass distributions from data are compared to signal and background templates using unbinned likelihood fit. Definition of likelihood is given bellow

$$\mathcal{L} = \mathcal{L}_{shape} \times \mathcal{L}_{bg}\,, \tag{57}$$

$$\mathcal{L} = \frac{e^{-(n_s+n_b)}(n_s+n_b)^N}{N!}\prod_{i=1}^{N}\frac{n_s P_{sig}(m_i;\Gamma_{top}) + n_b P_b(m_i)}{n_s+n_b}\,, \tag{58}$$

$$-\ln(\mathcal{L}_{bg}) = \frac{(n_b - n_b^{exp})^2}{2\sigma_{nb}^2}\,, \tag{59}$$

where $n_s, n_b$ are expected number of signal and background events, N is the observed number of events with observed top mass per event $m_i$. The likelihood $\mathcal{L}_{shape}$ is the joint probability density for sample of N reconstructed events with observed top mass $m_i$ and fraction of background $n_b/(n_s+n_b)$. Gaussian term $\mathcal{L}_{bg}$ constrains the number of background events to expected number of background events $n_b^{exp}$ within uncertainty $\sigma_{n_b}$. $\Gamma_{top}$ is determined by maximum likelihood fit to the observed top mass distribution. Method was tested on samples with fixed top width and fitted width distribution is shown in Fig. 56. To set a limit on top width Feldman-Cousins prescription [75] is employed. The FC prescription guarantees a physically meaningful result even in case when fitted values are close to unphysical or in unphysical region (e.g. $\Gamma < 0$). As an ordering principle for selecting acceptance region and creating acceptance bands likelihood ratio is used. Likelihood ratio is defined:

$$R(x) = \frac{P(x|\Gamma_0)}{P(x|\Gamma_{max})}\,,$$

where $R(x)$ is a likelihood ratio at $x$, $\Gamma_0$ is the given input top width and $\Gamma_{max}$ is the input top width that yields the maximum likelihood among all the possible width for a measured width $x$.

The systematic uncertainties are incorporated to the confidence bands by convolution prob-

ability density function of $\triangle\Gamma$ due to systematics with fitted width function. The new width function is used to create the confidence bands with systematics.

For analysis of data, the likelihood eq. (57) is used separately for single b-tag sample and 2 b-tag sample. Fit for single b-tag sample was $\Gamma_{top}^{fit} = -1.9$ GeV and for 2-b-tag sample $\Gamma_{top}^{fit} = -7.4$ GeV. A comparison of data and fit is shown in Fig. 57. Product of likelihoods for single b-tag sample and 2-b-tag sample is used for the fit of top width based on both samples. Result is $\Gamma_{top}^{fit} = -4.86$ GeV.

All fit results are in the unphysical region and mean that top width is small, close to 0 within resolution. In Fig. 58 95% Confidence Level bands produced by Feldman-Cousins prescription taking into account systematic errors are presented. Fitted value $\Gamma_{top}^{fit}$ for combined sample is marked there. It follows that $\Gamma_{top}^{fit} = -4.86$ GeV can be interpreted with 95 % CL as upper limit $\Gamma_{top} < 12.7$ GeV or top lifetime $\tau_{top} > 5.2 \cdot 10^{-26}$ s.

We can combine two independent measurement - top lifetime and top width measurement to set 95% CL for upper and lower limit on top quark lifetime.

It follows that in 95% CL experimentaly determined top mean lifetime is in range

$$5.2 \cdot 10^{-26} < \tau_{top} < 1.75 \cdot 10^{-13} s.$$

This result is consistent with lifetime expected for top mass 175 GeV/$c^2$ from Standard Model $\approx 4 \cdot 10^{-25}$ s!

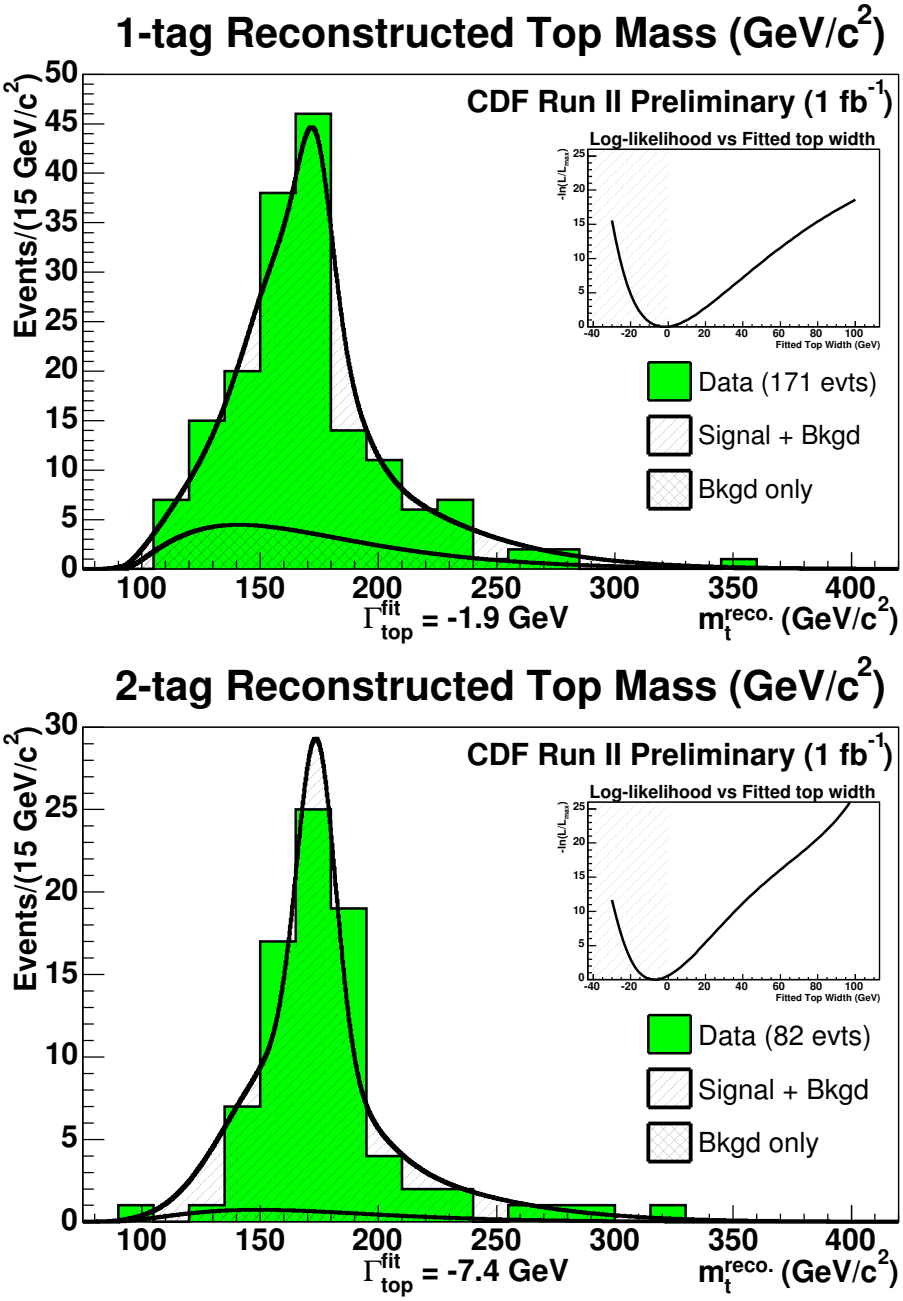


Fig. 57. Likelihood fit of top width to reconstructed top mass distribution of data. Upper plot for 1-b-tagged sample, lower plot for 2-b-tagged sample.

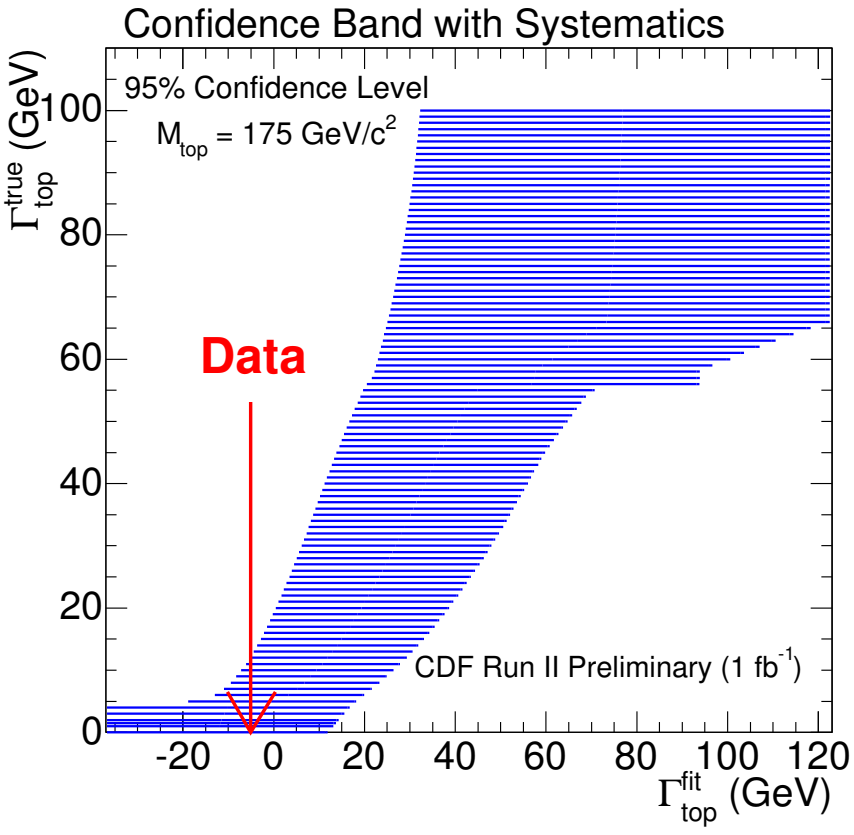


Fig. 58. Feldman-Cousins 95% Confidence Level bands. Mapping of fitted top width values to the range of corresponding true top width.

## 4 Concluding remarks

Over the past years was invested tremendous effort to the measurement of top quark physical parameters. Ingenious methods have been developed to push experimental limits as far as possible. Standard Model was challenged and up to now successfully passed all challenges. Still both experiments CDF and D0 did not say a final word. A realistic expectation is that at the end of run II the accumulated integrated luminosity will be around 6-8 $\mathrm{fb}^{-1}$. What kind of improvements can be still expected and what kind of questions will need to be answered by successors of TEVATRON - LHC and ILC?

Top quark pair candidate sample is also a region where new signals outside of the Standard Model can be present. Therefore it is necessary to carefully and critically analyze this sample. With larger statistics it will be possible to make detailed statistically significant studies based on specific subsamples. e.g. separate analysis for electron sample, muon sample.

Let's try to predict what will happen with topics discussed in this paper when integrated luminosity will be in the range from 6 to 8 $\mathrm{fb}^{-1}$.
$t\bar{t}$ **cross section** - uncertainty will be dominated by systematic errors.
**Top quark mass** - uncertainty will be dominated by systematic errors and it will be necessary to implement new ideas to push them down. For a long time most significant systematic error - jet energy scale is by in situ calibration reasonably under control. It can be pushed down inversely proportionally to square root of the statistics. Also combination with $Z \rightarrow b\bar{b}$ can be explored. That means that other systematic errors will dominate and there does not seem to exist similar solution like with jet energy scale. Statistical error of combined measurement is already below systematic error. New ideas are needed. One possibility is to concentrate on methods which methodically do not provide best resolution but have advantage of smaller systematic errors.
**Single top** - stage of discovery is expected to be achieved (5 $\sigma$). However detailed study of this channel will be probably left to LHC. Interesting topics can be measurement of top spin polarization and measurement of the top width. This channel is very sensitive to a new physics!
**Top charge** - definite answer achieved different ways in different channels. In two hypothesis scenario - rejection of of the wrong hypothesis with at least 4 $\sigma$ significance.
**W helicity** - a two dimensional model independent measurement of helicity fractions separately for electrons and muons in lept. + jets and dilepton channel, uncertainties factor two smaller than present
**Spin - Spin correlations** - measurement of the correlation coefficient, consistency with Standard Model prediction challenged
**Top quark lifetime and width** - improvements in the top mass methodology can push upper limit on top width to a more challenging values. Also combination with single top cross section can help. Direct lifetime measurement is saturated by resolution of detector element (silicon vertex detector). One can hardly expect improvement from this side.

What was mentioned is straightforward extrapolation but there is also space for surprises.

What will be left for experiments which take over from TEVATRON? Agenda of these experiments is focused on Higgs. But huge statistic of top production (pair and single) gives an opportunity for detailed studies which are impossible at TEVATRONN. e.g. Spin-Spin correlations measurements with few percent precision [76], measurement of cross section of $t\bar{t}\gamma$ channel (this way is direct measurement of the absolute value of the top charge possible).

Precision measurements of top quark mass based on measurement of threshold $t\bar{t}$ production

at International Linear Collider (ILC) will push uncertainty almost order of magnitude lower, ratio on $R = \frac{\sigma(e^+e^- \to hadrons)}{\sigma(e^+e^- \to \mu^+\mu^-)}$ after $t\bar{t}$ threshold will give definite support for true value of top charge.

LHC should start this year (2008) therefore interesting results can be expected soon.

**Acknowledgement:** Author takes an opportunity to thank all hard working people at TEVATRON collider, on experiments CDF and D0 for excellent work they have done. Special thanks go to my colleagues from CDF experiment. It was and still is very exciting time to work with these people on frontier of high energy physics. Very special thanks go to my very close collaborators Dr. A. Beretvas and Dr. Y.-C. Chen. Many ideas took a shape in discussion with them at our regular meetings.

Finally, support of Slovak grant agency APVV under contract APVV-20-057305 is respectfully acknowledged.

**References**


[1] W.-M. Yao et al.: *J. Phys. G* **33** (2006) 1

[2] F. Abe et al.: *Phys. Rev. Lett.* **74** (1995) 2626
S. Abachi et al.,: *Phys. Rev. Lett.* **74** (1995) 2632

[3] D. Chakraborty, J. Konigsberg and D. Rainwater:hep-ph/0303092

[4] A. Quadt: *Eur. Phys. J. C* **48** (2006) 835

[5] J. Ellis: *Nature* **448** (2007) 297

[6] N. Cabbibo: *Phys. Rev. Lett.* **10** (1963) 531
M. Kobayashi and T. Maskawa: *Prog. Theor. Phys.* **49** (1973) 652

[7] J. Pumplin et al.: hep-ph/0201195

[8] T. Arens and L.M. Sehgal: *Phys. Lett. B* **302** (1993) 501

[9] Z. Sullivan: *Phys. Rev. D* **70** (2004) 114012

[10] D. O. Carlson and C.-P. Yuan: hep-ph/9509208

[11] P. W. Jonson, F, I, Olness and Wu-Ki Tung: *Phys. Rev. D* **36** (1987) 291

[12] G.L. Kane, G.A. Ladinsky, and C.-P. Yuan: *Phys. Rev. D* **45** (1992) 124

[13] J.H. Kühn and G. Rodrigo: *Phys. Rev. D* **59** (1999) 054017

[14] CDF II Collaboration, FERMILAB-PUB-96/390-E(1996)

[15] D0 Collaboration: *Nucl. Instrum. Meth. A* **565** (2006) 463

[16] T. Sjostrand et al.: *Comput. Phys. Commun.* **135** (2001) 238

[17] G. Gorcella et al.: *JHEP* **01** (2001) 10

[18] http://www-cdf.fnal.gov/physics/new/top/2007/topProp/dil_xsection/xsec.html

[19] http://www-cdf.fnal.gov/physics/new/top/2007/topProp/secvtx_xsection_1invfb

[20] T. Affolder et al.: *Phys. Rev. D* **64** (2001) 03002

[21] T. Aaltonen et al.: *Phys. Rev. D* **76** (2007) 072009

[22] F. Abe et al.: *Phys. Rev. D* **45** (1992) 1448

[23] A. Bhatti et al.: *Nucl. Instrum. Meth. A* **566** (() 2 006)375

[24] D. Acosta et al.: *Phys. Rev. D* **96** (2006) 202002

[25] C. Peterson, T. Röngvaldsson, L. Lönngblad: *Comput. Phys. Commun.* **81** (1994) 185

[26] http://schwind.home.cern.ch/schwind/MLPfit.html

[27] http://root.cern.ch

[28] A. Ivanov for CDF and D0 collab., Hadron Structure Conf. 2007,Stara Lesna, September 2007

[29] M.Cacciari et al.: *J. High Energy Phys.* **04** (2004) 068

[30] N. Kidonakis and R. Vogt: *Phys. Rev. D* **68** (2003) 114014

[31] A.V. Gladyshev, D.I. Kazakov, M.G. Paucar: arXiv:0710.2322v1

[32] D. Chang, W.-F. Chang and E. Ma: *Phys. Rev. D* **59** (1999) 091503 D. Chang, and E. Ma: *Phys. Rev. D* **58** (1998) 097301

[33] private communication with W.-F. Chang

[34] M.C. Smith and S.S. Willenbrock: *Phys. Rev. Lett.* **79** (1997) 3825

[35] http://www-cdf.fnal.gov/physics/new/top/2007/mass/dil_Pt/DilMass_leptonPt_1_8.htm

[36] F. Abe et al.Phys. Rev. Lett.8019982779

[37] T. Aaltonen et al.: *Phys. Rev. D* **75** (2007) 111103

[38] C.S. Hill, J.R. Incandella and J.M. Lamb: *Phys. Rev. D* **71** (2005) 054029
[39] A. Abulencia et al.: *Phys. Rev. D* **75** (2007) 071102
[40] J. Antoš: *Acta. Phys. Slov.* **49** (1999) 127
[41] A. Abulencia et al.: *Phys. Rev. D* **73** (2006) 112006
[42] http://www-cdf.fnal.gov/physics/new/top/2007/mass/dil_kin
[43] http://www-cdf.fnal.gov/physics/new/top/2007/mass/dil_kin_xsec/
[44] T. Aaltonen et al.: *Phys. Rev. Lett.* **100** (2008) 062005
[45] T. Aaltonen et al.: *Phys. Rev. Lett.* **99** (2007) 182002
[46] A. Abulencia et al.: *Phys. Rev. D* **73** (2006) 032003
[47] M.L. Mangano et al.: *J. High Energy Phys.* **07** (2003) 001
[48] H.L. Lai et al.: *Eur. Phys. J. C* **12** (2000) 375
[49] T. Aaltonen et al.: *Phys. Rev. Lett.* **98** (2007) 142001
[50] The Tevatron Electroweak Working Group for the CDF and D0 Collaborations: FERMILAB-TM-2380-R
[51] S. Heinemeyer et al.: hep-ph/0412214 S. Heinemeyer et al.: hep-ph/0604147
[52] V.M. Abazov et al.: *Phys. Rev. Lett.* **98** (2007) 181802
[53] R. Brun and F. Carminati, CERN Program Library Long Writeup, Report No. W5013, 199
[54] http://www-d0.fnal.gov/Run2Physics/top/top_public_web_pages/top_public.html
[55] http://www-cdf.fnal.gov/physics/new/top/2008/singletop/combination
http://www-cdf.fnal.gov/physics/new/top/public_singletop.html
[56] A. Abulencia et al.: *Phys. Rev. D* **74** (2006) 072005
[57] A. Bhatti et al.: *Nucl. Instrum. Meth. A* **566** (2006) 375
[58] http://www-cdf.fnal.gov/physics/new/top/confNotes/cdf8967_publictq_15invfb.pdf
[59] A. Abulencia et al.: *Phys. Rev. D* **75** (2007) 052001
updated results http://www-cdf.fnal.gov/physics/new/top/2007/topProp/WHelicityFullReco2fb/
[60] http://www-cdf.fnal.gov/physics/new/top/2008/tprop/Whel_costhTemplate2fb/
[61] http://www-cdf.fnal.gov/physics/new/top/2007/topProp/Whel__ ME/
[62] V. M. Abazov et al.: *Phys. Rev. Lett.* **100** (2008) 062004
[63] A. Abulencia et al.: *Phys. Rev. D* **74** (2006) 072006
[64] F. Abe et al.: *Phys. Rev. D* **61** (1999) 032001
[65] G. Mahlon and S. Parke: *Phys. Rev. D* **53** (1996) 4886 D. Chang, S.-C. Lee and A. Soumarokov: *Phys. Rev. Lett.* **77** (1996) 1218
[66] W. Bernreuther, A. Brandenburg, Z. G. Si and P. Uwer: hep-ph/0107086
[67] W. Bernreuther, A. Brandenburg, Z. G. Si and P. Uwer:hep-ph/0304244
[68] private communication with S. Parke and G. Mahlon
[69] private communication with W. Bernreuther
[70] S.R.Slabospitsky and L.Sonnenschein: *Comput. Phys. Commun.* **148** (2002) 87
[71] W. Bernreuther et al.: hep-ph/0209202
[72] W. Bernreuther et al.: hep-ph/0410197
[73] http://www-cdf.fnal.gov/physics/new/top/2005/topProp/TopLifetime/index.html
[74] http://www-cdf.fnal.gov/physics/new/top/2007/mass/topwidth/topwidth.html
[75] G. Feldman and R. Cousins: *Phys. Rev. D* **57** (1998) 3873
[76] E. Hubaut et al.: *Eur. Phys. J. C* **44** (2005) 13